Adaptive PID Control of Interconnected Two-Area Photovoltaic Power Systems

Girma Abera Daba

A Thesis Submitted to the Department of Electrical Power and Control Engineering

School of Electrical Engineering and Computing

Office of Graduate Studies

Adama Science and Technology

September, 2024

Adama, Ethiopia

Adaptive PID Control of Interconnected Two-Area Photovoltaic Power Systems

Girma Abera Daba

Advisor: Dr. Tafesse Asrat

A Thesis Submitted to the Department of Electrical Power and Control Engineering

School of Electrical Engineering and Computing

Office of graduate studies

Adama Science and Technology University

September, 2024

Adama, Ethiopia

DECLARATION

I hereby state that the thesis titled “**Adaptive PID Control of Two-Area Photovoltaic Power Systems**" is my original effort. It has not been previously presented at all educational institution within a similar objective. The references utilized in this proposal have been appropriately recognized via accurate citations.

Girma Abera

Student’s Name	Signature	Date

ADVISOR’S RECOMMENDATION

As the advisor of this thesis, I confirm that I have provided close guidance and support to the student, **Girma Abera Daba**, during the development of the draft thesis proposal titled “**Adaptive PID Control of Interconnected Two-Area Photovoltaic Power Systems**". Having thoroughly reviewed the proposal, I recommend the submission of it to the department for additional review and evaluation.

Dr. Tafesse Asrat		
Advisor	Signature	Date

APPROVAL SHEET

I confirm that the suggestions and recommendations provided by the thesis review committee have been adequately included in the ultimate thesis titled "**Adaptive PID Control of Interconnected Two-Area Photovoltaic Power Systems**" by **Girma Abera**.

Dr. Tafesse Asrat

Advisor	Signature	Date

BOARD OF REVIEWERS APPROVAL PAGE

As members of the Board of Reviewers for the thesis open defence by Girma Abera, we have carefully reviewed and assessed the thesis titled "**Adaptive PID Control of Interconnected Two-Area Photovoltaic Power Systems**" to evaluate the candidate's comprehension of the proposed research. We hereby confirm the approval of the thesis and endorse the execution of the proposed thesis.

____________________	__________________	____________________
Chairperson	Signature	Date
____________________	__________________	____________________
Reviewer 1	Signature	Date
Dr Beteley Teka		Sept 22, 2024
Reviewer 2	Signature	Date

The final approval and acceptance of the thesis proposal are contingent up on the submission of its final version to the Office of Postgraduate Studies (OPGS) through the Department Graduate Council (DGC) and School Graduate Committee (SGC).

________________________	__________________	__________________
Department Head	Signature	Date
________________________	__________________	__________________
School Dean	Signature	Date
________________________	__________________	__________________
Office of Postgraduate Studies Dean	Signature	Date

ACKNOWLEDGEMENT

Primarily, I would like to convey my sincere appreciation to the All-Powerful God, the source of all existence and wisdom. He has given me the insight and endurance I needed to finish my research paper, and for that I am incredibly grateful. I am so grateful to God for giving me strength and the priceless gift of life. My adviser, Dr. Tafesse Asrat, has provided me with unwavering advice, encouragement, and unwavering support for both the technical and personal aspects of my research work. For this, I would like to genuinely appreciate and express my genuine gratitude. I am deeply touched by his persistent support for me during this process, as well as his steadfast motivation and patience. Also, I am truly thankful for Dr. Endalew Ayenew, who has provided me with wonderful advice and direction, for which I am very grateful. His unceasing support, perceptive advice, and strict oversight have all contributed to the development and improvement of this thesis. His patience and willingness to freely share his extensive knowledge have been greatly appreciated, and my study thesis has become much better as a result. I am really grateful to the head of the Electrical Power Control Engineering department for allowing me to use the lab. Finally, I would want to express my sincere thanks to my mother and father, who I will always love and miss dearly, as well as to my brother, sister, uncles, and aunts, whose unwavering love and sacrifices have laid the groundwork for my success. I am also incredibly appreciative of my close friends Girma Kushe and Gutema Gudunfa. Finally, I would want to express my sincere thanks to Adama Science and technology University, who I will always love.

TABLE OF CONTENTS

LIST OF FIGURES

LIST OF TABLES

LIST OF ACRONOMY

Abbreviation	Full Form
AC	Alternative Current
AFLC	Adaptive Fuzzy Logic Controller
APIDC	Adaptive Proportional-Integral-Derivative
BESS	Battery Energy Storage System Controller
DC	Direct Current
GA	Genetic Algorithm
IGBT	Insulated Gate Bipolar Transistor
LCL	Inductor-Capacitor-Inductor
LFC	Load Frequency Control
MOSFET	Metal-Oxide-Semiconductor Field-Effect
MPC	Model Predictive Controller
MPP	Maximum Power Point
MPPT	Maximum Power Point Tracking
MRAC	Model Reference Adaptive Controller
OAC	Optimal Adaptive Controller
PI	Proportional Integral
PID	Proportional Integral Derivative
PLL	Phase Lock Loop
PSO	Particles Swarm Optimization
PV	Photovoltaic
PWM	Pulse Width Modulation
ROCOF	Rate of Change of Frequency
SMC	Slide Mode Controller
STC	Self Tuning Controller Transistor

VSC	Voltage Source Control
VSI	Voltage Source Inverter
ESS	Energy Storage System
CSI	Current Source Inverter

ABSTRACT

There are a number of difficulties in integrating photovoltaic (PV) systems into contemporary power grids, especially in two-area power systems. Power sharing, frequency stability, and voltage regulation are problems in these systems, as each region is in charge of keeping its own power balance while also cooperating with nearby regions. This research highlights an important aspect of power systems, specifically the regulation of the frequency and voltage in a grid-on photovoltaic (PV) power system. In order to maintain stable operation and ensure optimal power generation, a Proportional-Integral (PI), Proportional-Integral Derivative (PID), step-up transformer, Alternative Current (AC) filter, Maximum Power Point Tracking (MPPT), DC to DC boost, inverters, DC link and voltage source converter ***(VSC)*** *controller are employed in this study. Furthermore, the PI and PID controller is designed based on maximum power point tracking through incremental conductance algorithm and Model Reference Adaptive Controller* ***(MRAC****) respectively to enhance its performance under uncertain system parameters. The optimal MRAC- PID and Maximum Power Point Tracking (MPPT) in DC-to-DC boost converter and PV panel to get stable voltage settled at 0.03 and 0.2 second respectively. Additionally, MRAC-PID used to stabilize frequency of the two-area grid-connected PV power system. The simulation results demonstrate that the controller effectively regulates the frequency of the system from 49-51 Hz, ensuring stable operation and maximizing power generation by using MATLAB software. This research contributes to the advancement of control strategies for PV power systems, enabling the efficient and reliable integration of renewable energy sources into the grid and the balancing of power between the two areas, i.e., tie line power. Finally, the results with and without optimal adaptive controller is discussed.*

Keywords: MPPT, PI/PID, Two-Area, PV system, DC-DC boost converter.

CHAPTER ONE

1. INTRODUCTION

1.1. Background of the Study

For many years, the world relied heavily on non-renewable energy sources such as coal, oil, and natural gas to meet its energy demands. These fossil fuels, while abundant and historically cheap, have significant drawbacks, including greenhouse gas emissions, environmental degradation, and finite availability. As a result, there has been a growing recognition of the need to transition to more sustainable energy sources.

In recent years, this awareness has led to an increasing focus on renewable energy, particularly wind and solar power. Renewable energy sources are inexhaustible and produce minimal environmental impact, making them key players in the fight against climate change. Solar energy, in particular, has gained prominence due to its vast potential (Dandoussou & Kenfack, 2023).

Solar energy systems capture sunlight using photovoltaic (PV) cells, converting it directly into electricity. These systems can be scaled from small rooftop installations to large solar farms that generate power for entire communities. Advances in technology have made solar panels more efficient and affordable, further driving their adoption. (Katinas et al., 2016), which may weakening the life qualities of people living nearby (Fu et al., 2016).

Harnessing the power of sunlight, solar photovoltaic (PV) systems utilize solar cells to generate electrical energy. These solar cells, also known as PV cells, are specialized devices that directly convert sunlight into electricity. As a renewable and clean energy source, solar PV systems have gained significant traction due to the surging demand for energy, the growing global interest in sustainable sources of energy, and the continuous advancements in solar PV technology and research (Fu et al., 2016).

Using photovoltaic (PV) solar power alone has several limitations. While solar energy is a valuable renewable resource, its effectiveness and reliability are influenced by various factors. Here are the primary reasons why combining PV solar power with hydropower, or other forms of energy, is often more practical and efficient:

i. Intermittency and variability

- Day-Night cycle: Solar power generation is limited to day light hours. During night there i no solar energy is produced.

- Weather Dependency: Solar output power varies with weather conditions, during rainy and cloudy season.

ii. **Difficulties with Energy Storage.**

- Storage Costs: Batteries and other large-scale energy storage technologies are pricy and not yet widely accessible or commercially viable for long-term energy storage.
- **Efficiency Losses:** The efficiency of solar power is decreased during the storage and retrieval of energy from batteries.

iii. **Variability Seasonal Variations**: Seasonal variations have an impact on solar power generation. In many areas, the winter months see less solar irradiance, which results in less energy being produced during periods of potentially high demand.

The imperative to transition from conventional energy systems to sustainable alternatives requires a paradigm shift in the energy supply. This shift entails a reliance on clean and renewable energy sources. Solar energy, in particular, emerges as a noteworthy option due to its pollution-free nature and limitless availability. It is widely accessible on a global scale. These attributes have played a role in the advancement of solar energy becoming the fastest growing renewable technology worldwide (Jiang et al., 2010). The solar panel generates a direct current (DC) input, which is influenced by factors like temperature and solar irradiance. This DC input is then fed into a DC-to-DC converter, which is responsible for increasing the level of voltage and transmitting it to a specific form of inverter used. Power electronic converters play a vital role in connecting distributed energy sources to the grid. In addition to transmitting the produced direct current power to the AC type of grid, these converters need to possess advanced capabilities. These include the ability to dynamically control voltage and frequency i.e., reactive and active power respectively, maintain stable operation within a defined frequency and voltage ranges, withstand fluctuations of voltage, inject reactive current when faults are occurred, and contribute to stabilization of grid activities such as primary frequency control, among other functions (Workshop, 2014). In this study solar energy is employed.

The primary objective of regulating frequencies by designing and developing PI (Proportional-Integral) controller specifically tailored for the regulation of frequency in two-area grid connected PV energy system. It means that in two distinct areas tie line's frequency and power levels within a defined range should be maintained. This aims to effectively manage fluctuations in power system demands and sudden disturbances, ensuring they meet varying load requirements and unforeseen changes in the system (Choudhary et al., 2019).

The concept of a PI controller involves using advanced control algorithms that can adapt to changing operating conditions and optimize the control actions for frequency regulation. It considers various factors such as solar irradiance, PV power output, load variations, and the interconnection between the two areas.

The controller aims to provide robust and efficient control performance by continuously monitoring and adjusting the power generation and consumption in real-time.

The main method of regulating the primary frequency and voltage involves managing uncertainty, i.e. irradiance, and temperature by means of various types of Maximum Power Point Tracking (MPPT)(D et al., n.d.).These are incremental conductance, perturb and observe and fractional short circuit current (Omar et al., 2018). Alternatively, the secondary frequency control aims to eliminate any permanent frequency error within the interconnected power grid by controlling the power flow between different regions (Civelek et al., 2018).

Table 1-1 Power Schedule

Time	**Loads**	**Area A**	**Area B**	**Total Power**
12:00 AM-6:00 AM	Load 1	20 kW	40 kW	60 kW
6:00 AM-12:00 PM	Load 2	40 kW	30 kW	70 kW
12:00 PM-6:00 PM	Load 3	40 kW	10 kW	50 kW
6:00 PM-12:00 AM	Load 4	10 kW	10kW	20 kW
Total Demand		110 kW	90 kW	200 kW

As shown in the Table 1-1 all loads Runs 6 hours per day.

1.2. Optimal Adaptive Controller

The Adaptive PID controller can actively monitor the frequency and voltage indirectly by, which match with the country grid code. In addition, it adjusts the output power of PV solar system to maintain a stable frequency and voltage within the specified limits. It can respond to frequency deviations by modulating the power generation of the PV solar system. This controller can balance the power produced from the PV solar system, which shared between the two areas based on their demand and requirements. It ensures that the power is efficiently allocated, minimizing imbalances and optimizing the overall system performance (Rohouma et al., 2020). In addition to frequency regulation, the OAC controller can also control the levels of voltage in the grid-on photovoltaic solar system. It can adjust the output power to maintain voltage stability within acceptable limits, ensuring reliable operation of the connected loads. In addition, it can adapt its control parameters and strategies based on the changing operating conditions and system dynamics. It can continuously monitor and analyze various parameters, such as solar irradiance, load demand, and grid conditions, to optimize the controllers (Mokhtar et al., 2022). Among the optimal adaptive controllers, MPC is commonly encouraged as a strategy of design in aspect of engineering electronics (Mirzaeva et al., 2016).

Generally, Model Reference Adaptive Controller(MRAC), Adaptive Model Predictive Controller (MPC) (Ortiz et al., 2020), c (N. Kumar et al., 2019), among various types of optimal adaptive controllers.

1.3. Statement of Problem

The renewable energy sources' integration, such as photovoltaic (PV), into power systems has led to a number of challenges, including frequency and voltage regulation as well as tie line power balance for two-area grid connected PV power system of solar energy. PV is a non-dispatch able generation source, meaning that its output cannot be controlled directly. This phenomenon creates difficulty to maintain the system frequency within acceptable limits, especially during the periods of low or high PV generation. Traditional frequency controllers, such as PID controllers, are not well suited for regulating the frequency and voltage of power systems with high penetrations of PV generation. This is because PID and PI controllers are not able to adapt to the changing dynamics of PV power output. This why adaptive Proportional-Integral-Derivative (PID) controller is a type of controller that can be used to regulate the voltage and power of solar power systems with high penetrations of PV generation. Adaptive Proportional-Integral-Derivative Controller (APIDC) are able to adapt to the changing dynamics of PV power output by adjusting their parameters in real-time.

1.4. Objectives of the Study

1.4.1. General Objective

The general objective is to develop an adaptive PID controller for regulating the voltage and frequency of two-area grid connected photovoltaic (PV) power systems.

1.4.2. Specific Objectives

- Model grid connected two-area PV power systems
- Design and develop an Adaptive PID Controller for the regulation of PV panel voltage.
- Synchronization of phase, frequency, and voltage with the electrical grid
- Power sharing between the two areas to meet load demand and power supply.

1.5. Motivation for writing this thesis.

The increasing global demand for sustainable and renewable energy sources has propelled the adoption of photovoltaic (PV) systems in power grids. As PV technology continues to evolve, its integration into multi-area grid systems becomes a crucial focus for enhancing grid reliability, stability, and efficiency. The two-area grid-connected PV system is particularly significant in this context, as it offers a promising solution to the challenges of balancing power supply and demand across different regions.

1.6. Scope of Thesis

The thesis aims to develop a system that controls the flow of active power. This control is achieved by implementing a rotating reference frame synchronously to control active power independently. The key components of this approach include:

- Modeling and simulating a photovoltaic (PV) array for a grid-on power system.
- Modeling and simulating a DC-to-DC boost converter integrated with an Incremental conductance MPPT controller.
- Regulating frequency between two areas which connected via tie-line.
- Modeling and simulating a DC to AC inverters alongside active component modeling.
- Simulating the entire grid-on PV power system.
- The simulation of models is implemented using MATLAB code/SIMULINK.

1.7. Thesis' Limitations

Thesis will focus on the simulation of the system using both MATLAB code and Simulink, demonstrating the interactions among several components of system. This approach is necessary because implementing the actual system is challenging, as the required components are expensive in our country. In addition, it limited to only one type of renewable energy, which is solar energy.

1.8. Significance of Thesis

A well-regulated frequency is essential for ensuring grid resilience and reliability. Fluctuations in frequency can lead to power outages, equipment damage, and even system-wide failures.

The PI and PID controller proposed in this research can respond to:

- Dynamic changes and disturbances in real-time, reducing the risk of blackouts and disruptions.
- Enhance the efficiency of power generation and utilization in the two-area PV power system by maintaining acceptable frequency regulation.
- Balance power supply and demand, minimizing wastage and improving overall energy efficiency.

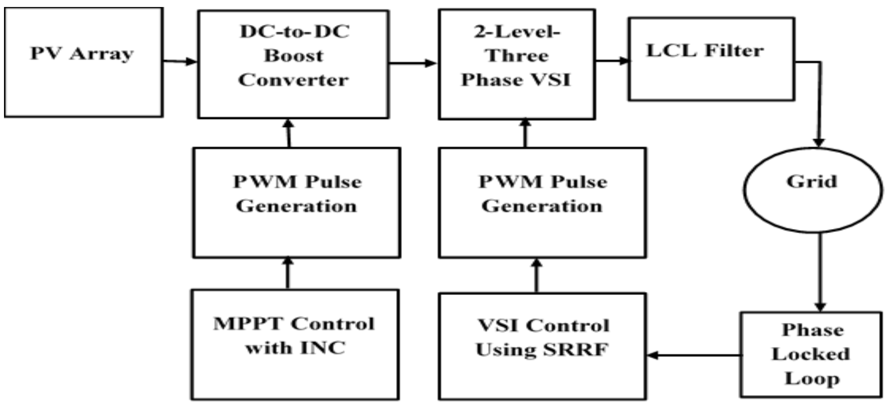

Figure 1-1 Block Diagram of Grid-on for a Single Photovoltaic Power System

1.9. Thesis Organization

The introduction is presented in Chapter One, and the thesis is organized into five chapters. Here is the structure of the rest of the thesis: Chapter Two covers the literature review and theoretical analysis of both DC-to-DC and adaptive controllers. Chapter Three focuses on adaptive control design, two-area solar panel power systems, and the mathematical modeling of non-linear systems. Chapter Four discusses the simulation and results. Finally, Chapter Five concludes the thesis and offers recommendations for further research.

CHAPTER TWO

2. LITERATURE REVIEWS

Researchers from various backgrounds have devoted their efforts to enhancing the quality, stability, and efficiency of grid-connected PV systems through the utilization of diverse techniques and methods. In their study published in the Middle-East Journal of Scientific Research in 2017,A.Angela Sheril and Ramesh Babu demonstrated that the control of voltage, current, and frequency synchronization in a grid-connected photovoltaic system can be achieved through the use of phase-locked loops(PLL) and the stationary reference frame method (Minda, 2019). However, they noted that the control of active and reactive power flow from the inverter's output to the grid was not addressed. This lack of independent control over these two powers hinders the improvement of system stability and efficiency (Sheril & Ramesh Babu, 2017). Additionally, MPPT is based on a control system that aims at maintaining the PV system operation in the most effective conditions of maximum power output done by Roberts is consider temperature and irradiance, however it is not consider sudden change of loads (Roberts, 2020). A.H. Azad, and H. Shateri in their "A Novel Control Strategy for On-Grid Photovoltaic Systems Based on Adaptive PI Control" (Azad & Shateri, 2019) use the inductor only as a filter, however the LCL filter is the most common for grid connected systems, and depend on the one area only.

Abd-Elazim and E. S. Ali developed LFC via FA for two areas Grid connected PV and thermal energy. However, they couldn't develop adaptive control for system and the type of filter used was not clear (Abd-Elazim & Ali, 2018).

On the other hand, the study of Choudhary compares the performance of the proposed whale optimization technique with genetic algorithm (GA) and firefly algorithm. While this provides some insights into the relative performance, it does not consider other potential optimization techniques or benchmarking against established methods in the field of load frequency control(Choudhary et al., 2019).

2.1. Review Summary

Finally, Zhang Ruiping designed, "Single phase Photovoltaic Grid-connected Inverter Current Control using MRAC controller" (Zhang et al., 2018). This thesis is limited to single phase, off grid connected. This off-grid system uses additional storage device, which make it costlier. The DC-link voltage is converges and overshoot up to final sampling time and after overshoot result settled after 0.1 second in (Mokhtar et al., 2022) thesis and above 0.1 seconds in all mentioned reviews. Hence in this thesis MRAC-PID is applied to DC-to-DC converter and settling time is improved.

2.2. Overview of Photovoltaic Panels

Photovolaic cells are also called solar cell,which takes energy directly from the sun light and convert it into electrical energy.These cells of psolar panels are made up of electronic devices,such as diode,transistors,integrated circuit and semiconductors.

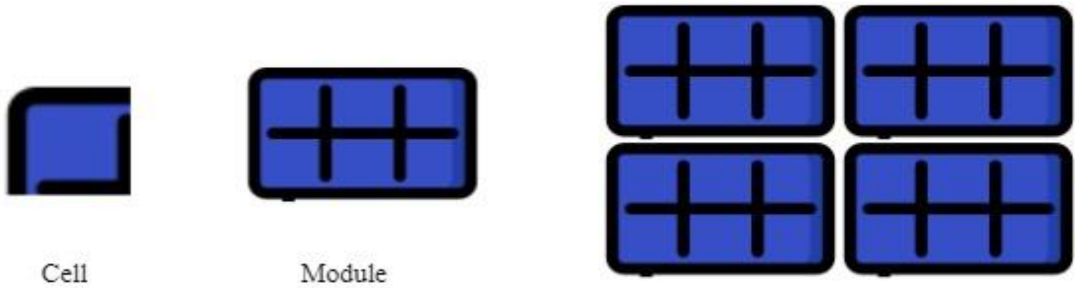

Figure 2-1 PV cell, Module and Array,L_{in1} ay

2.2.1. Types of Photovoltaic Cells

There are various types of photovoltaic cells available on the market, among them:

2.2.1.1. Mono-crystalline Solar Cells

These types of solar cells are made from a single continuous crystal structure, which allows electrons to move more freely through the cell, resulting in higher efficiency when compared to polycrystalline and amorphous silicon cells. It has efficiency of 15-20% and more expensive. In the study, this type of solar is employed.

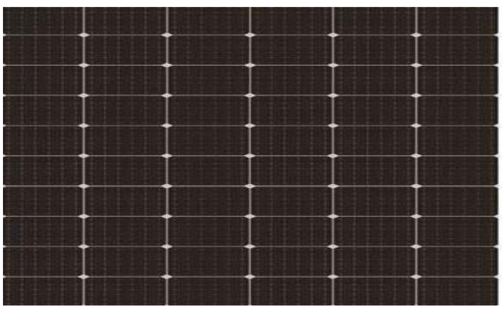

Figure 2-2 Mono-crystalline solar cell, L_{in2}

2.2.1.2. Polycrystalline Solar Cells

Polycrystalline solar cell is made from silicon wafers composed of multiple crystals structures. These crystals are smaller and less uniform compared to those in mono-crystalline cells. They are bluish in color, cost effective and have efficiency of 13% to 18%.

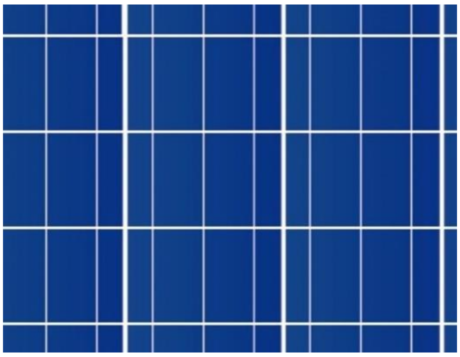

Figure 2-3.Polycrystalline solar cell, L_{in3}

2.2.1.3. Amorphous Silicon Cells

Amorphous silicon cells are known as thin film solar cells, made by depositing a thin layer of non-crystalline silicon into a substrate such as glass or metal. They have lower efficiency (6% to 10%) and cheap price.

Figure 2-4 Amorphous silicon cell, L_{in4}

2.3. Types of PV solar System

- Based up on application view, Photovoltaic power systems are categorized into grid-on, grid-off, hybrid PV system and micro grid PV system are among their categories.

2.3.1. Grid-on PV system

PV panels generate DC power from sun radiation. This DC power converted into AC power system in grid connected system. Hence, this is why inverter is playing a great role in conversion of power. In grid-on system any excessive power is fed into grid and when there is inadequate or absence of sunshine, supply of power is maintained from the grid.

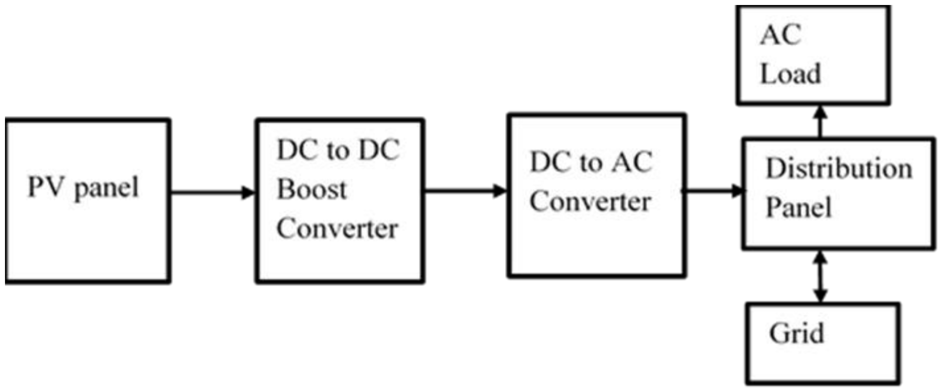

Figure 2-5 Grid connected photovoltaic system

2.3.2. Grid-off PV system

Stand-alone solar system is used without power grid, specifically the place or site where far away from the grid such as, offshore islands or rural areas. In this system, in order to feed load at night storage device like batteries are used.

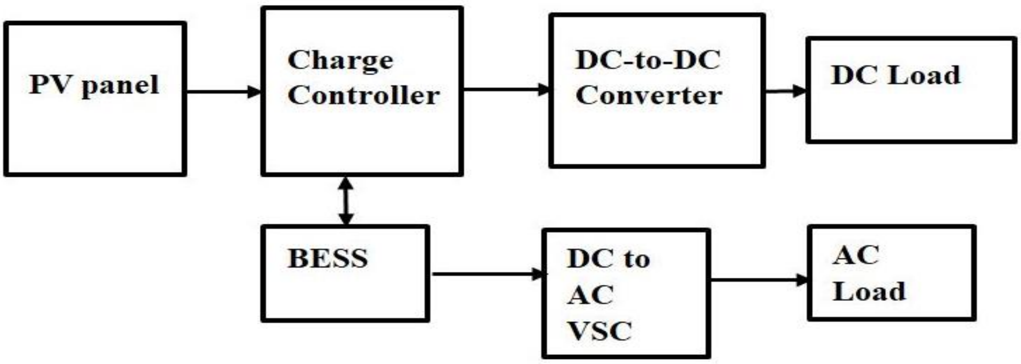

Figure 2-6 Stand-alone photovoltaic power system.

2.4. Maximum Power Point Tracking (MPPT)

2.4.1. Background

Early Development: In the 1950s, the idea behind MPPT started to take shape. The first useful photovoltaic cell was created at Bell Laboratories in 1954.Researchers soon discovered that operating these cells at their maximum power point (MPP), which fluctuates with temperature and solar intensity, was essential to maximizing their effectiveness.

Advancements in the 1980s: In 1985, an Australian company called AERL developed one the first commercial MPPT devices. This device, known as a “Power Optimizer,” significantly improved the efficiency of PV systems by dynamically adjusting the load to maintain operation at the MPP.

Maximum power point tracking is the cornerstone of a solar PV system, serving as its pivotal component. It is paramount for optimizing the systems performance by extracting the maximum power from the PV panels. The output power is affected by radiation

2.4.2. Application Areas of MPPT

- Photovoltaic (PV) Solar Power Systems
- Battery Charging Systems
- Electric Vehicles (EVs)
- Wind Energy Systems:
- Space Applications:

CHAPTER THREE

3. METHODOLOGY AND SYSTEM MODELING

3.1. PV PANEL MODELING

Photovoltaic (PV) systems convert solar energy directly into electrical power using semiconductor materials. The modeling of PV systems plays a crucial role in simulating and understanding the behavior of solar panels under varying environmental conditions, such as sunlight intensity and temperature. Accurate PV modeling is essential in designing and optimizing energy systems, ensuring maximum efficiency and reliability.

Table 3-1 Resistive Load Profile

Time (24 hrs.)	Loads	Area 1(A_a)	Area 2(A_b)
12 AM-6 AM	Load 1	20 kW	40 kW
6 AM-12 PM	Load 2	40 kW	30 kW
12 PM-6 PM	Load 3	40 kW	10 kW
6 PM -12 AM	Load 4	10 kW	10 kW
Total		110 kW	90 kW
Overall Two-Area Load		200 kW	

Energy required per day

$$1. For\ A_a, Load\,1a \times 6\,hrs + Load\,2a \times 6\,hrs + Load\,3a \times 6\,hrs$$
$$Load\,4a \times 6\,hrs \quad (3.1)$$

$$E = 20\,kW \times 6\,hrs + 40\,kW \times 6\,hrs + 40\,kW \times 6\,hrs + 10\,kW \times 6\,hrs$$

$$120\,kWh + 240\,kWh + 240\,kWh + 60\,kWh$$

$$660\,kWh$$

Design the PV for ' A_a ' system:

Since the lost energy in PV cell to consider for energy loss, multiply the output energy by 1.3

$$E_{Aa} = 660\,kWh \times 1.3 = 858\,kWh$$

Take: Mono-crystalline 350Wp with $V_{pm} = 43.0V$ from datasheet table below

Table 3-2 Datasheet of selected PV solar panel

Model	1 STH-350-WH
Peak Power (P_{max}) in W	350 W
Module efficiency	16.22%
Maximum power voltage (V_{mp})	43.0 V
Maximum power current (I_{mp})	9.94 A
Open circuit voltage (V_{oc})	51.5 V
Short circuit current (I_{sc})	8.13 A
Power tolerance	±3 % W
Maximum system voltage nominal	1000 V
Operating cell temperature	44.4 ± 2 °C
Maximum series Fuse Rating	15A
Temperature Coefficient of I_{sc} (Tk I_{sc})	0.09% /°C
Temperature Coefficient of V_{oc} (Tk V_{oc})	-0.28% /°C
Temperature Coefficient of P_{max} (Tk P_{max})	-0.37% /°C
Cell Type	166×83mm Mono
Dimension	1652×1306×40mm
Weight	24kg
Number of cells	80

$$Efficiency\ of\ the\ system = MPPT \times Inverter \times DC - DC \times Others \tag{3.2}$$

$$= 0.95 \times 0.94 \times 0.96 \times 0.90 = 0.77$$

$$Power\ required\ from\ PV\ panel = \frac{Total\ energy\ required\ per\ day\ for\ A_a}{Sun\ shine\ hours \times system\ efficiency} \quad (3.3)$$

$$= \frac{858\,kWh}{6.5\,hr \times 0.77} = 171.42\,kW$$

$$Power\ required\ (selected) = 300\,kW$$

Solar panel selection: since the power required from solar is 300 *kW*, then how many panels should be used? Select 350 *Wp* solar panel, then

$$N_o\ panels\ required = \frac{Power\ required\ from\ PV\ panel}{Output\ power\ of\ solar\ panel} \quad (3.4)$$

$$= \frac{300\,kW}{350\,W} \approx 856\ panels\ of\ 350\,W\ should\ be\ utilized$$

$$Powe\ required1 = N_{pa} \times N_{se} \times Wp \quad (3.5)$$

Select, $V_{mp} = 43\ V$, $N_{se} = 400V / 43V = 10$, from Equation (3.5), $N_{pa} = \frac{Power}{\left(N_{se} * Wp\right)} = 86$

$$2.\ For\ A_b, Load\ 1b \times 6\,hrs + Load\ 2b \times 6\,hrs + Load\ 3b \times 6\,hrs + Load\ 4b \times 6\,hrs \quad (3.6)$$

$$E = 40\,kW \times 6\,hrs + 30\,kW \times 6\,hrs + 10\,kW \times 6\,hrs + 10\,kW \times 6\,hrs$$

$$= 240\,kWh + 180\,kWh + 60\,kWh + 60\,kWh = 540\,kWh$$

Design the PV for 'A_b' system:

Since the lost energy in PV cell to consider for energy loss, multiply the output energy by 1.3

$$E_{Ab} = 540\,kWh \times 1.3 = 702\,kWh$$

Take: Mono-crystalline 350 Wp with $V_{pm} = 43V$

$$Efficiency\ of\ system = Effi\ of\ MPPT \times Inverter \times DC - DC \times Others \quad (3.7)$$

$$= 0.95 \times 0.94 \times 0.96 \times 0.90 = 0.77$$

$$Power\ required\ from\ panel = \frac{Total\ energy\ required\ per\ day\ for\ A_b}{sun\ shine\ hours \times Efficiency\ of\ system} \quad (3.8)$$

$$= \frac{702\,kWh}{6.5\,hrs \times 0.77} = 140.25\,kW$$

To feed load select $Power\ required = 280\,kW$

Solar panel selection: since we the power required from solar is 280 kW, then how many panels should be used. Select 350W solar panel, then according to Equation (3.4)

$$N_o\ panel\ required = \frac{power\ required\ from\ PV}{output\ power\ of\ solar\ panel} = \frac{280\,kW}{350\,W} \cong 800$$

$800\ panels\ of\ 350W\ should\ be\ utilized.$

$$Power\ required\ 2 = N_{se} \times N_{pa} \times W_p \quad (3.9)$$

Where, W_p is watt-peak (maximum power, which the single solar panel generated).

Select, $V_{mp} = 43$ V , $N_{se} = \frac{800V}{43V} = 20$, from Equation (3.9) $N_{pa} = \frac{Power}{N_{se} * Wp} = 40$

In addition, we can design solar based on its area, efficiency and irradiance as shown in Equation (3.10) at STC

$$P = \eta * A * G \quad (3.10)$$

Where P, η, A, G are output power, efficiency area and irradiance of solar panel respectively.

From Table 3-2 , $\eta = 16.22\%, A = 1652\,mm * 1306\,mm, G = 1000\,W / m^2$

$$P = 0.1622 * (1.652\,m * 1.306\,m) * 1000\,W / m^2$$

$$= 349.9465\,W \rightarrow This\ show\ us\ the\ chosen\ solar\ panel\ is\ correct.$$

In a **single-diode single-solar panel in** Figure 3-1, the solar panel is modeled as a current source in parallel with a diode, representing the p-n junction of the cells. The panel's current is proportional to sunlight, while the diode helps explain the non-linear I-V characteristics, such as the effects of shading or temperature. In Figure 3-2 **parallel-series combination** shown as, solar panels are connected in series to increase voltage and in parallel to increase current. This configuration helps meet specific power requirements and improves the efficiency and reliability of photovoltaic systems, especially in larger arrays.

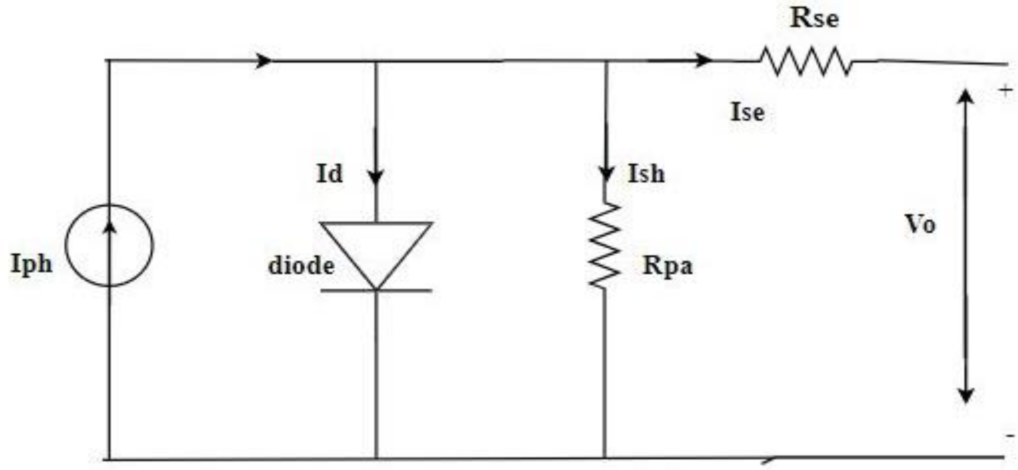

Figure 3-1 General Photovoltaic cell circuit diagram.

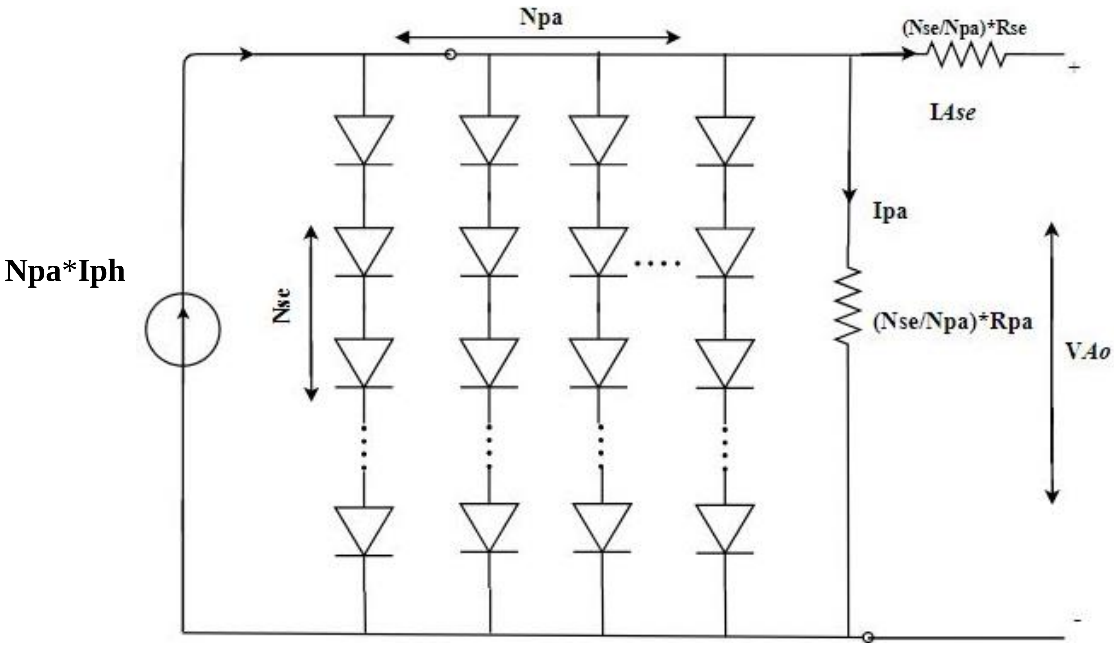

Figure 3-2 Area A and Area B General solar array representation

3.1.1. General solar cell equations for one diode single solar panel from Figure 3-1.

The Equations from (3.11-3.17) describe solar cell equations (Naz, 2021). Apply Kirchhoff's current law to the Figure 3-1circuit. we have:

$$I_{ph} = I_d + I_{sh} + I_{se} \tag{3.11}$$

$$I_{se} = I_{ph} - I_{sh} - I_d \tag{3.12}$$

$$I_d = I_{Rs}\left(e^{\frac{V_d}{a \times V_T}} - 1\right), V_T = \frac{KT}{Q} \tag{3.13}$$

$$I_{se} = I_{ph} - I_{sh} - I_{Rs}\left(e^{\frac{V_d}{a \times V_T}} - 1\right) \tag{3.14}$$

$$I_{se} = \frac{V_d - V_o}{R_{se}} \tag{3.15}$$

$$V_d = I_{se} \times R_{se} + V_o \tag{3.16}$$

$$I_{sh} = \frac{V_d}{R_{pa}} = \frac{I_{se} \times R_{se} + V_o}{R_{pa}} \tag{3.17}$$

Substitute Equation (3.13) and Equation (3.14) into Equation (3.11) gives

$$I_{se} = I_{ph} - \frac{I_{se} \times R_{se} + V_o}{R_{pa}} - I_{Rs}\left(e^{\frac{I_{se} \times R_{se} + V_o}{a \times V_T}} - 1\right) \tag{3.18}$$

Where; I_d = current flow through diode circuit

I_{ph} = photo-current at given irradiance and temperature

I_{sh} = current flow through shunt resistor (R_{pa})

I_{se} = current flow through series resistor (R_{se})

I_{Rs} = reverse saturation current in a diode

V_o = output voltage of the system

V_d = voltage across diode terminal

V_T = thermal voltage produced in p-n junction due to temperature

a = ideality factor

N_{pa} = Number of parallel solar panel

N_{se} = Number of series solar panel

K = Boltzmann's constant 1.38×10^{-23}

T = junction temperature in degree kelvin

Q = Charge of electron ($1.602 \times 10^{-19} c$)

3.1.2. General solar cell equations for series and parallel connected solar panels

From Figure 3-2 circuit diagram we derive:

$$I_{Ase} = I_{ph} N_{pa} - I_0 N_{pa} \left\{ e^{\left[\frac{Q}{a \times KT} \left(\frac{V_{Ao}}{N_{se}} + \frac{I_{Ase} \times R_{se}}{N_{pa}} \right) \right]} - 1 \right\} - \frac{N_{pa}}{R_{pa}} \left(\frac{V_{Ao}}{N_{se}} + \frac{I_{Ase} \times R_{se}}{N_{pa}} \right) \quad (3.19)$$

$$V_{Ao} = \frac{N_{se} KaT}{Q} \ln \left(\frac{N_{pa} I_{ph} + N_{pa} I_0 - I_{Ase}}{N_{pa} I_0} \right) - I_{Ase} R_{se} \frac{N_{se}}{N_{pa}} \quad (3.20)$$

Multiplying Equation (3.19) by output voltage, gives

$$P_{PvA} = I_{Ase} V_{Ao} \quad (3.21)$$

$$P_{PvA} = N_{pa} V_{Ao} I_{ph} - N_{pa} V_{Ao} I_0 \left[\exp\left(\frac{V_{Ao} + R_{se} I_{Ase}}{N_{se} V_T} \right) - 1 \right] - \left(\frac{{V_{Ao}}^2 + R_{se} I_{Ase} V_{Ao}}{R_{pa}} \right), \quad (3.22)$$

Where, P_{PvA} = output power of solar array

V_{Ao} = PV array's output voltage

I_{Ase} = PV array's output current

R_{pa} = Shunt resistance

R_{se} = Series resistance

G_n = Reference irradiance

T_n = Reference Temperature

In Simulink below, the parameters I0, Iph, IRS, Ish, and Ise represent different characteristics of the solar cell. I0, or saturation current, indicates the small amount of current that flows when the cell is reverse-biased and is temperature-dependent, playing a crucial role in determining the diode characteristics. Iph, or photocurrent, is the current generated by the solar cell when exposed to sunlight, directly proportional to the solar irradiance and the effective area of the solar cell. I_{RS} refers to reverse saturation current, which also flows in reverse bias and can influence the efficiency of energy conversion. Ish represents the shunt current, indicating leakage current that flows through the solar cell when it's not generating power, potentially reducing overall efficiency by providing a path for current that bypasses the load. Lastly, Ise is the series current, which flows through the series resistance of the solar cell.

$$I_{ph} = I_{sc} + K_i \left(T - T_n\right) \times \frac{G}{G_n} \tag{3.23}$$

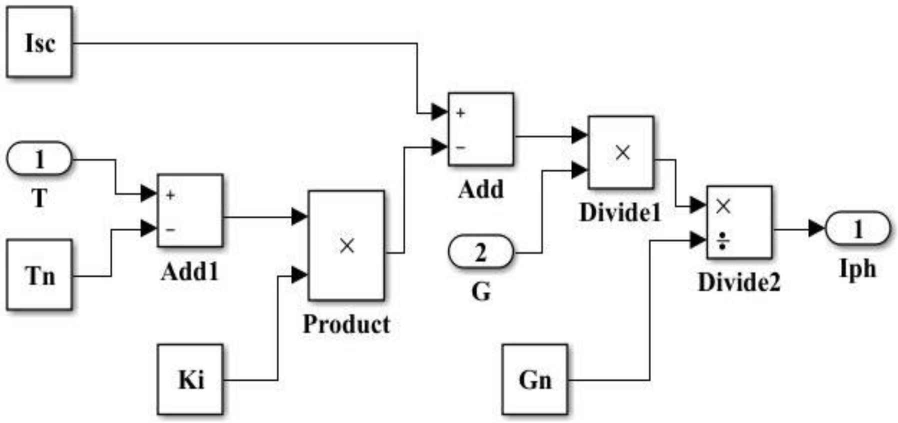

Figure 3-3 Modeling of photocurrent in solar panel(Workshop, 2014)

$$I_{pa} = \frac{I_{Ase} \times R_{se}}{N_{pa}} + \frac{N_{pa} \times V_{Ao}}{N_{se} \times R_{pa}} \tag{3.24}$$

Equation (3.24) is derived in similar manner with single solar module.

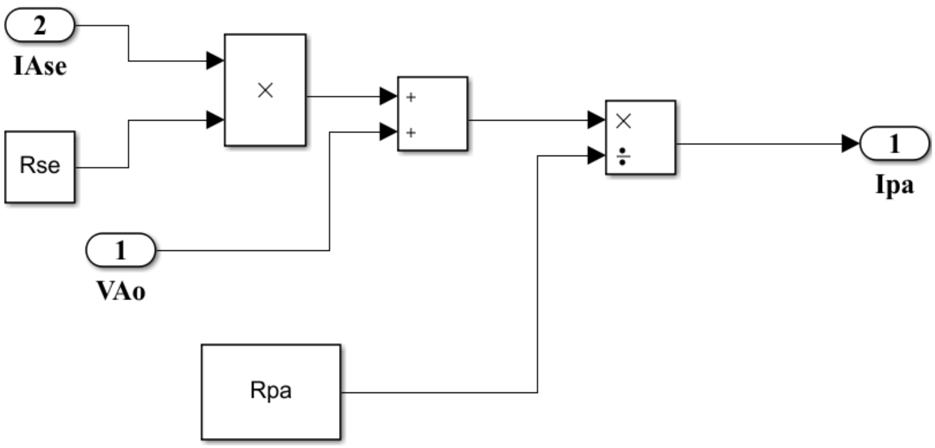

Figure 3-4 Current flows through shunt resistor of the cell (Dandoussou & Kenfack, 2023)

$$I_{Rs} = I_{sc} \div \left(e^{\frac{Q \times V_{oc}}{aN_{se}KT}} - 1 \right) \tag{3.25}$$

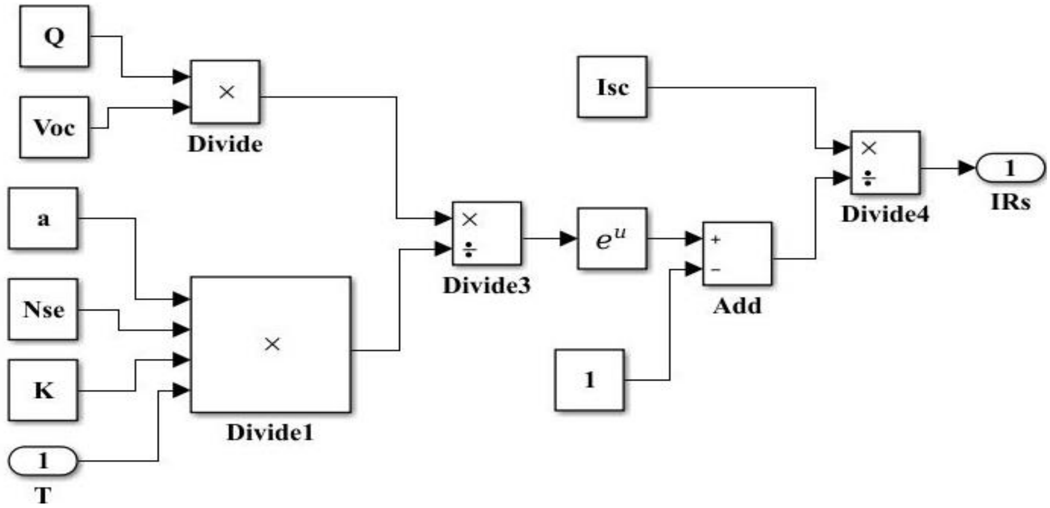

Figure 3-5 Reverse diode saturation current at STC (Azad & Shateri, 2019)

$$I_0 = I_{Rs} \times \left(\frac{T}{T_n} \right)^3 e^{\left(\frac{Q \times E_{Go}}{aK} \left(\frac{1}{T_n} - \frac{1}{T} \right) \right)} \tag{3.26}$$

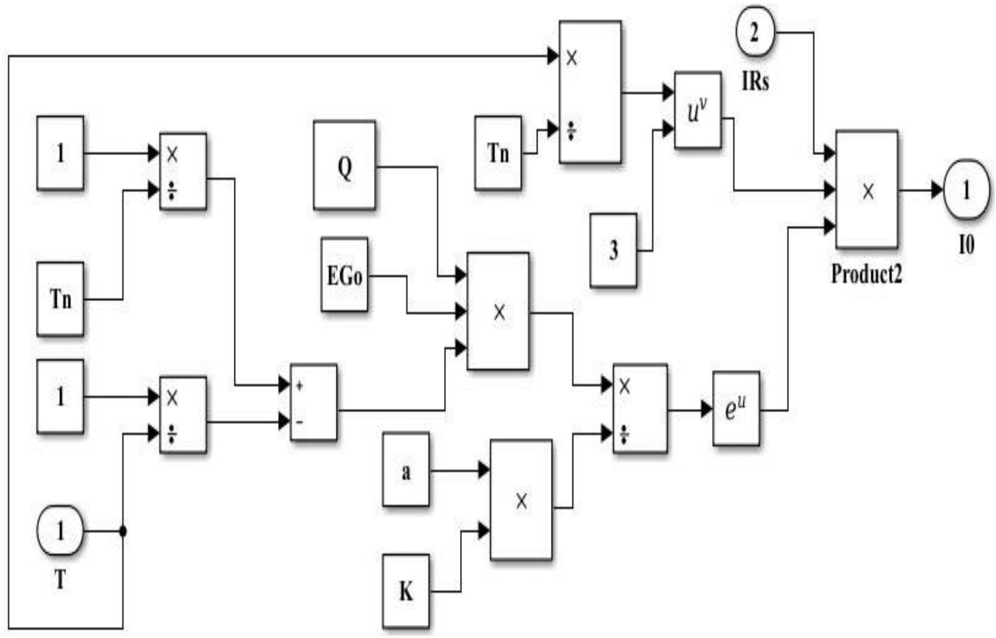

Figure 3-6 Temperature dependent Reverse diode saturation current(Choudhary et al., 2019)

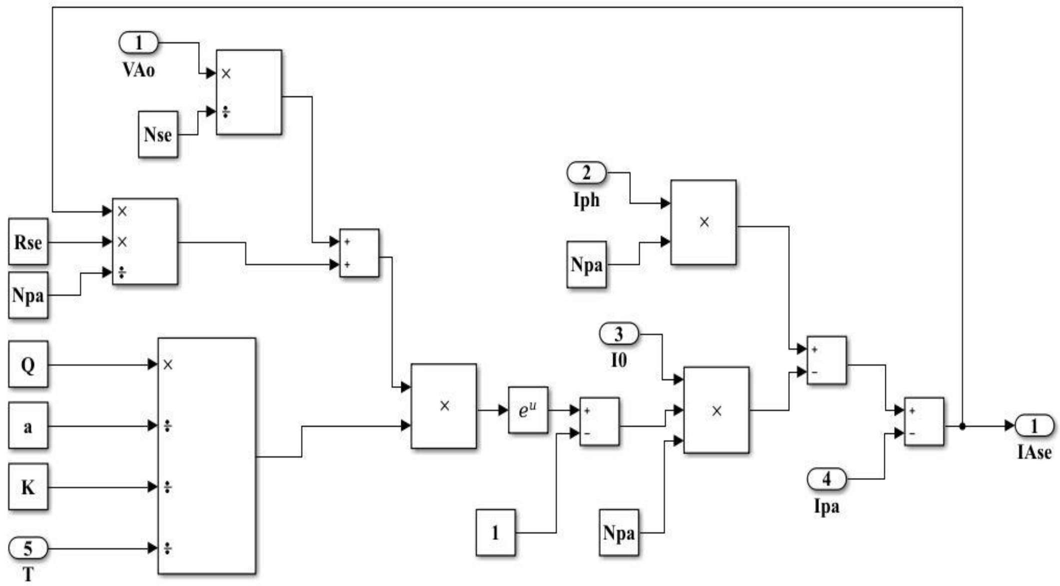

Figure 3-7 Mathematical model of PV array output current (I_{Ase}) drawn according to equation (3.19)(Choudhary et al., 2019)

3.1.3. Electronics Converters

An electronic converter is a device that changes electrical energy from one form to another, such as converting AC to DC (rectifier), DC to AC (inverter), or altering voltage levels (like a transformer or DC-DC converter). Among electronics converters, a DC-to-DC converter is an electrical device that converts direct current (DC) from one voltage level to another. It can increase (boost converter), decrease (buck converter), or invert (buck-boost converter) the voltage while maintaining the same current direction, enabling efficient power management in various applications. DC-DC converters have several types. Some of these are:

i. Boost converter
ii. Buck boost converter
iii. Buck converter

3.1.4. DC to DC boost converter (Step up converter)

This is electronic equipment, which is considered whenever different level of DC electrical power efficiently from one voltage level to another is required. As its name indicates, it is fed voltage to get high amount of voltage output, which is greater than the input voltage. In addition, it is applicable to solar panel to increase the output voltage of its module.

3.1.5. DC to DC buck converter

Others converter like buck converter reduce voltage and increase current.

3.1.6. DC to DC buck boost converter

Buck boost converters are increasing both current and voltage. The main reason why we use converter is that transformers are unable to function on DC, due to DC's constant flux. In this study boost converter is employed due to its simplicity (Ghosh & Kandpal, n.d.).

3.1.7. Different Operation mode of Boost Converter

Continuous Conduction Mode: A DC-to-DC converter is said to be operating in CCM, if inductor current never reaches to zero and remains for certain time period.

Discontinues Conduction Mode: DC-to-DC is operating in DCM, if inductor current reaches zero and remains zero for certain time period (Ghosh & Kandpal, n.d.).

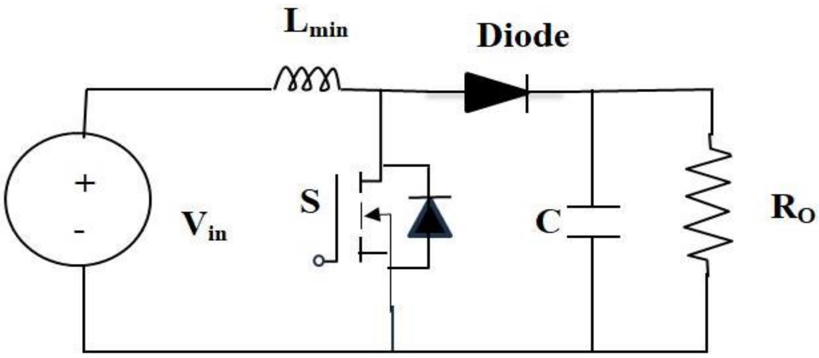

Figure 3-8 DC to DC Boost converter circuit diagram (Minda, 2019)

The voltage across the inductor and the current flowing through the capacitor in Figure 3-8 are defined as follows:

$$V_L = L_{\min} \times \frac{dI_L}{dt} \tag{3.27}$$

$$I_c = C \times \frac{dV_c}{dt} \tag{3.28}$$

Where: I_c, V_c, C ,current flow in capacitor, Voltage across capacitor ($V_c = V_o$) and capacitor respectively.

Boost conversion initiates with the commencement of the switching process, leading to the formation of two circuit configurations illustrated in figure. The inductor V_L (voltage across inductor), corresponding to the ON and OFF switching conditions, is depicted in Equations (3.27) and (3.29) respectively, as shown in

Figure 3-9.

$$V_L = V_{in} \times PMW \tag{3.29}$$

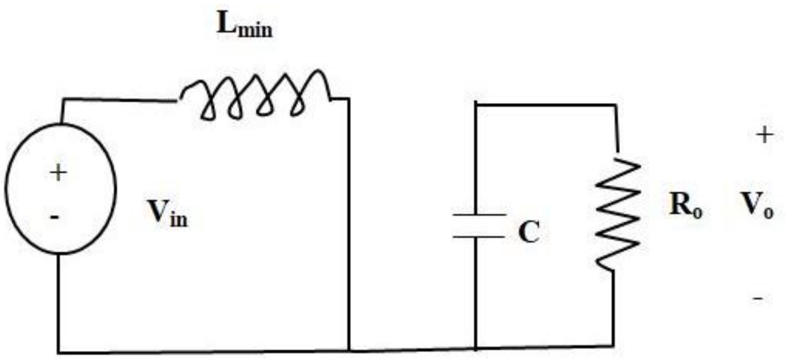

Figure 3-9 DC-to- DC Boost converter in ON state condition (Roberts, 2020).

The inductor L_{min} stores energy during the T_{ON} period. In order to raise the load output voltage above the source voltage, this energy storage in inductor is necessary. In a step-up chopper, a high value of inductor is therefore necessary.

When MOSFET is in ‘ON’ state:

Apply KVL and KCL to the Figure a circuit

$$V_{in} - L_{\min}\frac{dI_L}{dt} = 0, \frac{dI_L}{dt} = \frac{V_{in}}{L_{\min}} \tag{3.30}$$

$$\frac{V_c}{R_o} + C\frac{dV_c}{dt} = 0, \frac{dV_c}{dt} = -\frac{V_c}{R_o C} \tag{3.31}$$

$$V_{in} - L_{\min}\frac{dI_L}{dt} - V_c = 0, \frac{dI_L}{dt} = \frac{V_{in}}{L_{\min}} + \frac{V_c}{L_{\min}} \tag{3.32}$$

State space equation: $$\begin{bmatrix} \frac{dI_L}{dt} \\ \frac{dV_c}{dt} \end{bmatrix} = \begin{bmatrix} 0 & 0 \\ 0 & -\frac{1}{R_o C} \end{bmatrix} \begin{bmatrix} I_L \\ V_c \end{bmatrix} + \begin{bmatrix} \frac{1}{L_{\min}} \\ 0 \end{bmatrix} V_{in}, V_o = \begin{bmatrix} 0 & 1 \end{bmatrix} \begin{bmatrix} I_L \\ V_c \end{bmatrix} \tag{3.33}$$

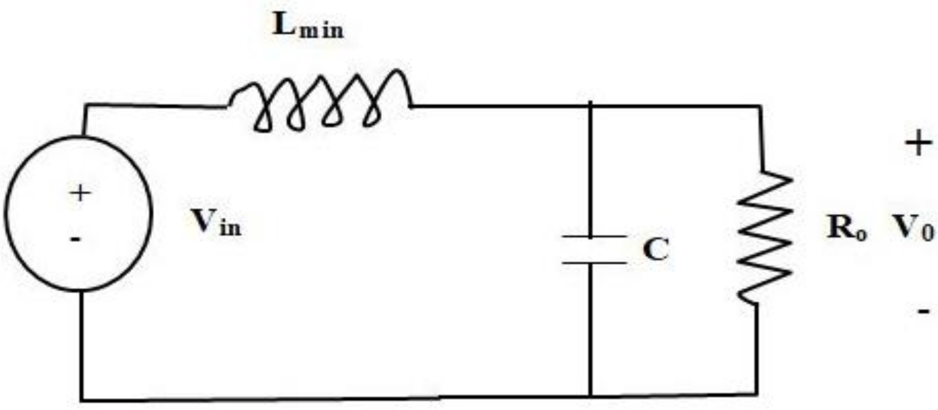

Figure 3-10 DC to DC Boost converter in OFF state (Roberts, 2020)

Apply both KVL and KCL to the

Figure 3-10

$$V_{in} - L_{min}\frac{dI_L}{dt} - V_c = 0, \frac{dI_L}{dt} = \frac{V_{in}}{L_{min}} + \frac{V_c}{L_{min}} \quad (3.34)$$

$$I_L - C\frac{dV_c}{dt} - \frac{V_c}{R_o} = 0, \frac{dV_c}{dt} = \frac{I_L}{C} - \frac{V_c}{R_o \times C} \quad (3.35)$$

Applying Laplace transform to Equations (3.34) and (3.35) gives:

$$V_{in}(s) - L_{min}(s) * sI_L(s) - V_o(s) = 0, sI_L(s) = \frac{V_{in}(s)}{L_{min}(s)} + \frac{V_0(s)}{L_{min}(s)} \quad (3.36)$$

Overall Transfer function of DC-to-DC boost is:

$$G(s) = \left(\frac{V_o}{1-D}\right) * \frac{R_o(1-D)^2 - L_{min}s}{R_o L_{min} C s^2 + L_{min}s + R_o(1-D)^2} \quad (3.37)$$

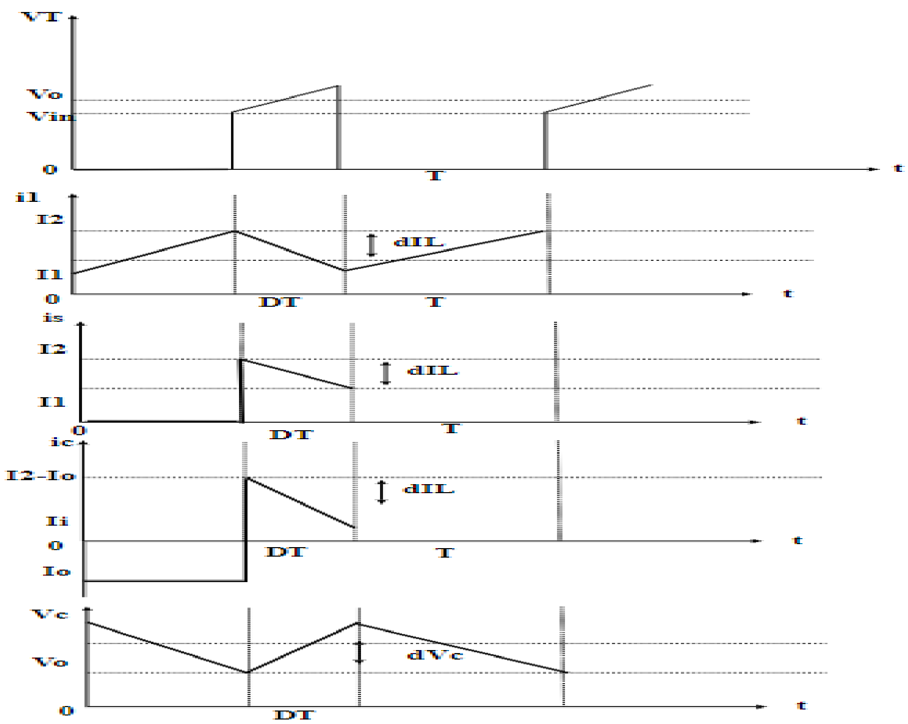

Figure 3-11 Step-up converter current and voltage wave forms **(**Naz, 2021**)**

3.1.8. Boost converter Derivation

Suppose a linear rise in inductor current from I1 to I2 we obtain

$$V_{in} = L_{min}\left(\frac{I_2 - I_1}{T_{on}}\right) = L\frac{\Delta I}{T_{on}} \quad (3.38)$$

$$T_{on} = L\frac{\Delta I}{\Delta V_{in}} \tag{3.39}$$

By assuming a linear fall in the inductor current at t=T_{off} from I2 to I1, we have

$$V_{in} - V_o = -L_{\min}\frac{\Delta I}{T_{off}} \tag{3.40}$$

$$T_{off} = L_{\min}\frac{\Delta I}{V_o - V_{in}} \tag{3.41}$$

From Equations (3.38) and (3.41), the Peak to peak ripple current of inductor is derived as,

$$\Delta I = V_{in}\frac{T_{on}}{L_{\min}} = \left(V_o - V_{in}\right)\frac{T_{off}}{L_{\min}} \tag{3.42}$$

Substituting T_{on}=DT and T_{off}=T (1-D), we have,

Average output voltage,

$$V_o = V_{in}\frac{T}{T_{off}} = \frac{V_{in}T}{(1-D)T} \tag{3.43}$$

i. **Duty cycle**

$$\frac{V_o}{V_{in}} = \frac{1}{1-D} = \frac{800V \times 0.9}{430V}, D = 48\% \tag{3.44}$$

ii. **Inductor Design**

$Input\ Power = Output\ Power\ (Pin = Po)$

$$\left.\begin{aligned} P_{in} &= V_{in}I_i \\ P_o &= V_oI_o \end{aligned}\right\} \tag{3.45}$$

From Equation(3.45):

$$I_o = \frac{P_o}{V_o} \tag{3.46}$$

$$= \frac{300\,kW}{800V} = 375\,A$$

Ripple current equation

$$\Delta I_L = \frac{V_{in} \times D}{f_{sw} \times L_{\min}} \tag{3.47}$$

According to IEC harmonics standards, ripple current is 20% to 40% of load current. After substitute values $\Delta I_L = 0.2 \times 375\,A = 75\,A$

From Equation(3.47), we have:

$$L_{\min} = \frac{V_{in} \times D}{\Delta I_L \times f_{sw}} = \frac{430 \times 0.48}{75 \times 20000} = 1.38 \times 10^{-4} H$$

iii. Minimum Capacitor Requirement

Select 1% of V_o , $\Delta V_o = V_o * 0.01 = 8V$

$$C\min = \frac{Vo \times D}{f \times \Delta Vo \times R_o} \tag{3.48}$$

$$= \frac{800V \times 0.48}{2.13\Omega \times 20000Hz \times 8V} = 1.1 \times 10^{-3} F$$

iv. Resistor selection (Load)

$$R_o = \frac{V_o}{I_o} \tag{3.49}$$

$$R_o = \frac{V_o}{I_o} = \frac{800V}{375A} = 2.13\Omega$$

Equation (3.43) to (3.49) area derived depending up on Faraz Naz's paper.(Naz, 2021)
For area two, procedures are the same starting from Equations (3.43) to (3.49) except numerical difference.

Table 3-3 Area b DC-to-DC converter specification(Naz, 2021)

Components	**Size**	**Unit**
Inductor ($L_{\min}$)	1.493×10^{-5}	Henry
Capacitor ($C_{\min}$)	6.25×10^{-4}	Farad
Load resistor (R_o)	3.2	Ω
Duty cycle (D)	50	%
ΔI_L	60	Ampere
V_o	800	Volt
V_{in}	400	Volt
Switching Frequency (f_{sw})	2.4×10^{4}	Hertz

3.1.9. MPPT Algorithm:

Multiple Maximum Power Point Tracking (MPPT) methods are available for maximizing the output powers. This serves as adjustment to match the source and load's impedance. MPPT is typically used in conjunction with a DC-DC converter. Among the MPPT current techniques are:(Zhang et al., 2018)

i. P&O method
ii. Incremental conductance method
iii. Voltage based peak power tracking method

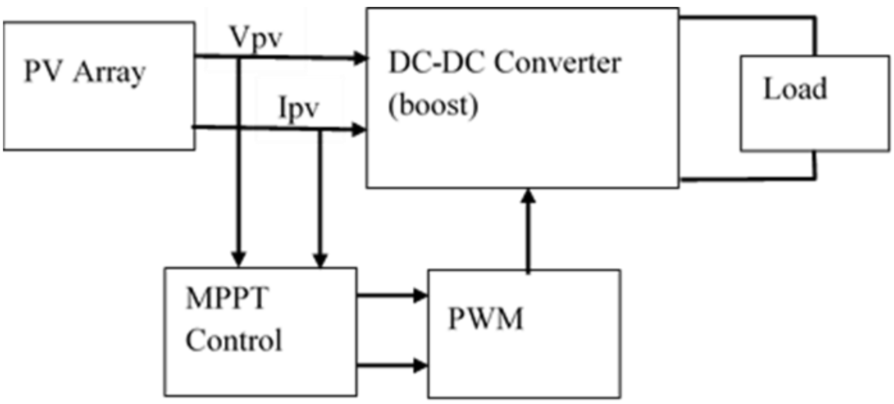

Figure 3-12 MPPT controller and DC-DC boost converter for PV array (Minda, 2019)

From all others MPPT algorithms, P&O, and incremental conductance are the most often utilized due to their ease of use, shorter tracking times for the maximum power point, and other financial considerations. In our study, incremental conductance is employed.

3.1.10. Incremental Conductance:

The incremental conductance algorithm, as shown below based on the fact that the slope of the PV array power curve become zero at maximum power point, positive on the left side and negative on the right of MPP, as given by:

$$P = VI \tag{3.50}$$

Where $V = V_{Ao}, I = I_{Ase}$

$$\frac{dP}{dV} = 0 \quad \text{, at MPP} \tag{3.51}$$

$$\frac{dP}{dV} > 0 \quad \text{, at the Left of MPP} \tag{3.52}$$

$$\frac{dP}{dV} < 0 \quad \text{, at the Right of MPP} \tag{3.53}$$

To get the MPP point, differentiation of Equation (3.50) with respect to V should be zero

$$\frac{dP}{dV} = I + V\frac{dI}{dV} \cong I + V\frac{\Delta I}{\Delta V} \tag{3.54}$$

$$\frac{\Delta I}{\Delta V} = -\frac{I}{V} \tag{3.55}$$

From Equation (3.55) $\frac{\Delta I}{\Delta V} = -\frac{I}{V}$ is called dynamic conductance or Incremental conductance and $-\frac{I}{V}$ is known as static conductance.

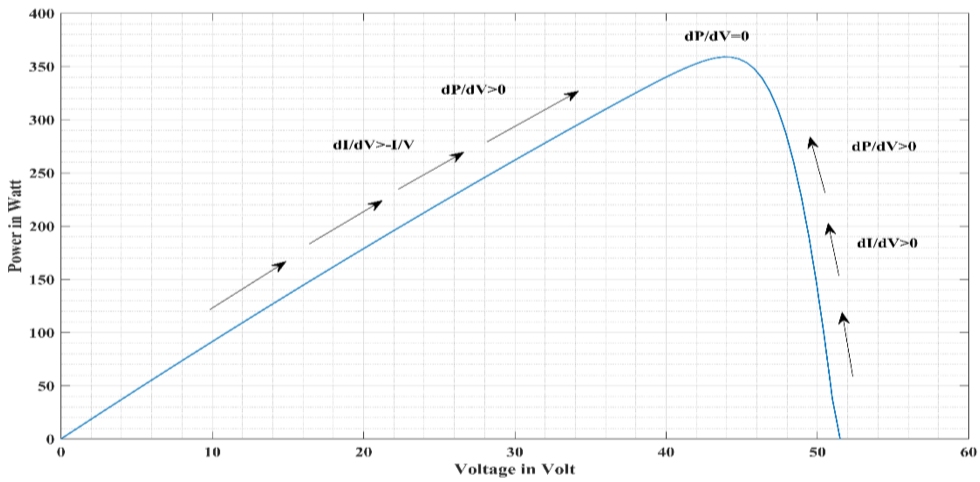

Figure 3-13 P-V curve of single solar panel

From the above p-v curve (
Figure 3-13), it can be shown that if $dV = 0$ but $dI > 0$, the solar irradiance has increased and voltage at the maximum power point rises. Therefore, the operating PV modules' voltage has to be increased in order to track maximum power point.

If $\frac{dP}{dV} < 0$, the MPP point is at the left side of $\frac{dP}{dV} < 0$ because the P-V curve's slope is negative. Reduce voltage to obtain MPP. The MPP point lies right side of $\frac{dP}{dV}$ if $\frac{dP}{dV} > 0$, and the slope is positive. Increase voltage to follow the maximum power point tracking. If the $\frac{dP}{dV} = 0$, then maximum power point tracking is satisfied.

3.1.11. Perturb and Observe (P & O) algorithm

- **Perturb:** The algorithm starts by slightly changing (perturbing) the operating
- voltage or current of the solar panel system. This perturbation could be an increase or decrease in the voltage or current.
- **Observe:** After the perturbation, the algorithm observes the resulting power output of the solar panel. If the power output increases due to the perturbation, the algorithm continues to perturb the system in the same direction. If the power output decreases, the algorithm reverses the direction of the perturbation.
- **Iteration:** This process of perturbing and observing continues iteratively until the maximum power point (MPP) is reached, where the solar panel generates the maximum possible power.

Main Difference between Incremental Conductance and Perturb and Observe is that:

- **P&O** relies on perturbing the system and observing the outcome, leading to potential oscillations around the MPP.
- **INC** uses a more precise calculation method to identify the MPP, resulting in more stable and accurate performance, especially in dynamic conditions.

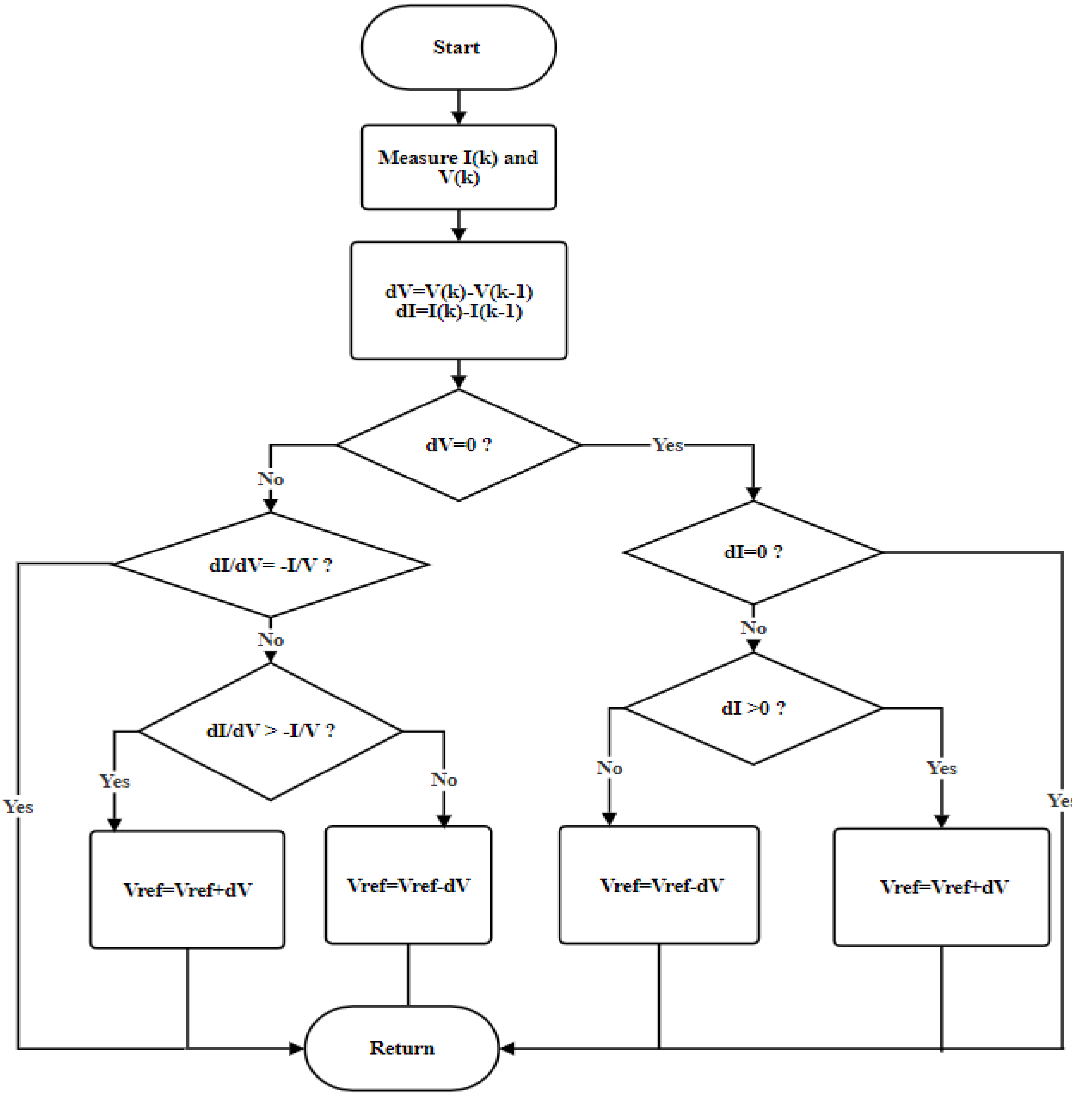

Figure 3-14 Flow chart INC algorithm of MPPT (Dandoussou & Kenfack, 2023)

3.1.12. Incremental Conductance Flow chart discussion

Step1: Measure the current (I) and voltage (V): Examine the solar panel's current and voltage readings in real time.

Step2: Determine whether $dV = 0$ or not. If so check for $dI = 0$:If both dV and dI are zero, which means maximum power tracking is satisfied, then return. If $dV = 0$, and $dI \neq 0$, check $\frac{dI}{dV} < -\frac{I}{V}$, if so increase reference voltage V_{ref} by dV and if $\frac{dI}{dV} > -\frac{I}{V}$, increase duty cycle or the derivative of current (I) with respect to voltage (V), to find the incremental conductance. As ($\frac{dP}{dV} = \frac{P_{new} - P_{old}}{V_{ref} - V_{old}}$), it is computed.

Step3: Compute $\frac{dI}{dV}$: Additionally, compute the derivative of voltage in relation to current.

Step4: Compare Zero and Incremental Conductance: Compare zero to $\frac{dP}{dV}$; verify that $\frac{dP}{dV}$ equals zero. The system is probably getting close to the Maximum Power Point (MPP) if it is close to zero.

Step5: Modify the operating point: Not Zero Incremental Conductance: Should $\frac{dI}{dV}$ be negative and $\frac{dP}{dV}$ be positive: Lower the voltage by moving the I-V curve to the left. In case, $\frac{dP}{dV}$ is minus.

3.1.13. DC-link design and selection

A DC link is an electrical connection that facilitates the transfer of direct current (DC) between various components in a power system, such as converters, inverters, or energy storage systems. It acts as a bridge, enabling efficient energy flow and control, particularly in renewable energy applications, electric vehicles, and grid integration. By stabilizing voltage levels and minimizing losses, the DC link plays a crucial role in enhancing the performance and reliability of power electronics systems.

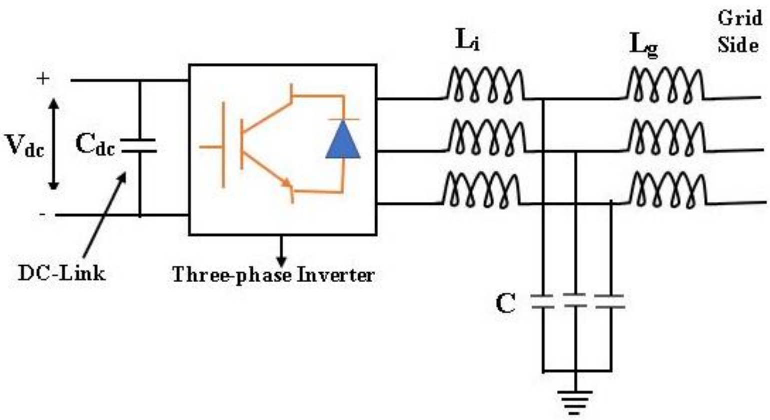

Figure 3-15 DC-link with inverter diagram (Minda, 2019)

$$C_{dc} = \frac{I_{dc}}{2\omega \tilde{V}_{dc}} = \frac{P_{dc}}{2\omega V_{dc} \tilde{V}_{dc}} \quad (3.56)$$

$$\text{Where, } I_{dc} = \frac{P_{dc}}{V_{dc}}$$

Where P_{dc} is the average DC-link power, ω is the grid frequency), $\langle V_{dc} \rangle$ is the average DC-link voltage and $\tilde{V}_{dc}$ is the amplitude of the ripple voltage (5% of the dc link voltage). The flow of current cannot be controlled if the dc link voltage is less than the peak grid-voltage plus the drop in between grid and inverter (i.e. filter loss and semiconductor loss in inverter). (Fay, 2017)

3.1.14. Controller of voltage

The voltage controller is employed to control the VSI DC-link voltage. The inner control loop receives the equivalent d-axis amount from the dc voltage controller in order to generate the reference signal. The typical PI controller, current control block (which may be thought of as a response delay of current), dc coefficient (k_{dc}) (to balance the power between dc quantity and d-q coordinate), and dc link capacitor make up the general dc voltage control loop in Figure 3-16 sample block, which can only be used in the forward loop or feedback loop, is additionally considered for digital control analysis.

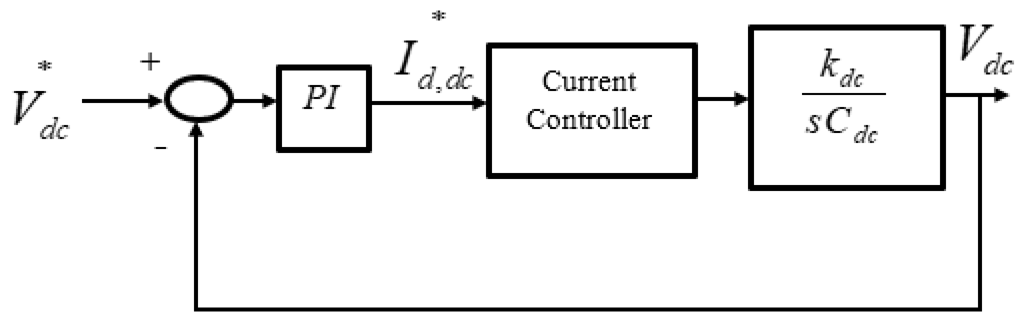

Figure 3-16 DC-link controller (Mokhtar et al., 2022)

The relationship between the direct components of the current fed to the VSI and the DC current was used to derive the DC coefficient. We express the direct component and DC component relationship between the input and output power at equation (3.57)

$$V_{dc} \times I_{dc} = \frac{3}{2} V_d \times I_d \qquad (3.57)$$

So, the dc coefficient (k_{dc}) can be computed as

$$k_{dc} = \frac{I_{dc}}{I_d} = \frac{3V_d}{2V_{dc}} \qquad (3.58)$$

The relationship of dc link voltage (V_{dc}) and line-to-line grid voltage (VLL) in Equations (3.57) and (3.58) gives an expression

$$\frac{V_d}{V_{dc}} = \frac{m}{2}, k_{dc} = \frac{3}{4} m \qquad (3.59)$$

Where: **m** is the modulation index between zero and one for sinusoidal PWM switching.

The parameters used in DC-link is calculated according to Equations (3.57) to (3.59)

Table 3-4 Parameters used at DC-link stage(Fay, 2017)

Components	Magnitude & Units
m	0.1
k_{dc}	0.075
I_{dc}	250 A
C_{dc}	20 mF
V_{dc}	800 V
V_d	5%*800 V=40 V
Frequency of grid	50 Hz

3.1.15. Adaptive PID design:

An adaptive controller automatically adjusts its parameters to maintain optimal performance in the presence of varying conditions or uncertainties in the system. The adaptive controller consists of two subcomponents: the adaptation mechanism, which modifies the adaptive PID controller based on the error, and the adaptive PID controller, which has an input error derived from the variation in the plant's output at the set point. There are many different types of Optimal Adaptive Controller (OAC). Adaptive PID is one of those adaptive controllers.

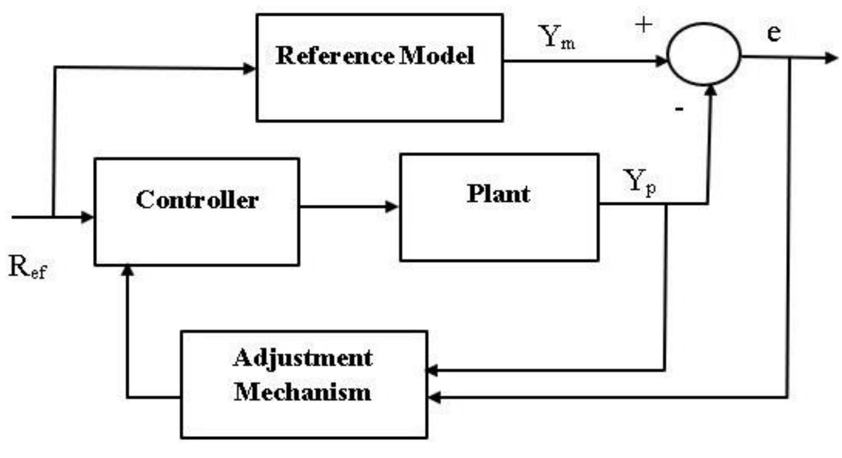

Figure 3-17 Model Reference Adaptive Control(Azad & Shateri, 2019)

3.1.15.1. Adaptive PID to the DC-to -DC boost converter

Error Tracking: The formulas eV = $V_{out} - V_{ref}$ and eI = Ipv − Iref determine the tracking voltage error (eV) and tracking current error (eI), respectively. Figure 3-17 displays the adjustment procedure, which produces an estimate of the controller parameters. By observing the structure of the controller and the principle of the MRAC algorithm, we will have as a condition the relations

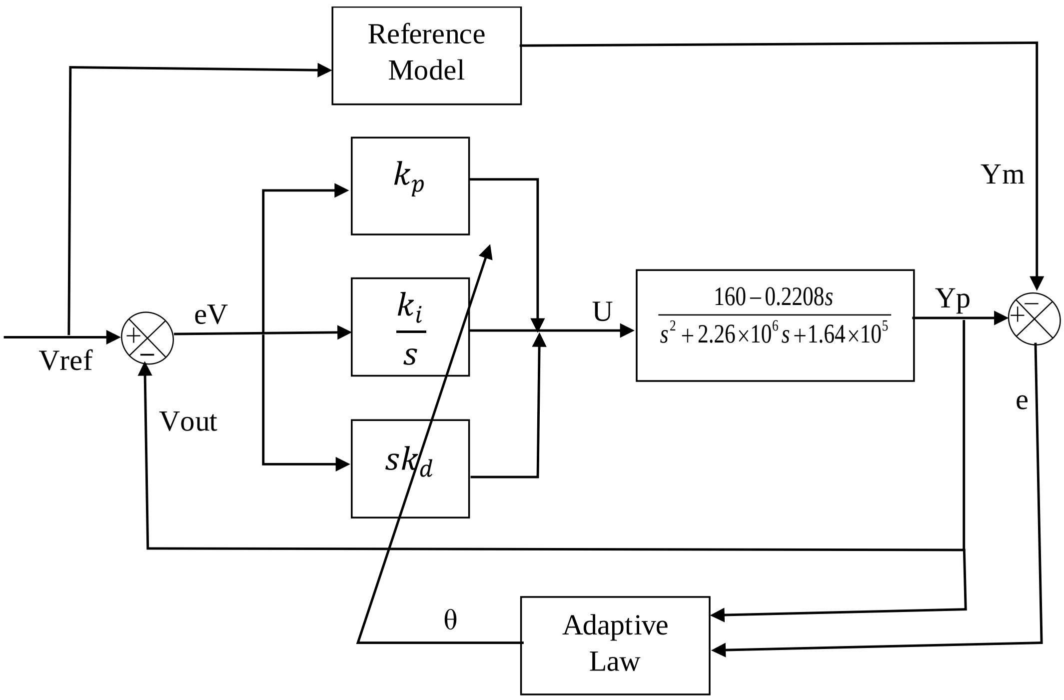

Figure 3-18 Adaptive Law for Controller

MIT Rule

The MIT rule was initially created in 1960 by scientists at Massachusetts Institute of Technology (MIT) and was applied to the development of aircraft autopilot systems. Any system can be used to build a controller utilizing the MRAC scheme by using the MIT rule. The following is how this rule defines a cost function(Negi et al., 2023):

$$J(\theta) = \frac{e^2}{2} \tag{3.60}$$

where θ is the variable parameter of PID controller and 'e' is the difference between the outputs of the plant and the outputs of the model. A change in the parameter may result in a reduction of the cost function to zero. Consequently, the θ parameter change is sustained in the direction of J's negative gradient, that is to say:

$$\frac{d\theta}{dt} = -\gamma \frac{\partial J}{\partial \theta} \tag{3.61}$$

$$\frac{d\theta}{dt} = -\gamma e \frac{\partial e}{\partial \theta} \tag{3.62}$$

The system's sensitivity derivative is denoted by the partial derivative phrase ∂e, ∂θ. The way the error varies with the parameter θ is explained in this sentence. Equation (3.61) illustrates how the parameter can be varied over time to reduce the cost function J(θ) to zero. The adaptation gain of the controller is represented by the positive integer γ in this case. Let us assume that the process is linear and that the transfer function is KG(s), where G(s) is a known first-order transfer function and K is an unknown parameter(Negi et al., 2023). Our goal is to develop a controller that will enable our process to use the transfer function Gm(s) = Ko*G(s), where Ko is a known parameter, to monitor the reference model. Derivation from Figure 3-17 is:

$$e(t) = Y_p(t) - Y_m(t) \tag{3.63}$$

$$e(s) = KG(s)u(s) - K_o G(s) u_c(s) \tag{3.64}$$

$G(s) = \dfrac{160 - 0.2208s}{s^2 + 2.26\times10^6 s + 1.64\times10^5}$ & $G_m(s) = \dfrac{1}{Ts+1}$ are plant and model reference respectively.

Define PID control law, = K_p, K_i, K_d,

$$u(t) = K_p e(t) + K_i \int e(t)dt + K_d \frac{de(t)}{dt} \tag{3.65}$$

$$\begin{aligned}\frac{dk_p}{dt} &= -\gamma_p e \frac{d}{dk_p}\left(k_p e(t) + k_i \int e(t)dt + k_d \frac{de(t)}{dt} \right) \\ &= -\gamma_p e^2\end{aligned} \tag{3.66}$$

$$\begin{aligned}\frac{dk_i}{dt} &= -\gamma_i e \frac{d}{dk_i}\left(k_p e(t) + k_i \int e(t)dt + k_d \frac{de(t)}{dt} \right) \\ &= -\gamma_i e \int e(t)dt\end{aligned} \tag{3.67}$$

$$\begin{aligned}\frac{dk_d}{dt} &= -\gamma_d e \frac{d}{dk_d}\left(k_p e(t) + k_i \int e(t)dt + k_d \frac{de(t)}{dt} \right) \\ &= -\gamma_d e \frac{de(t)}{dt}\end{aligned} \tag{3.68}$$

Where: $\gamma_p, \gamma_{i,}, \gamma_d$ are kp, ki and kd adaptation gain respectively and $k_p, k_i, k_d, e(t), y(t), Rref$ are proportional gain, integral gain, derivative gain, error, plant output and input of reference model respectively.

Laplace domain of Equation (3.65) is given by:

$$U(s) = \left(K_p + \frac{K_i}{s} + sK_d \right) E(s) \tag{3.69}$$

3.1.16. Grid inverter modeling and explanation

Inverter is an electronic converter that converts DC supply into AC supply through switching mechanism. Consider all possible switching states of a three-phase, two-level voltage source inverter. Switching states of inverter are given by:

3.1.17. Types of Inverters

A Voltage source Inverter (**VSI**): It is a device that transforms a DC voltage into a three-phase AC output at the input. Owing to its simple management and dependable performance, this kind of inverter is frequently utilized in grid-connected systems and industrial motor drives. This inverter is used in this paper.

Current Source Inverter (CSI): A CSI generates a three-phase AC output by operating with a DC current source at its input. When accurate current regulation is crucial, as in high-power industrial drives, CSIs are preferred.

Multilevel Inverter (MLI): An MLI combines many DC voltage levels to generate a three-phase AC output. Large-scale industrial motors and renewable energy systems are two high-power applications that benefit greatly from this design's minimal harmonic distortion.

3.1.18. Size Inverters for Loads

Inverters are chosen from 20-30 % greater than the total power of the loads. The maximum load of Area1 is 90 kW and Area 2 load is 110 kW.

Calculate the Combined Maximum Load:

Combined Maximum Load**:** 90 kW+110 kW=200 determine the Sizing Strategy: There are couples of strategies you can employ. These are: each inverter is capable of handling the entire combined load (200 kW). This ensures that if one inverter fails, the other can take over completely. Secondly each inverter is sized to handle its own area’s load but with some margin to share the load during peak times or minor failures. Take 20% and efficiency above 90 % then, $0.20 \times 200\ kW + 200\,kW = 240\,kW$ .In particular case inverters sizes were 100 kW-250 kW. Each inverter has been selected to handle approximately $250\,kW$ in this work.

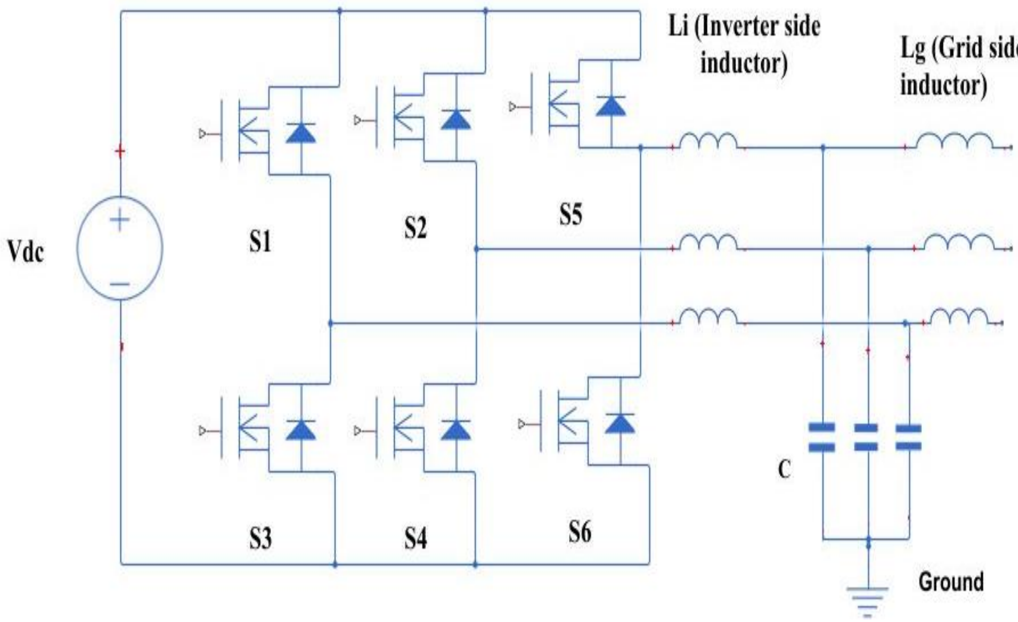

Figure 3-19 Three phase Voltage source Inverter (VSI)(Naz, 2021)

The voltage (V_{dc}) is the DC-link output, which is given to three phase inverters, and then inverter side connected to the LCL filter to avoid harmonics and distortion of voltage and current. There are internal R_g and R_i in inverter and grid side wire.

Table 3-5 DC-to-DC converter specification

Switches			Three Phase Voltages		
S1	S2	S3	V^{ab}	V^{bc}	V^{ca}
0	0	0	0	0	0
0	0	1	0	-$V_{\_dc}$	+$V_{\_dc}$
0	1	0	0	-$V_{\_dc}$	+$V_{\_dc}$
0	1	1	-$V_{\_dc}$	0	+$V_{\_dc}$
1	0	0	+$V_{\_dc}$	0	-$V_{\_dc}$
1	0	1	+$V_{\_dc}$	-$V_{\_dc}$	0
1	1	0	0	$V_{\_dc}$	-$V_{\_dc}$
1	1	1	0	0	0

By considering inverter's possible switching states of three phase, which are eight combinations ($2^3 = 8$) in the Table 3-5 switching conditions are defined as follows: The voltages V^{ab}, V^{ca} and V^{ca} represent the line-to-line voltages in a three-phase inverter. These voltages can be calculated based on the switching states of the inverter, where each phase (A, B, C) can either be connected to the positive or negative rail of the DC bus.

Switching states

- Phase-by-phase transfer to the negative rail in 000 switching combination in.
- For 001 combination: Two phases to the negative rail, C-phase to the positive rail.
- For 010 combination: Phase-A and phase-C to the negative rail, B-phase to the positive rail.
- For 011 combination: A to negative, B and C to the positive rail.
- For 100 combination: Some go to the negative rail, A-phase to the positive rail.
- For 101 combination: B to negative, A and C to the positive rail.
- For 110 combination: C to negative, A and B to the positive rail.
- For 111 combination: Every step to the rail that is positive.

3.1.19. The theory of synchronous reference frame (SRFT)

The theory of synchronous reference frame (SRFT) in the indirect current control mode, synchronous reference frame theory (SRFT) control is used. For the purpose of controlling VSI, references for three phase ac grid currents are generated. SRF theory's basic method is to use transformation equations to convert the three phase control parameters that rotate the d-q frame synchronously. For the conversion of abc to dq0, the transformation equation is:

$$\begin{bmatrix} \alpha(t) \\ \beta(t) \end{bmatrix} = \begin{bmatrix} \cos(\omega t) & \cos(\omega t - \frac{2\pi}{3}) & \cos(\omega t + \frac{2\pi}{3}) \\ \cos(\omega t) & \sin(\omega t - \frac{2\pi}{3}) & \sin(\omega t + \frac{2\pi}{3}) \end{bmatrix} \begin{bmatrix} x_a \\ x_b \\ x_c \end{bmatrix} \tag{3.70}$$

$$\begin{bmatrix} x_d \\ x_q \end{bmatrix} = \begin{bmatrix} \cos(\omega t) & \sin(\omega t) \\ -\sin(\omega t) & \cos(\omega t) \end{bmatrix} \begin{bmatrix} \alpha(t) \\ \beta(t) \end{bmatrix} \tag{3.71}$$

$$\begin{bmatrix} x_a \\ x_b \\ x_c \end{bmatrix} = \begin{bmatrix} \cos\theta & \sin\theta & 1 \\ \cos\left(\theta - \frac{2\pi}{3}\right) & \sin\left(\theta - \frac{2\pi}{3}\right) & 1 \\ \cos\left(\theta + \frac{2\pi}{3}\right) & \sin\left(\theta + \frac{2\pi}{3}\right) & 1 \end{bmatrix} \begin{bmatrix} x_d \\ x_q \\ x_0 \end{bmatrix} \tag{3.72}$$

Where **x** could be either voltage or current, and are produced by a three-phase PLL.

An average (dc) component plus an oscillating (harmonic) component can make up the d-q component of voltage and current. To achieve selective compensation, the load current is broken down using the SRF method. Intermediate quantity transformation, or αβ components, is required for selective compensation. As we discussed above, Equation (3.70) and Equation (3.71) are Clarke transformation, Park transformation, respectively.

$$\begin{bmatrix} i_\alpha \\ i_\beta \end{bmatrix} = \sqrt{\frac{2}{3}} \begin{bmatrix} 1 & -\frac{1}{2} & -\frac{1}{2} \\ 0 & \frac{\sqrt{3}}{2} & -\frac{\sqrt{3}}{2} \end{bmatrix} \begin{bmatrix} i_a \\ i_b \\ i_c \end{bmatrix} \tag{3.73}$$

$$\begin{bmatrix} i_d \\ i_q \end{bmatrix} = \sqrt{\frac{2}{3}} \begin{bmatrix} \cos\theta & \sin\theta \\ -\sin\theta & \cos\theta \end{bmatrix} \begin{bmatrix} i_\alpha \\ i_\beta \end{bmatrix} \tag{3.74}$$

The load current's d-q component, which is calculated, using the above equation, has positive components. By mathematically altering the angle's sign and rotating the frame in the opposite direction, the negative component of the load current is calculated. The Equation (3.68) to (3.73) is Park and Clarke transformation (Naz, 2021).

$$\begin{bmatrix} i_d^* \\ i_q^* \end{bmatrix} = \sqrt{\frac{2}{3}} \begin{bmatrix} \cos\theta & -\sin\theta \\ \sin\theta & \cos\theta \end{bmatrix} \begin{bmatrix} i_\alpha \\ i_\beta \end{bmatrix} \tag{3.75}$$

The low pass filter (LPF) is used to isolate the dc component of the d-q quantities of load current for both the positive and negative sequence components. The fundamental component of the positive sequence that is calculated using the d-q components and transformed into three phase reference quantities.

3.1.20. LCL filter Design

System second order transfer function is:

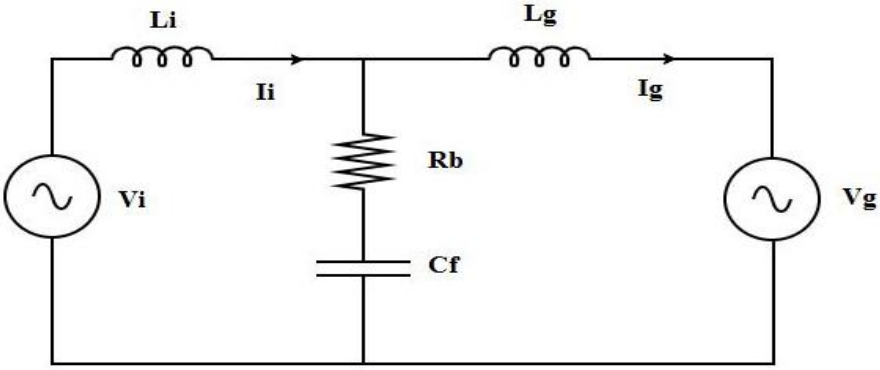

Figure 3-20 Simple LCL filter circuit diagram (Dandoussou & Kenfack, 2023)

Applying Kirchhoff voltage and current laws to

Figure 3-20 gives

$$V_i = L_i \frac{dI_i +}{dt} R_i I_i + R_b (I_i - I_g) + V_c \tag{3.76}$$

$$I_c = I_i - I_g = C_f \frac{dV_c}{dt} \tag{3.77}$$

$$R_b \left(I_i - I_g\right) + V_c = L_g \frac{dI_g}{dt} + R_g I_g + R_L I_g \tag{3.78}$$

After re-arranging Equations (3.76), (3.77) and (3.78), we get the following state space equation.

$$\begin{bmatrix} \dot{x}_1 \\ \dot{x}_2 \\ \dot{x}_3 \end{bmatrix} = \begin{bmatrix} \frac{-R_i + R_b}{L_i} & \frac{R_b}{L_i} & -\frac{1}{L_i} \\ \frac{R_i}{L_g} & -\frac{\left(R_i + R_g + R_L\right)}{L_g} & \frac{1}{L_g} \\ \frac{1}{C} & -\frac{1}{C} & 0 \end{bmatrix} \begin{bmatrix} I_i \\ I_g \\ V_c \end{bmatrix}_{abc} + \begin{bmatrix} \frac{1}{L_i} \\ 0 \\ 0 \end{bmatrix} \left[V_i\right] \tag{3.79}$$

Maximum allowable current for the filter is:

$$I_{\max} = \frac{P_N \sqrt{2}}{3V_{ph}} \tag{3.80}$$

The ripple current for LCL filter is given by:

$$\Delta I_{\max} = \left(1 - 5\%\right) I_{\max} \tag{3.81}$$

$$L_i = \frac{0.49 \times V_{dc}}{3\Delta I_{\max} f_{sw}} \tag{3.82}$$

Design grid side inductance and Damping resistor of

$$L_g = \frac{1 + \sqrt{\frac{1}{K_a^{\ 2}}}}{C\omega_{sw}^{\ 2}} \tag{3.83}$$

$$R_b = \frac{1}{3C\omega_{re}} \tag{3.84}$$

$$\omega_{re} = \frac{1}{2\pi}\sqrt{\frac{L_i + L_g}{L_g \times L_i \times C}} \tag{3.85}$$

$$C = \frac{1}{\left(2\pi\omega_{re}\right)^2} \times \frac{L_i \times L_g}{L_i + L_g} \tag{3.86}$$

$$R_b = K_a \times \sqrt{\frac{L_i + L_g}{C}} \tag{3.87}$$

Where K_a is typically between 0.1 to 1 $R_b, \omega_{re}, \omega_{sw}, K_a, f_{sw}, P_N, V_{ph}, L_g, R_g, L_i, R_i, I_g, I_i, R_b, R_L$ are damping resistor, resonant

frequency, Phase voltage, grid side resistor, grid side inductor, grid side current, inverter side inductor, inverter side resistor, inverter side current.

When designing an LCL filter, several key parameters are important to consider. First, you need to select the values of the input inductor (Li) and output inductor (Lg) to limit current ripple and reduce harmonic distortion. The capacitance value (C) is also crucial, as it helps filter out unwanted harmonics and sets the cutoff frequency of the filter. Additionally, it's important to determine the cutoff and resonant frequencies to ensure effective filtering without unwanted amplification. Damping factors should be included to avoid resonance peaks that can cause instability. Table 3-6 show the parameters quantities.

Table 3-6 Parameters used to design filter

Parameters	Value
Li	9 mH
Lg	2.7 mH
fsw	10 kHz
C	3.2 µF
Rb	8.6 Ω
ωre	12000 rad/s
Rg	0.000001Ω
ωsw	2*pi*10^4 rad/se

The vector equations are split into their real and imaginary components to yield the real valued state space description of the output LCL filter model. The complex d − q frame differential equations are then obtained by assuming that R_i and R_g are distinct from zero.

$$\frac{dI_{id}}{dt} = -\frac{R_i}{L_i} I_{id} + \omega I_{iq} + \frac{1}{L_i} V_{id} - \frac{1}{L_i} V_{cd} \tag{3.88}$$

$$\frac{dI_{iq}}{dt} = -\frac{R_i}{L_i} I_{iq} - \omega I_{id} + \frac{1}{L_i} V_{iq} - \frac{1}{L_i} V_{cq} \tag{3.89}$$

$$\frac{dV_{cd}}{dt} = \omega V_{cq} + \frac{1}{C_f} I_{id} - \frac{1}{C_f} I_{cd} \tag{3.90}$$

$$\frac{dV_{cq}}{dt} = -\omega V_{cq} + \frac{1}{C_f} I_{iq} - \frac{1}{C_f} I_{cq} \tag{3.91}$$

$$\frac{dI_{gd}}{dt} = \omega I_{gq} + \frac{1}{L_2} V_{gd} - \frac{1}{L_g} V_{cd} - \frac{R_g}{L_g} I_{gd} \tag{3.92}$$

$$\frac{dI_{gq}}{dt} = -\omega I_{gd} + \frac{1}{L_g} V_{gq} - \frac{1}{L_g} V_{cq} - \frac{R_g}{L_g} I_{gq} \tag{3.93}$$

The d − q frame's complex valued state description shows that the vectors' rotation orientation affects how the output LCL filter behaves. L_i, C_f , and L_g are the three reactive elements, resulting in a third order system. The grid voltage (V_{gdq}) and the inverter voltage (V_{idq}) is the inputs. The system's state and output variables are the capacitor voltage (V_{cdq}) and the currents flowing through L_i (I_{idq}) and L_i (I_{gdq}).

3.1.21. Gide-side current controller

The grid side current controller block diagram, which includes all feed forward and feedback terms, is displayed in

Figure 3-21. The current controller's input is divided into two terms: the inputs for reference (I^*_{gdq}) and feedback (I_{gdq}). Inverter with output current is attained using conventional P-I controllers. The matching state formulas are:

$$\Delta I_{gd} = I_{gd}{}^* - I_{gd} \tag{3.94}$$

$$\Delta I_{gd} = I_{gd}{}^* - I_{gd} \tag{3.95}$$

The d-q reference frame complex equation becomes of equation:

$$L_g \frac{d}{dt}\left(I_{gd}{}^*\right) + R_g I_{gd} - \omega L_g I_{gq} + V_{gd} - V_{cd} = L_g \frac{d}{dt}\left(\Delta I_{gd}\right) \tag{3.96}$$

$$L_g \frac{d}{dt}\left(I_{gq}^{\ *}\right) + R_g I_{gq} + \omega L_g I_{gd} + V_{gq} - V_{cq} = L_g \frac{d}{dt}\left(\Delta I_{gq}\right) \tag{3.97}$$

Where:

$$\begin{aligned} V_{cd}^{\ *} &= L_g \frac{d}{dt}\left(I_{gd}^{\ *}\right) + R_g I_{gd} - \omega L_g I_{gq} + V_{gd} \\ V_{cq}^{\ *} &= L_g \frac{d}{dt}\left(I_{gq}^{\ *}\right) + R_g I_{gq} - \omega L_g I_{gd} + V_{gq} \end{aligned} \tag{3.98}$$

An error is produced on the current injected into the network by the difference between the measured V_{cdq} and the reference voltage, V_{cdq}^{*}. Two terms make up the voltage V_{cdq}^{*}, according to Equation (3.98). The immediately measurable network voltage V_{cdq} is represented by the first term. In contrast, the second term indicates the corresponding impedance's voltage drop when there is a current I_{gdq} that crosses it. As per (Choudhary et al., 2019), existing controllers need to explain on words in Equation (3.98) as seen in Figure 3-21.

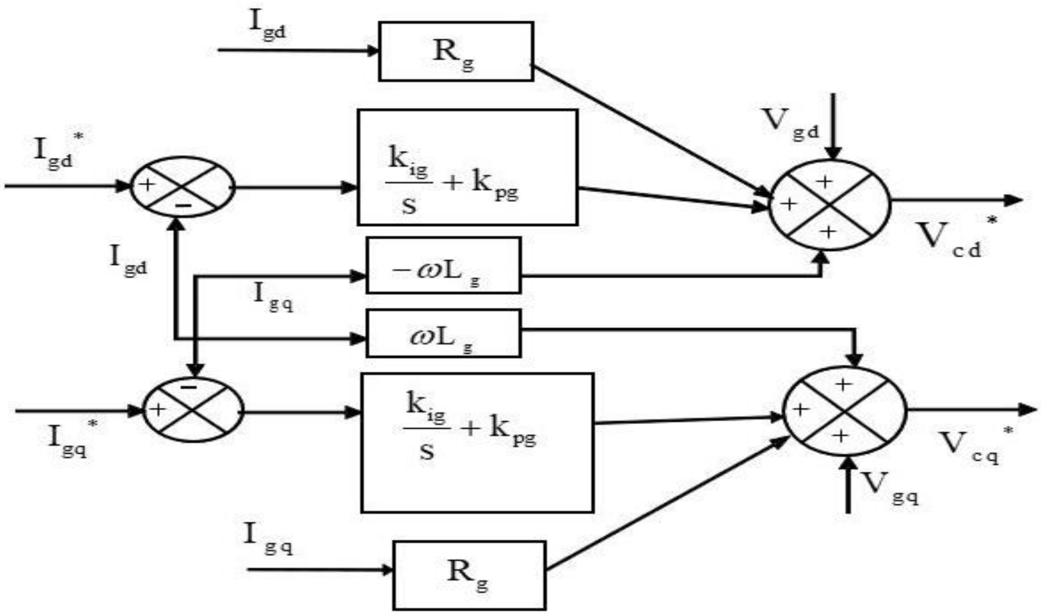

Figure 3-21 Grid-side current control with the PI controllers

3.1.22. Voltage Controlling

$$\Delta V_{cd}^{\ *} = V_{cd}^{\ *} - V_{cd} \tag{3.99}$$

$$\Delta V_{cq}^{\ *} = V_{cq}^{\ *} - V_{cq} \tag{3.100}$$

Figure 3-22 shows the voltage controller block diagram. It includes feedback and feed forward terms. The capacitor voltage control is made with a P-I controller. The corresponding state equations are:

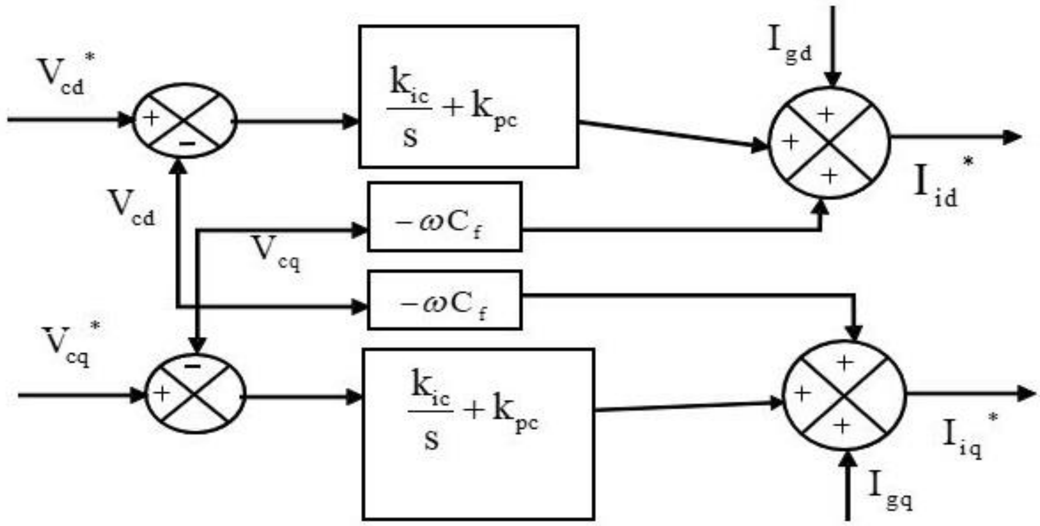

Figure 3-22 Voltage control with the PI controllers

The differential equations for the d − q frame become:

$$C_f \frac{dV_{cd}^*}{dt} - \omega C_f V_{cq} + I_{gd} - I_{id} = C_f \frac{d}{dt}\left(\Delta V_{cd}\right) \quad (3.101)$$

$$C_f \frac{dV_{cq}^*}{dt} + \omega C_f V_{cd} + I_{gq} - I_{iq} = C_f \frac{d}{dt}\left(\Delta V_{cq}\right) \quad (3.102)$$

$$I_{id}^* = C_f \frac{dV_{cd}^*}{dt} - \omega C_f V_{cq} + I_{gd} \quad (3.103)$$

$$I_{iq}^* = C_f \frac{dV_{cq}^*}{dt} + \omega C_f V_{cd} + I_{gq} \quad (3.104)$$

An inaccuracy on the capacitor voltage is caused by the difference between the measured I_{idq} and the reference current i.e. I_{idq}^*. As per Equations (3.103) and (3.104) the present I_{idq}^* consists of two terms. While the second term reflects the current that crossed the capacitor when it was fed by a voltage V_{cdq}, the first term represents the immediately observable network current I_{idq}. Voltage controllers in Figure 3-22 are required to elaborate terms in Equations (3.103) and (3.104).

3.1.23. Inverter-side current controlling mechanism

Figure 3-23 depicts the side inverter current controller. A P-I corrector is used to achieve an inductor current controller. The matching state equations are as follows:

$$\Delta I_{id} = I_{id}^{*} - I_{id} \tag{3.105}$$

$$\Delta I_{iq} = I_{iq}^{*} - I_{iq} \tag{3.106}$$

The differential equations for the d − q frame become:

$$L_i \frac{d}{dt}\left(I_{id}^{*}\right) + R_i I_{id} - \omega L_i I_{iq} + V_{cd} - V_{id} = L_i \frac{d}{dt}\left(\Delta I_{id}\right) \tag{3.107}$$

$$L_i \frac{d}{dt}\left(I_{iq}^{*}\right) + R_i I_{gd} + \omega L_i I_{id} + V_{cq} - V_{iq} = L_i \frac{d}{dt}\left(\Delta I_{iq}\right) \tag{3.108}$$

Where:

$$V_{id}^{*} = L_i \frac{d}{dt}\left(I_{id}^{*}\right) + R_i I_{id} - \omega L_i I_{iq} + V_{cd} \tag{3.109}$$

$$V_{iq}^{*} = L_i \frac{d}{dt}\left(I_{iq}^{*}\right) + R_i I_{iq} + \omega L_i I_{id} + V_{cq} \tag{3.110}$$

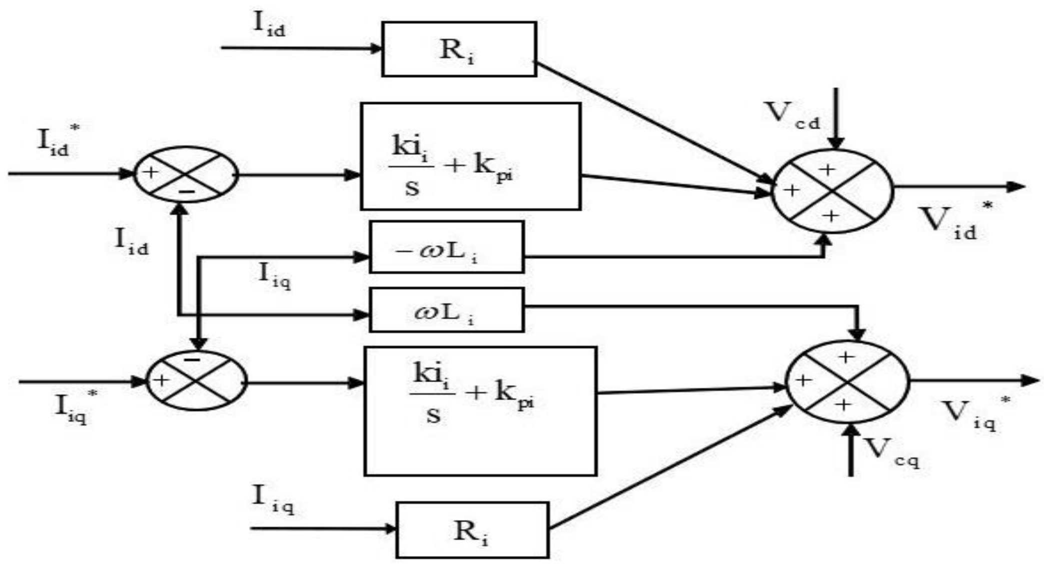

Figure 3-23 Inverter-side current controller

The mistake on the current delivered by the inverter is caused by the difference between the measured V_{idq} and the reference voltage V_{idq}^{*}.Equations (3.109) and (3.110) state that the voltage V_{idq} is made up of two words. The first term is the directly observable capacitor voltage (V_{cdq}), and the second is the voltage drop across the filter impedance caused by a current (I_{idq}). Current controllers need to elaborate terms of Equations (3.109) and (3.110) in accordance with Figure 3-23.

$$I_{dref} = I_{do} + \left(V_{do\_ref} - V_{do}\right)\left(\frac{K_{pv} + K_{iv}}{s}\right) - V_{qo}C_f\omega \tag{3.111}$$

$$I_{qref} = I_{qo} + \left(V_{qo\_ref} - V_{qo}\right)\left(\frac{K_{pv} + K_{iv}}{s}\right) + V_{do}C_f\omega \tag{3.112}$$

$$V_d = V_{do} + I_{di}R_f + \left(I_{dref} - I_{di}\right)\left(\frac{K_{pv} + K_{iv}}{s}\right) - I_{qi}L_f\omega \tag{3.113}$$

$$V_q = V_{qo} + I_{qi}R_f + \left(I_{qref} - I_{qi}\right)\left(\frac{K_{pa}s + K_{ia}}{s}\right) - I_{di}L_f\omega \tag{3.114}$$

$$V_{PWM} = \begin{bmatrix} V_{aref} \\ V_{bref} \\ V_{cref} \end{bmatrix} = \begin{bmatrix} \sin(\omega t) & \cos(\omega t) & 1 \\ \sin(\omega t - 120^o) & \cos(\omega t - 120^{o)} & 1 \\ \sin(\omega t + 120^o) & \cos(\omega t + 120^o & 1 \end{bmatrix}\begin{bmatrix} V_d \\ V_q \\ V_0 \end{bmatrix} \tag{3.115}$$

Where, V_{PWM} = reference input voltage to PWM generator

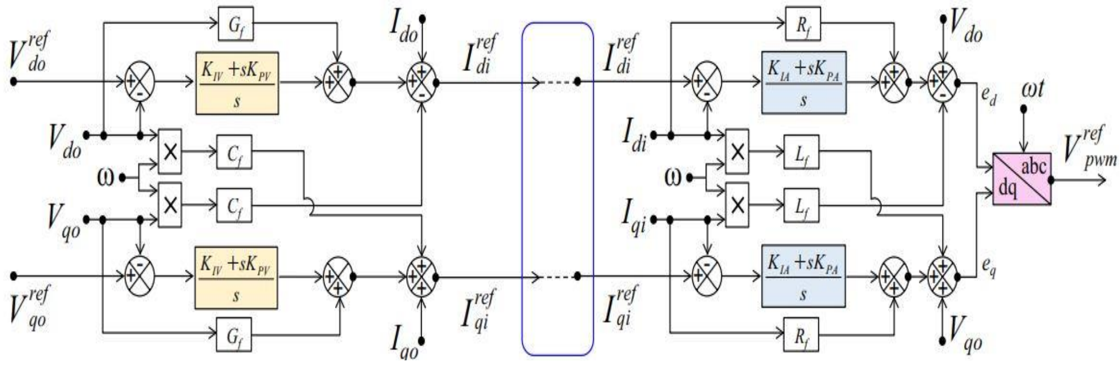

(a) voltage control module (b) current control module

Figure 3-24 Voltage and current controller model (Y. V. P. Kumar & Bhimasingu, 2021)

I_{qref}, I_{dref}, V_{do_ref} and V_{qo_ref} is reference input current to current and voltage controller

I_{qo}, I_{do}, V_{qo} and V_{do} is dq equivalent of I_{o_abc}, V_{o_abc}

I_{di}, I_{qi} is d-q component of I_{i_abc} V_d, V_q is d-q component of V_{PWM}

$$I_{il} = I_{g0}(s) + I_c(s) \text{ and } I_c(s) = I_{il}(s) - I_{g0}(s) \tag{3.116}$$

$$V_{g0}(s)=\frac{V_{\sin}(s)-(R_f+sL_f)I_{g0}(s)}{1+sC_f(sL_f+R_f)} \tag{3.117}$$

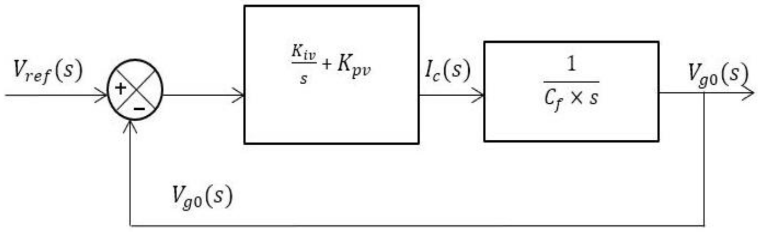

Figure 3-25 Simple equivalent model(Y. V. P. Kumar & Bhimasingu, 2021)

Where, V_{sin}, V_{g0}, V_{il} is single-phase equivalent $V_{sin\_abc}, V_{g0-abc}, V_{il\_abc}$.

I_{il}, I_{g0}, I_c is single phase equivalent of $I_{il\_abc}, I_{g0\_abc}, I_{c\_abc}$.

Internal current and voltage controller transfer function

By simulating the inner current control loop and disregarding the voltage control outer loop, the current controller draws the system current (Y. V. P. Kumar & Bhimasingu, 2021). On the other hand, the voltage controller ignores the inner control loop and models the control loop to control the voltage.

$$\frac{I_{il}(s)}{I_{il\_ref}(s)}=\frac{K_{i_a}s+K_{p_a}}{s^2L_f+s(K_{p_a}+R_f)+K_{i_a}} \tag{3.118}$$

To determine the integral and proportional gain values for the current controller. The closed-loop current control system's characteristic equation, which has a second-order dynamic characteristic equation, is;

$$s^2+2\varsigma\times\omega_n s+\omega_n^2=0 \tag{3.119}$$

$$s^2L_f+s(R_f+K_{pa})+K_{ia}=0 \tag{3.120}$$

To achieve both transient stability and a satisfactory dynamic response, the closed-loop system's desired damping ratio (ζ) was determined to be 0.707.

Proportional gain K_{pa} calculated as:

$$K_{p_a}=2\varsigma\times\omega_n-R_f=1\times0.707\times11.7\times10^2-1.2=8.32\times10^2$$

The integral gain K_{ia} calculated as:

$$K_{i_a}=\omega_n^2\times L_f=(11.7\times10^2)^2\times2.7\times10^{-3}=3.696\times10^3$$

$$\frac{V_{g0}(s)}{V_{ref\_0}(s)} = \frac{sK_{pv} + K_{iv}}{s^2 C_f + K_{pv}s + K_{iv}} \tag{3.121}$$

The values of the proportional gain K_{pv} and the integral gain K_{iv} for the voltage controller.

$$K_{pv} = 2\varsigma\omega_n - R_f = 1\times 0.707\times 11.7\times 10^2 - 1.2 = 8.32\times 10^2$$

The integral gain K_{iv} calculated as:

$$K_{iv} = \omega_n^2 \times L_f = (11.7\times 10^2)^2 \times 2.7\times 10^{-3} = 3.696\times 10^3$$

$$\frac{V_{og}(s)}{V_{oref}(s)} = \frac{sK_{pv} + K_{iv}}{s^2 C_f + K_{pv}s + K_{iv}} \tag{3.122}$$

The values of the proportional gain K_{pv} and the integral gain K_{iv} for the voltage controller.

3.1.24. Two-Areas Connected Through Tie-Line Modelling

$$P_{pv} = Area \times \eta \times G \tag{3.123}$$

Where: G is irradiance, $\eta = 16.22\%$ $Area = 1652\,mm \times 1306\,mm = 2.15\,m^2$ calculated from Table 3-2 for single solar panel. However, there is $40\times 10 = 400$ in second $Area\ B$, then $Area\ B = 400\times 2.15\,m^2 \approx 800\,m^2$ and for $Area\ \mathrm{A} = 86\times 10\times 2.15\,m^2 \approx 1800\,m^2$

$$P_{pv\_j} = Area_j \times \eta \times G_j \tag{3.124}$$

Assuming P_{pv_j} represents the power generated by PV in Area $_j$ (where j=A, B).

Power Balance for Each Area $_j$:

$$P_{pv\_j} = P_{L\_j} + P_{Tie} + P_{grid} \tag{3.125}$$

- P_{Tie} : Power exchange via the tie line is positive if exporting and negative if importing.
- P_{grid} : Power exchanged with the grid is positive if exporting and negative if importing.

Tie Line Power Flow:

Take tie line is purely inductive with reactance of X_{tie}.

$$P_{Tie} = \frac{V_A \times V_B}{X_{Tie}} \sin(\delta_1 - \delta_2) \tag{3.126}$$

V_A, V_B Voltage magnitudes in Area A and Area B and δ_1, δ_2 area phase angles in Area A and Area B(Negi et al., 2023).

Power Flow Based on Excess and Deficit.

- If Area A has excess power (P_{exc}) and Area B has a deficit (P_{def}):

$$P_{Tie} = \min(P_{exc\_A}, P_{def\_B}) \tag{3.127}$$

Similarly, if Area B has excess power and Area A deficit, then

$$P_{Tie} = -\min(P_{exc\_B}, P_{def\_A}) \tag{3.128}$$

Power Export to The Grid:

When both areas have excess power, the total excess sent to the grid (P_{grid}) is:

$$P_{grid} = P_{exc\_A} + P_{exc\_B} - |P_{Tie}| \tag{3.129}$$

3.2.Two-Area Solar Power System Model (with Droop Control)

For a solar power plant connected to the grid, the **inverter control** takes over the functions traditionally handled by the generator. We use **Droop Control** for frequency and voltage regulation, but the dynamics change because there's no mechanical inertia.

3.2.1. Frequency Regulation Using Droop Control:

Droop control adjusts the frequency based on the active power imbalance(Negi et al., 2023):

$$f_j = f_0 - m_j(P_{pv\_j} - P_{L\_j}) \tag{3.130}$$

f_j : Frequency of Area_j

f_0: Nominal frequency (50 Hz)

m_j : Droop coefficient for Area_j

Frequency Balancing between Areas

$f_A \approx f_B$ should close to 0 to ensure frequency stability.

$$\Delta f = -\frac{1}{R_j}\Delta P_j \tag{3.131}$$

Where: $m_j = \frac{1}{Rj}$, ΔP_j is change in active power delivered by the inverter.

For each area, the frequency deviation dynamics can be simplified to the following for an inverter-based system:

$$\frac{d\Delta f_j}{dt} = -\frac{1}{R_j}\Delta P_j - T_{ji}\left(\Delta f_j - \Delta f_i\right) \tag{3.132}$$

Equation (3.132) includes the droop control term and the tie-line power sharing term(Mokhtar et al., 2022).

3.2.2.Voltage Control (Using Reactive Power with Droop)

For voltage control in inverter-based solar systems, reactive power (Q) is controlled to regulate voltage via reactive power-voltage droop:

$$\Delta V_j = -\frac{1}{x_j}\Delta Q_j \tag{3.133}$$

Where: x_j, ΔQ_j, droop coefficient for reactive power-voltage control in Area j and change in reactive power delivered by the inverter respectively.

The inverter-based voltage dynamics equation in each area is:

$$\frac{dV_j}{dt} = -\frac{1}{x_j}\Delta Q_j \tag{3.134}$$

No mechanical dynamics or automatic voltage regulators (AVR) are involved, as the inverters directly control the reactive power to regulate the voltage.

3.2.3. Reference Model for Frequency (Inverter-Based System)

In this case, we still use a second-order system to represent the desired frequency behavior, but now it models the inverter response (Sheril & Ramesh Babu, 2017):

$$M_f(s) = \frac{\omega_n^{\ 2}}{s^2 + 2\xi\omega_n + \omega_n^{\ 2}} \tag{3.135}$$

ω_n, ζ are the desired natural frequency of the system and the desired damping ratio respectively. The output of the reference model is Δf_{ref}, which represents the desired frequency deviation in each area.

3.2.4. Reference Model for Voltage (Inverter-Based System)

$$M_v(s) = \frac{K_{ref}}{T_{ref}s + 1} \tag{3.136}$$

Where: K_{ref} *and* T_{ref} are the desired voltage regulation parameters respectively.

The reference model provides the desired voltage deviation ΔV_{ref} .

3.2.5. MRAC PID Controller Design (With Droop Control)

The MRAC-PID controller will dynamically adjust the active power and reactive power delivered by the inverters in response to frequency and voltage deviations, respectively.

3.2.5.1. PID Control for Frequency (With Droop)

For each area, the MRAC PID control for frequency will adjust the **active power** delivered by the solar inverters:

$$u_f = k_{pf}e_f + k_{if}\int e_f dt + k_d \frac{de_f}{dt} \tag{3.137}$$

Where: $e_f = \Delta f_{ref} - \Delta f$ is the frequency error (difference between reference and actual frequency) and u_f represents the control signal that adjusts the **active power** output of the inverter to match the reference frequency(Negi et al., 2023).

3.2.5.2. PID Control for Voltage (With Droop)

For voltage control, the MRAC PID controller adjusts the **reactive power** output of the inverters to regulate the voltage(Mokhtar et al., 2022):

$$u_v = k_{pv}e_v + k_{iv}\int e_v dt + k_{dv} \frac{de_v}{dt} \tag{3.138}$$

Where: $e_v = \Delta V_{ref} - \Delta V$ is the voltage error (difference between reference and actual voltage) and u_v is the control signal that adjusts the reactive power output of the inverter to match the desired voltage.

3.2.6. Adaptive Law for Gain Tuning

The adaptive laws for MRAC PID dynamically adjust the gains $k_p, k_i, and\, k_d$ in response to the error signals. A typical adaptive law could be based on gradient descent (Minda, 2019):

$$\frac{dk_{pf}}{dt} = -\gamma_p \frac{de^2{}_f}{dk_{pf}} \tag{3.139}$$

$$\frac{dk_{if}}{dt} = -\gamma_i e_f \int e_f \, dt \tag{3.140}$$

$$\frac{dk_{df}}{dt} = -\gamma_d e_f \frac{de_f}{dt} \tag{3.141}$$

Where γ is a learning rate. The same adaptive law applies for voltage control.

Control Logic for Power Distribution:

$$\begin{aligned} P_{exc\_A} &= P_{pv\_A} - P_{L\_A} \\ P_{exc\_B} &= P_{pv\_B} - P_{L\_B} \end{aligned} \tag{3.142}$$

$$\begin{aligned} P_{def\_A} &= P_{L\_A} - P_{pv\_A} \quad (if \; P_{pv\_A} < P_{L\_A}) \\ P_{def\_B} &= P_{L\_B} - P_{pv\_B} \quad (if \; P_{pv\_B} < P_{L\_B}) \end{aligned} \tag{3.143}$$

If both areas have deficit, $P_{Tie} = 0$ and P_{grid} may supply the deficit if connected.

3.2.7. Transformer Introduction and Modelling

3.2.7.1. Introduction Transformer

A transformer is an electrical device that uses electromagnetic induction to transmit electrical energy between two or more circuits. It operates on the basis of Faraday's law of electromagnetic induction, in which a fluctuating current in one transformer coil causes a fluctuating magnetic field, which in turn causes a second coil to induce a fluctuating voltage. A transformer that raises the voltage from the primary side (input) to the secondary side

(output) is called a step-up transformer. This indicates that the secondary coil has a higher number of wires turns than the primary coil. The transformer's task is to synchronize and step up the voltage to the grid in this study.

3.2.7.2. Model of Transformer

Base Impedance Calculation: connect 400 V_{rms} to the primary winding of transformer,

$$Z_{base\_primary,400V} = \frac{(400V)^2}{2300kVA} = 0.069\Omega$$

$$Z_{base\_secondary,33kV} = \frac{(33kV)^2}{2300kVA} = 0.47391k\Omega$$

$$Z_{base\_secondary,230kV} = \frac{(230\,kV)^2}{2300\,kVA} = 23\,k\Omega$$

$$I_{primary,400\,V} = \frac{P_{rated}}{\sqrt{3}\times V_{rms}} = \frac{230\,kVA}{\sqrt{3}\times 400V} = 332.6\,A$$

$$I_{secondary,33kV} = \frac{P_{rated}}{\sqrt{3}\times V_{rms}} = \frac{2300\,kVA}{\sqrt{3}\times 33\,kV} = 10.4\,A$$

$$I_{secondary,230kV} = \frac{P_{rated}}{\sqrt{3}\times V_{rms}} = \frac{2300\,kVA}{\sqrt{3}\times 230\,kV} = 5.77\,A$$

Linkage inductance (L) and winding resistance (R)

$$L_{primary,400\,V} = \frac{0.5\times Z_{base\_primary,400kV}}{2\pi\times 50\,Hz} = 0.000111\,H$$

$$L_{secondary,33kV} = \frac{0.5\times Z_{base\_secondary,33kV}}{2\pi\times 50\,Hz} = 0.00074\,H$$

$$L_{secondary,230kV} = \frac{0.5\times Z_{base\_secondary,230kV}}{2\pi\times 50\,Hz} = 0.036674\,H$$

$$R_{secondary,230kV} = 0.01\times Z_{base\_secondary,230kV} = 0.23\,k\Omega$$

$$R_{primary,400\,V} = 0.01\times Z_{base\_primary,400V} = 0.00069\,k\Omega$$

$$R_{secondary,33\,kV} = 0.01\times Z_{base\_secondary,33kV} = 0.0047\,k\Omega$$

Magnetizing Inductance (L_m) and Core Loss Resistance (R_m):

$$R_{m\_400V} = 500\times Z_{base\_primary,400\,V} = 34.5\,\Omega$$

$$R_{m\_33kV} = 236.95\,k\Omega$$

$$R_{m\_230kV} = 11.5\,M\Omega$$

$$L_{m\_400V} = 100\times L_{primary,400\,V} = 0.0111\,H$$

$$L_{m\_33kV} = 237.7\,\Omega$$

$$L_{m\_230kV} = 230\,H$$

Note: For Area B, the procedure is the same except the input voltage to the primary winding of the first transformer.

Table 3-7 Area B electrical components specification(Negi et al., 2023)

Electrical Components	Magnitude	Units
P_{rated} in both Transformer	2300	kVA
$L_{m\_600\ V}$,	0.0248	H
$L_{m\_33\ kV}$	74.8	H
$L_{m\_230\ kV}$	3.18	kH
$I_{\_600\ V}$	20	A
$I_{\_33\ kV}$	8.4	A
$I_{\_230\ kV}$	4.5	A
$L_{\_600\ V}$	0.000248	H
$L_{\_33\ kV}$	0.748	H
$L_{\_230\ kV}$	31.8	H
$Z_{base\_600\ V}$	0.156	Ω
$Z_{base\_33\ kV}$	0.47	kΩ
$Z_{base\_230\ kV}$	20	kΩ
$R_{m\_600\ V}$	78	Ω
$R_{m\_33\ kV}$	235	kΩ
$R_{m\_230\ kV}$	10	MΩ

3.2.8. Phase Locked Loop Grid synchronization

Phase locked loops, or PLLs, are typically used to synchronize grid frequency with signal phase locking. Phase detector, loop filter, and voltage-controlled oscillator (VCO) make up the generalized fundamental structure of PLL, as illustrated in Figure 3-26. the precise phase and frequency detection needed to generate reference signals that are appropriate for compensating for various quantities. By transforming three phase quantities into two phase rotating frames (abc-to-dq) and setting the reference quantity ($\dot{V}d$) to zero, the synchronous reference frame (SRF) is utilized to create PLL. PI (Proportional-Integrator) controllers are typically used to control system variables by acting as filters. The fundamental grid frequency, which is further processed through a VCO and realized by an integrator, is the output of the PI controller. An angle is the integrator's output and this angle fed into transformation block as shown in Figure 3-26.

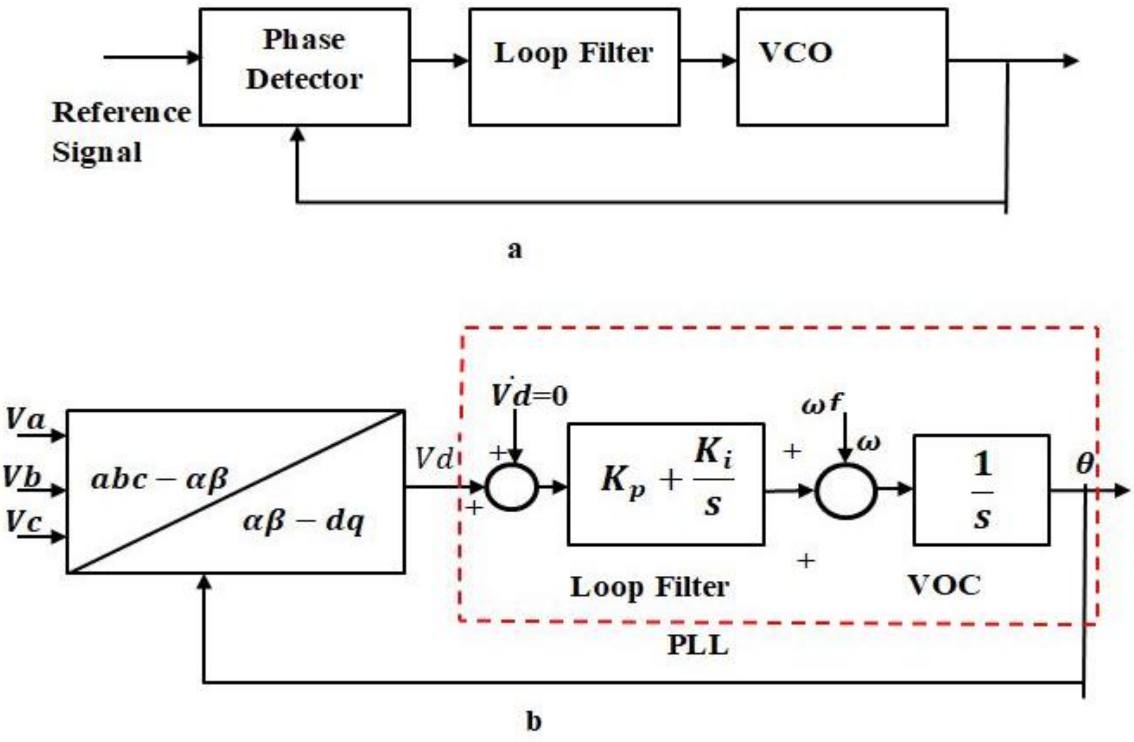

Figure 3-26 Phase Locked Loop (Omar et al., 2018)

a) PLL block diagram,

b) PLL algorithm development in a power system

$$M_{pLL}(s) = \frac{sK_p + K_i}{s^2 + sK_p + K_i} = \frac{sK_p + \dfrac{K_p}{T_i}}{s^2 + sK_p + \dfrac{K_p}{T_i}} \qquad (3.144)$$

In practical design, M_{PLL} (s) is approximated to second order transfer function in standard form as the following:

$$M(s) = \frac{(2\zeta\omega_n)s + \omega_n^{\,2}}{s^2 + (2\xi\omega_n)s + \omega_n^{\,2}} \qquad (3.145)$$

$$\omega_n = \sqrt{\frac{K_p}{T_i}} ; \xi = \frac{K_p}{2\omega_n} \qquad (3.146)$$

The standard scenario with an overshoot of less than 5% for a step reaction led to the selection of 0.707 as the damping factor (ζ) and frequency 100 Hz. Filtering and tracking performance K_p and T_i, as well as settling time (T_{set}), can all be adjusted.

$$K_p = \frac{2\omega_n\zeta}{V_d} = \frac{0.707\times2\times2\times3.14\times100}{400} = 2.2$$

$$K_i = \frac{\omega_n^{\;2}}{V_d} = \frac{(2\times3.14\times100)^2}{400} = 985$$

Table 3-8 Controller and Grid side parameters used in simulation.

Parameter name	Value	Units
Grid Voltage (VLL) in V_{rms}	400 and 800	Volt
Frequency of the system (in Hz)	50	Hearz
Current controller gain (Kp, Ki)	10,4000	-
Voltage controller gain (Kp, Ki)	10,180	-
Lgrid	0.0001e-9	H
Rgrid	0.0001e-6	Ω
Ri	0.001e-4	Ω
Li	9e-3	H
Cf	9.86e-6	F

3.2.9. Circuit breakers

A circuit breaker is an electrical device designed to protect an electrical circuit from damage caused by overcurrent, short circuits, or other electrical faults. It automatically interrupts the flow of electricity when it detects that the current exceeds a certain threshold, thereby preventing damage to the system, fires, or even electric shock hazards. Since,

$$\begin{aligned} P_{active} &= \sqrt{3}V_{LL}I_{LL}\times\cos(\phi) \\ I_{LL} &\Rightarrow \frac{P_{active}}{\sqrt{3}V_{LL}\times\cos(\phi)} = \frac{230\,kVA}{600V\times1.73} = 221.6\,A \end{aligned} \tag{3.147}$$

Approximate ϕ to 90 $^0{}_C$

- 600 V Inverter Output: Breaker rated for 600 V and >221.6 A.
- 600 V Side of Transformer: Breaker rated similarly as above.
- 230 kV Side of Transformer: High-voltage breaker rated for 230 kV.
- Grid Connection: Another high-voltage breaker at the grid connection point coordinated with grid protection systems.

3.2.10. Electrical Grid

The electrical grid is a complex and interconnected network designed to deliver electricity from power plants to homes, businesses, and other users. Here is a breakdown of how it works:

Coordination of the generation, transmission, distribution, and consumption of electrical energy throughout a network is necessary for an electrical grid to function. An electrical grid is a large, networked system that guarantees the dependable transmission of electricity from power plants to final consumers, such as residences, commercial buildings, and industrial facilities. The functioning of an electrical grid is broken down as follows:

CHAPTER FOUR

4. SIMULATION AND RESULTS DISCUSSION

4.1. Solar Panel I-V and P-V curves

A solar panel's **I-V curve** (Current-Voltage curve) is a graphical representation that shows how the current (I) delivered by the solar panel varies with the voltage (V) across its terminals. This relationship is fundamental to understanding the electrical behavior of the solar panel under different operating conditions, such as varying sunlight (irradiance) and temperature. Understanding the I-V curve is essential for optimizing solar panel performance and maximizing energy output under varying conditions.

The **P-V curve** (Power-Voltage curve) for a solar panel is a graphical representation that shows how the power output (P) of the panel varies with the voltage (V) across it.

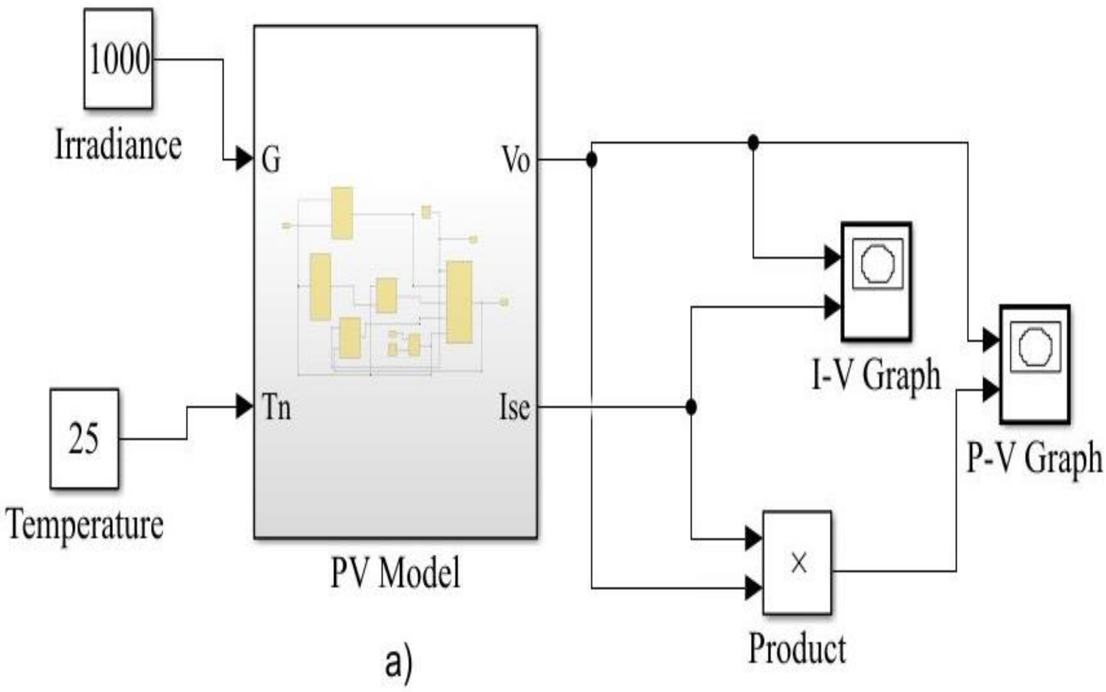

Figure 4-1 Photovoltaic Model

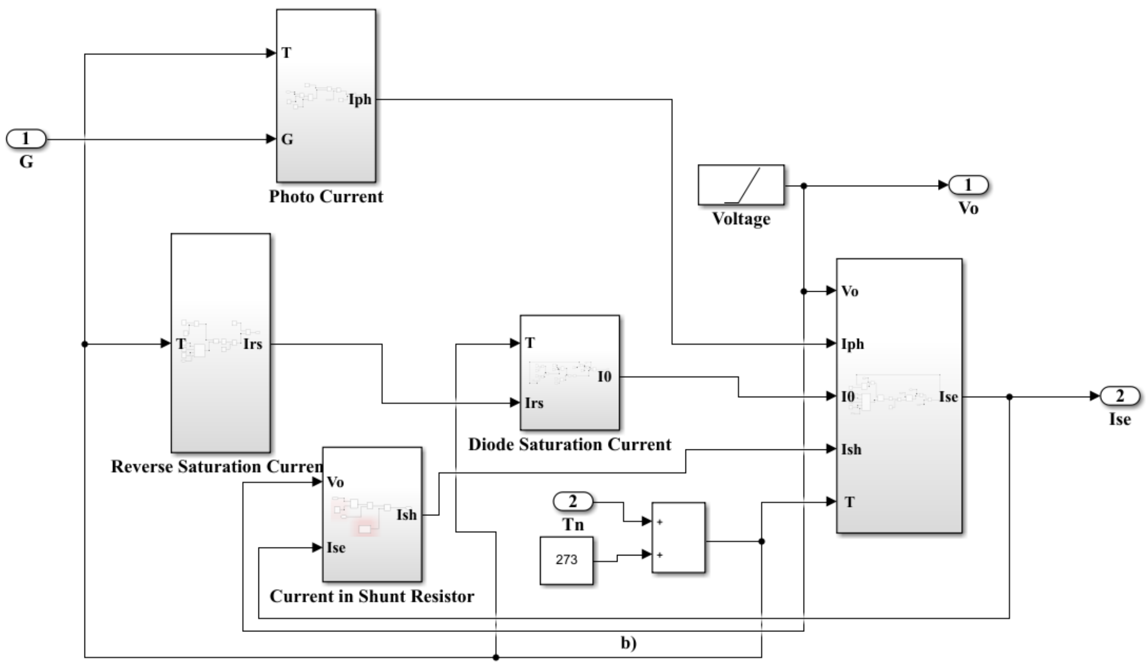

Figure 4-2 (a) Simulink of PV panel. (b) Internal part of PV Array

Figure 4-1 (a) is the modeled PV panel to generate the P-V and I-V curve. Figure 4-2 (b) shows the internal part of model.

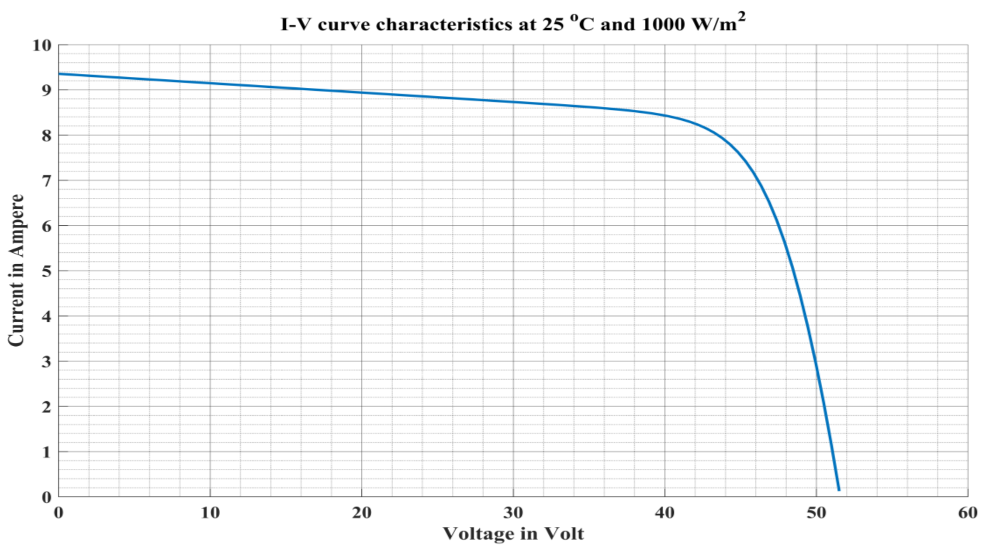

Figure 4-3 Single solar panel current-voltage curve

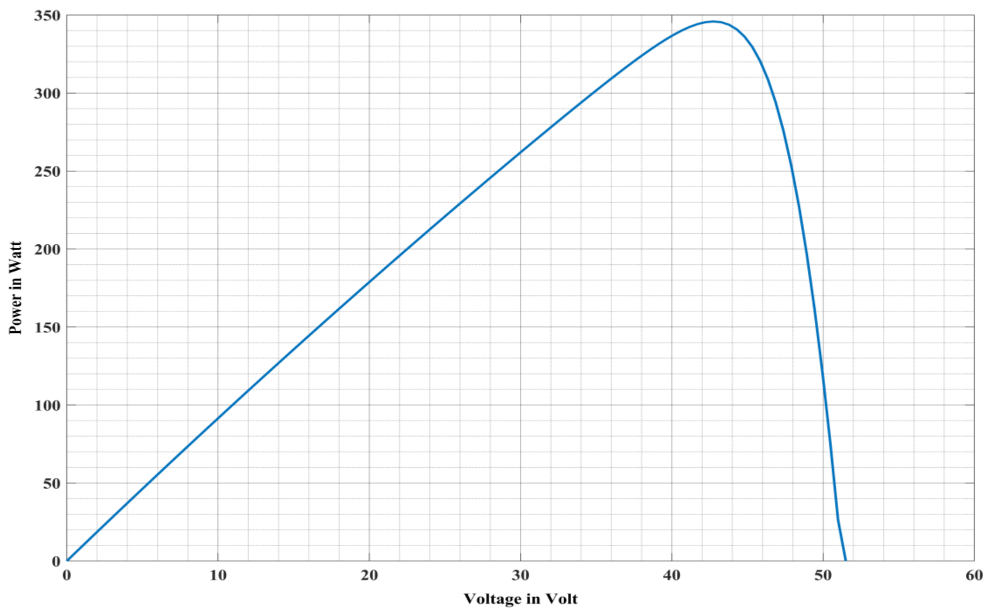

Figure 4-4 Single solar panel power-voltage curve

4.2. PV arrays Power-Voltage and Current-Voltage Curve

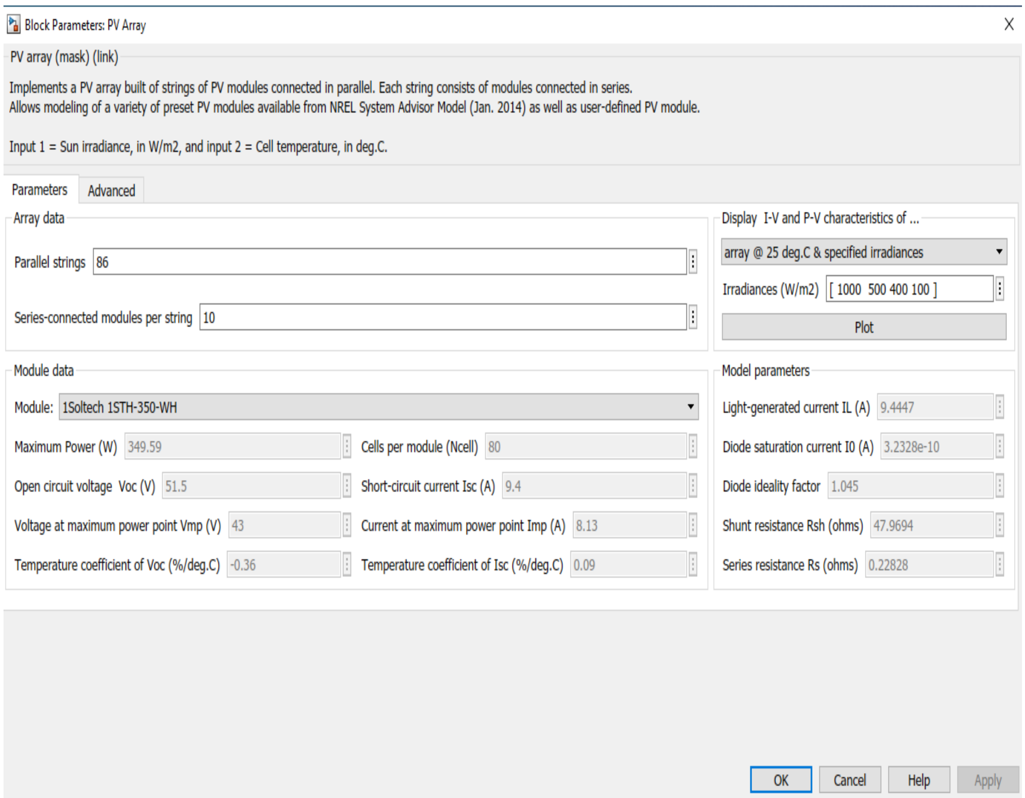

Figure 4-5 Parallel and series Area A solar array specification

The current in the I-V curve is directly proportional to irradiance. As irradiance increases, the photocurrent generated by the solar panel also increases, leading to a higher short-circuit current (I_{sc}). Conversely, as irradiance decreases, the short-circuit current decreases. On the other hand, the open-circuit voltage (V_{oc}) is less sensitive to changes in irradiance but still increases slightly as irradiance rises. The voltage remains relatively stable because, it is more influenced by temperature than by irradiance as shown in

Figure 4-6 . Finally, the power output of the PV system is the product of current and voltage ($P = I \times V$). With constant temperature, as irradiance increases, the current increases, leading to a higher maximum power point (MPP). The P-V curve shifts upward with increasing irradiance, indicating higher power generation.

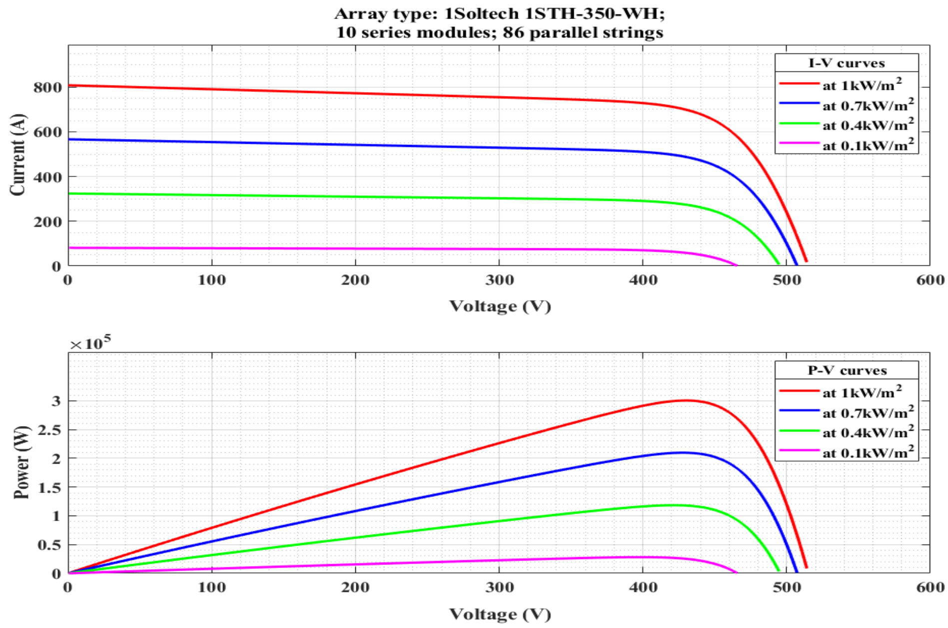

Figure 4-6 PV array's Current-Voltage curve and Power-Voltage curve at 25^0c.

4.2.1. P-V and I-V curve for solar panel array at specific irradiance and vary temperature

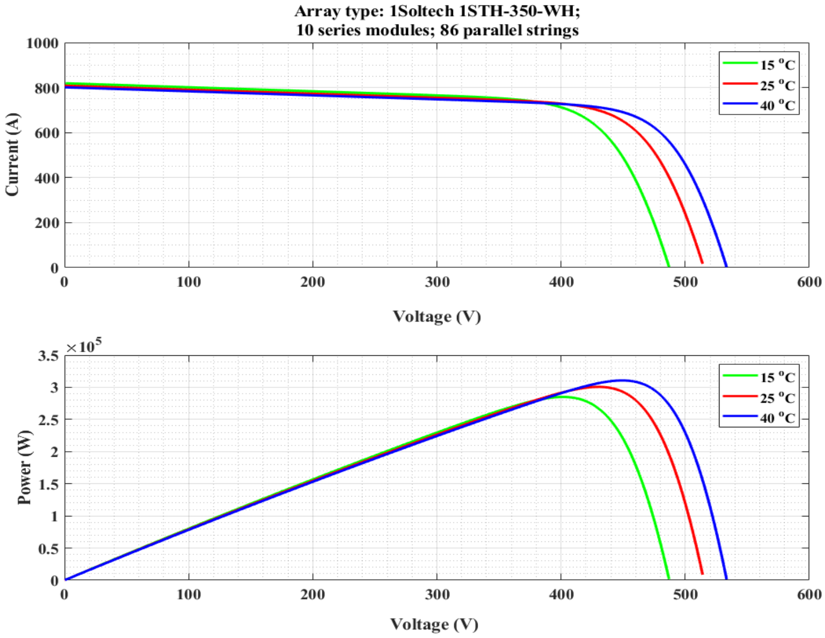

Figure 4-7 Solar array output curves at specific irradiance (1000 w/m^2)

As Figure 4-7 temperature varies while irradiance remains constant, the P-V (power-voltage) and I-V (current-voltage) curves of a photovoltaic (PV) module exhibit distinct behaviours. In the I-V curve, the current remains largely unaffected by temperature changes, maintaining a relatively consistent value at the maximum power point (MPP). However, the voltage at the MPP decreases as temperature increases, leading to a shift in the I-V curve to the left. This results in a reduction of the overall power output, which is reflected in the P-V curve. The P-V curve shows a decrease in both the peak power and the voltage at which this peak occurs as temperature rises. Consequently, the MPP shifts leftward on the voltage axis, indicating reduced efficiency in power generation at higher temperatures.

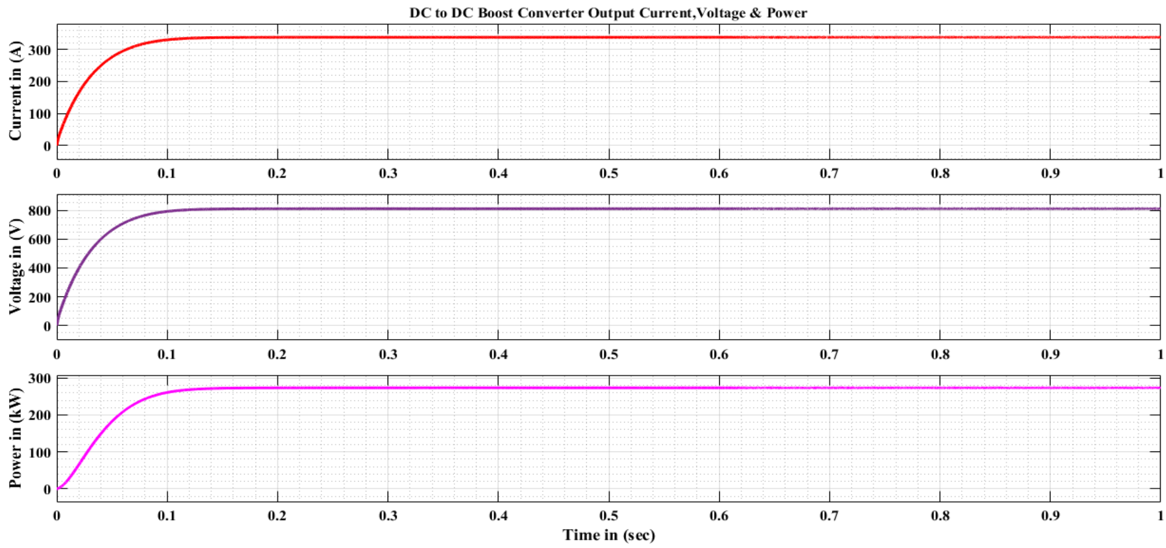

Figure 4-8 DC-DC Boost Converter outputs with constant irradiance (1000 W/m^2)

All inputs and outputs of DC-to-DC boost converter are different.

The DC to DC output shown in

Figure 4-9 is not rapidly converge without both Model Reference Adaptive Controller (MRAC) or Maximum Power Point Tracking (MPPT) with Incremental Conductance (INC). The result approximately converges to 0.2 sec. This is why MRAC_PID and MPPT is employed.

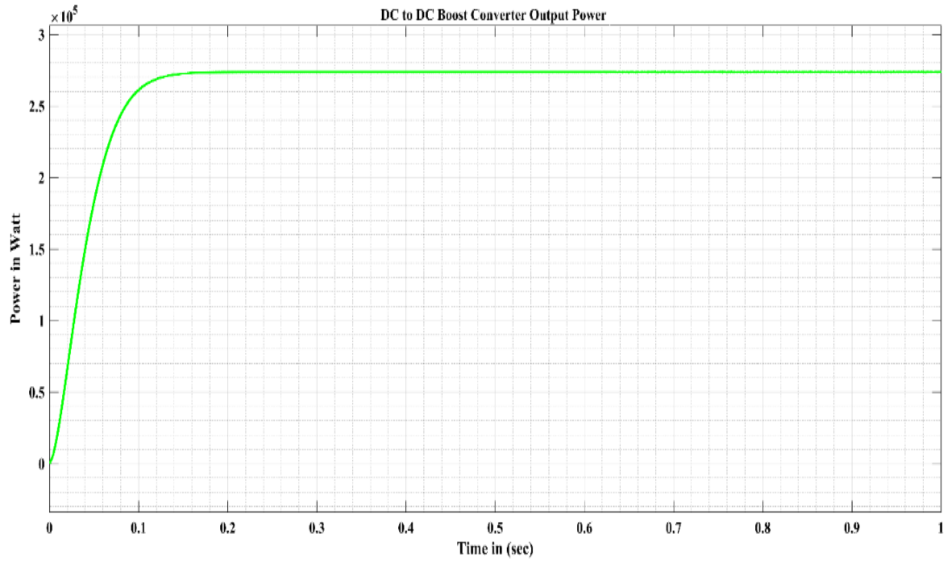

Figure 4-9 DC to DC boost converter output power

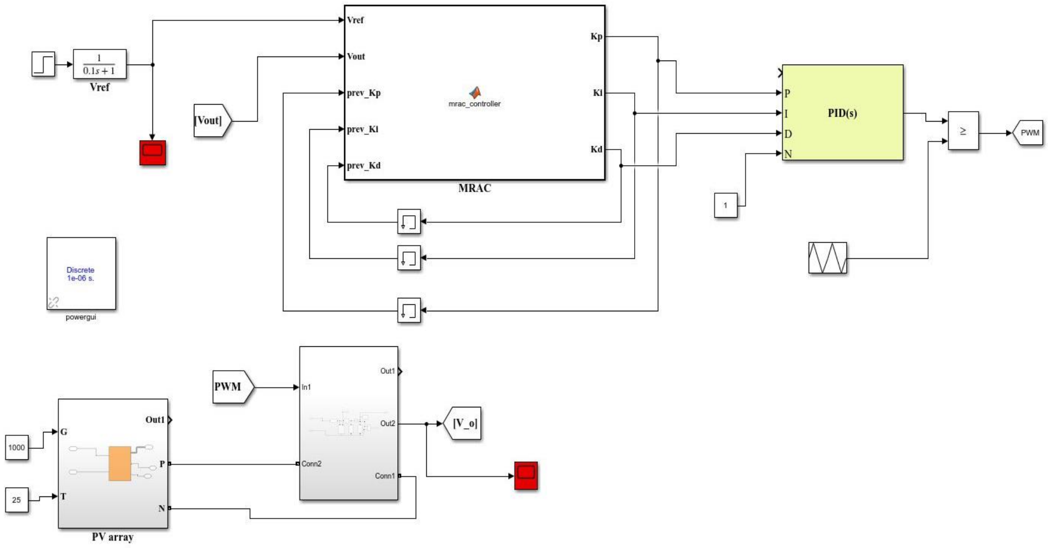

Figure 4-10 MRAC_PID Simulink

Selected reference model is $V_{ref} = \dfrac{1}{0.1s+1}$ which, is first order transfer function.

V_{out} is DC-to-DC boost converter output voltages.

How MRAC-PID works?

V_{ref} (reference model) is compared with the desired output, which is V_{out}. Then, the error generated in the MRAC function block. Then after, the error is multiplied by the adaptation rate and connected to the PID block; finally, the PID gains as well as the triangle pulse generator are connected to the relation operation block; after all, it is given to the MOSFET by PWM.

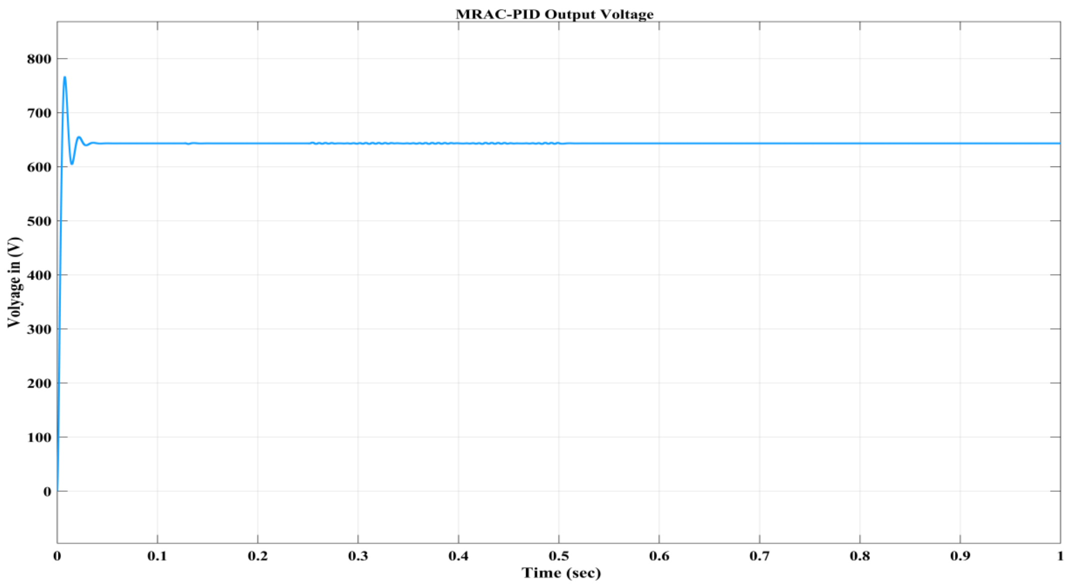

Figure 4-11 Area A: Model Reference Adaptive PID Controller output voltage

Using a Proportional-Integral-Derivative (PID) controller in conjunction with Model Reference Adaptive Control (MRAC) is a potent technique that attempts to adjust the controller's settings in real-time to achieve desired performance, even in the presence of system uncertainties or changes. With a settling time of only 0.03 seconds, the system can quickly stabilize and approach the reference value.

Maximum Power Point Tracking with Incremental Conductance (MPPT_INC) applied to the PV array output voltage or connected to PV array before DC-to-DC boost converter. The result would be good, which is fast to converge to the desired output as shown at Figure 4-13.This result obtained by using Proportional Integral (PI) controller, 20 kHz frequency switching frequency for MOSFET.

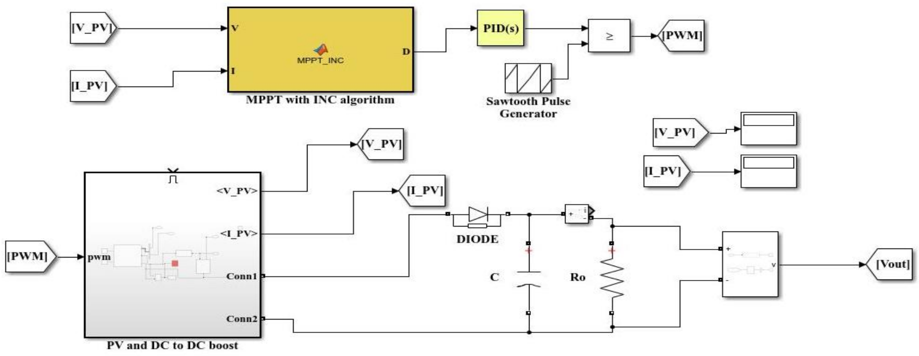

Figure 4-12 Photovoltaic with MPPT_PID controller

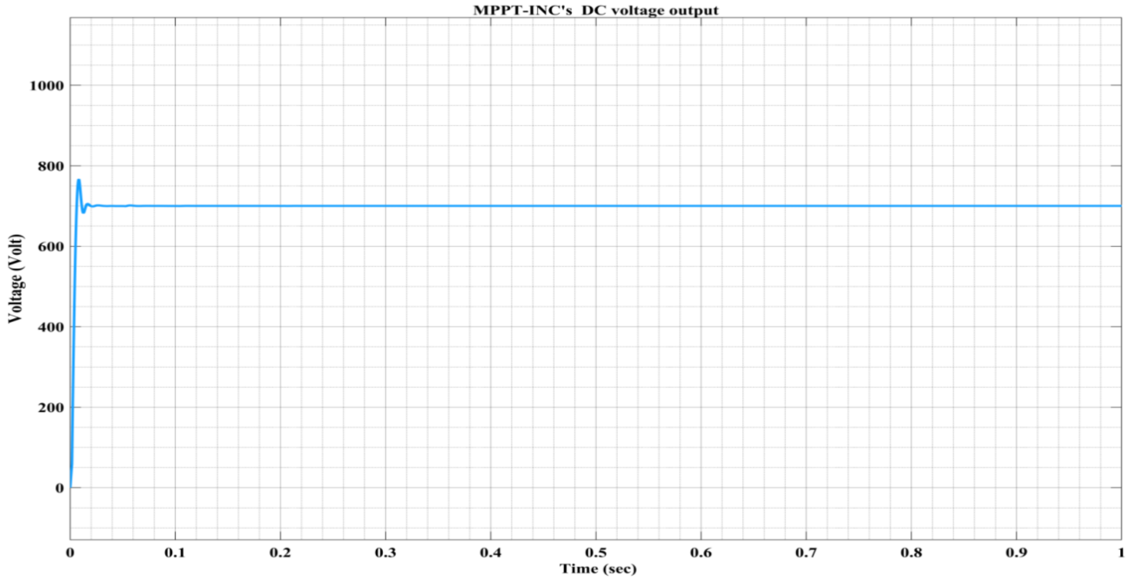

Figure 4-13 MPPT_INC output voltage

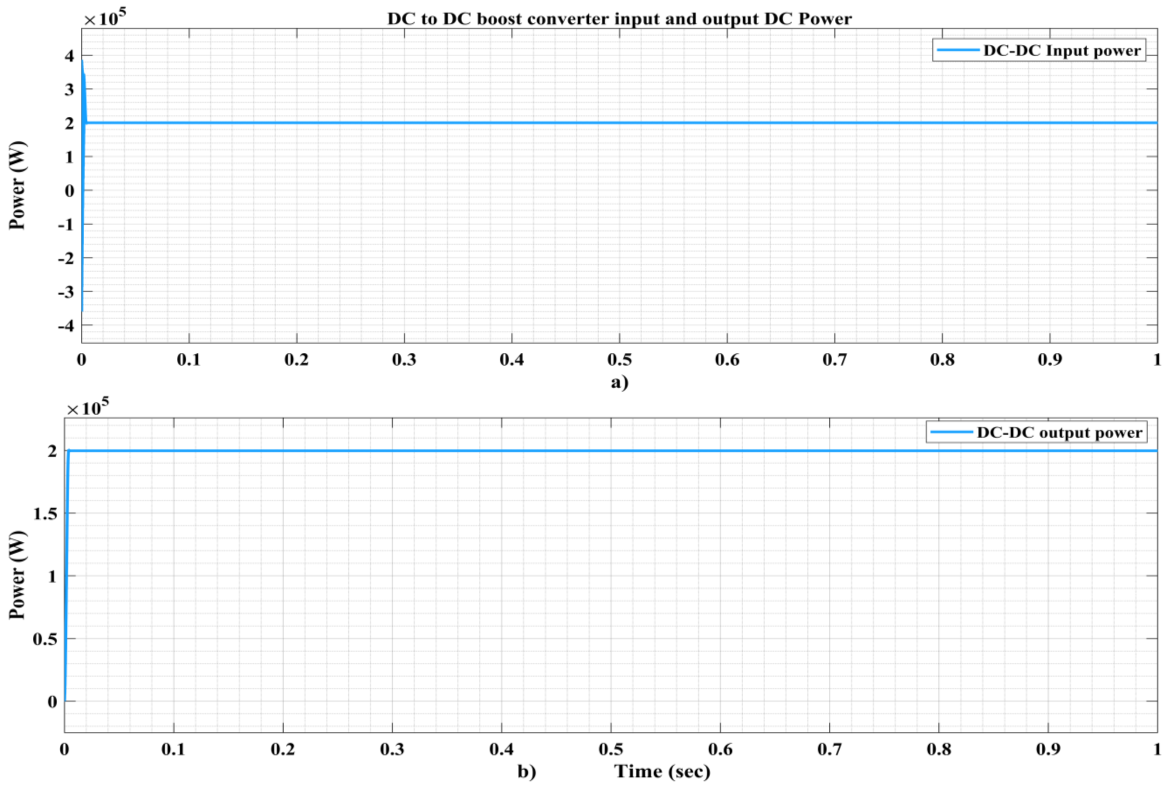

Figure 4-14 DC-Link Power Output

DC-Link output: After application of MRAC and MPPT, the output is given to DC-Link to remove small harmonic, which is almost zero. This DC-Link voltage is given to three-phase inverter.

Pulse Width Modulated (PWM), voltage waveform will be produced by the inverter from the DC input. Due to the lack of a filter, the voltage will be a high-frequency square wave (or PWM signal) with severe harmonic distortion, reflecting the inverter's switching activity. Similarly, because there is no filtering, the output current waveform has high-frequency harmonics that resemble the voltage waveform Figure 4-15. Within help of filter, voltage and current waveforms become more smoother and more akin to a sinusoidal shape after going through the LCL filter. The fundamental frequency component is largely retained after the high frequency components are removed by the LCL filter Figure 4-16.

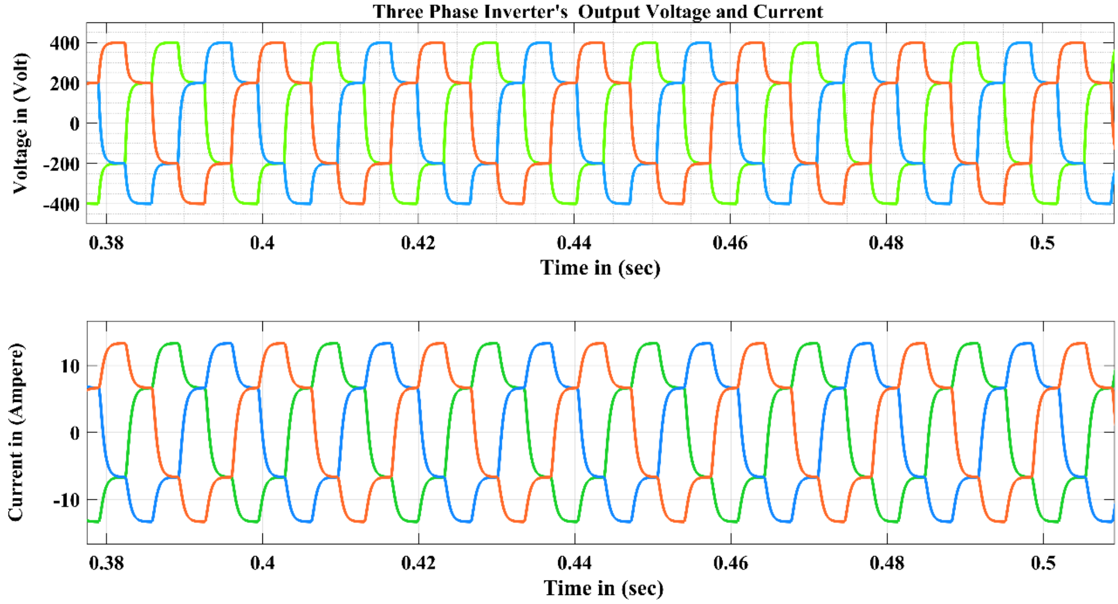

Figure 4-15 Area B: Inverter side current and voltage waveform without LCL filter application.

As demonstrated in Figure 4-16, an inverter generates three phase voltages that are regulated with a magnitude of 600 Vrms line-to-line and 100 A maximum current for Area A, as well as three phase currents that are controlled by a voltage control loop and three phase voltages 415 Vrms line-to-line with a maximum of 50 A for second area(Area B). The LCL filter is very effective in lowering harmonics.

4.2.2. Inverter Side Voltage and Currents

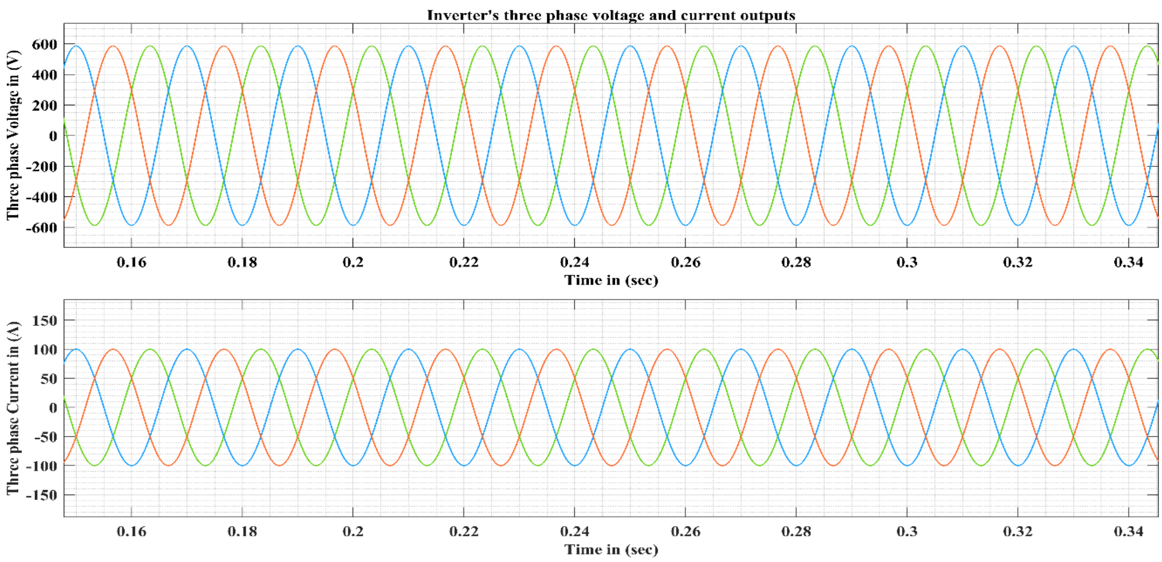

Figure 4-16 Area A controlled and filtered 3Φ-phase current and voltage

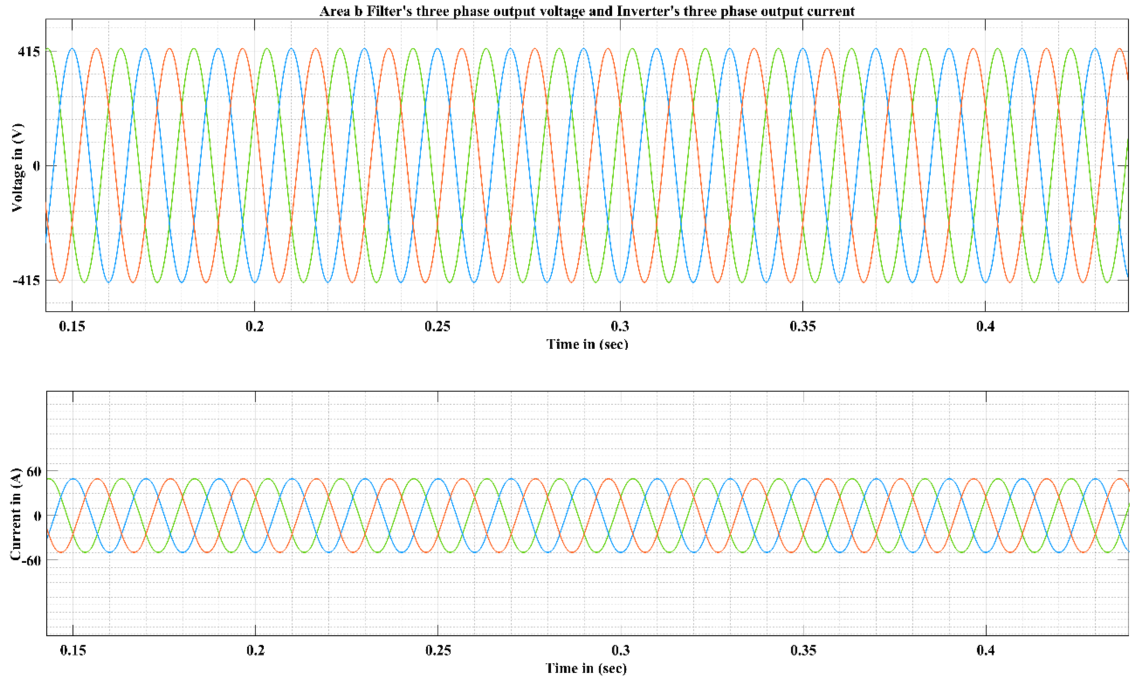

Figure 4-17 Area B controlled and filtered 3-Φ current and voltage

4.2.3. Grid side three phase Voltage and Current

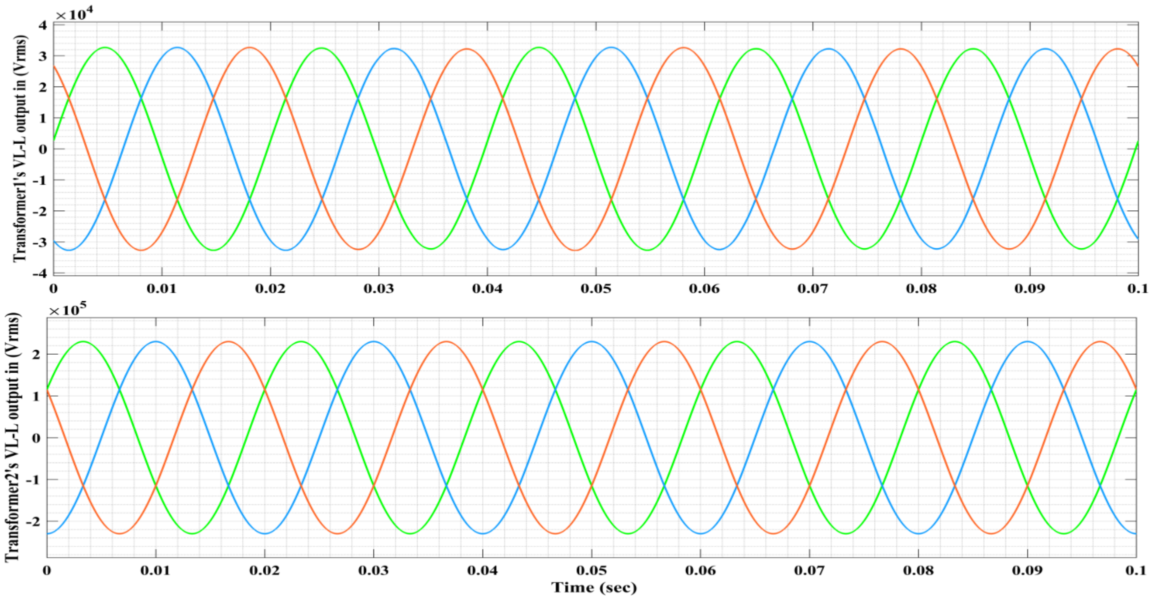

Figure 4-18 Voltage Synchronized to the Electrical Grid

The lack of a transformer that can step up 400 V to 230 kV is the primary reason why two transformers are used. Direct step-up is difficult in the second scenario. It is impossible to step up voltage straight from 400 V to 230 kV in a single transformer due to the enormous turns ratio required. Large transformers, intricate designs, and insulation problems would arise from this. By using an intermediate voltage level (33 kV in this case), the step-up method is divided into two manageable pieces, simplifying and enhancing the efficiency of each transformer's construction.

Transformers designed for extremely high voltage ratios would need to be large and employ highly advanced insulating techniques. Each transformer's size and insulating needs are more reasonable and achievable.

Purpose of using powergui: The powergui block initializes and manages the simulation of electrical systems by handling the initial conditions, such as initializing the states of electrical components like capacitors and inductors.

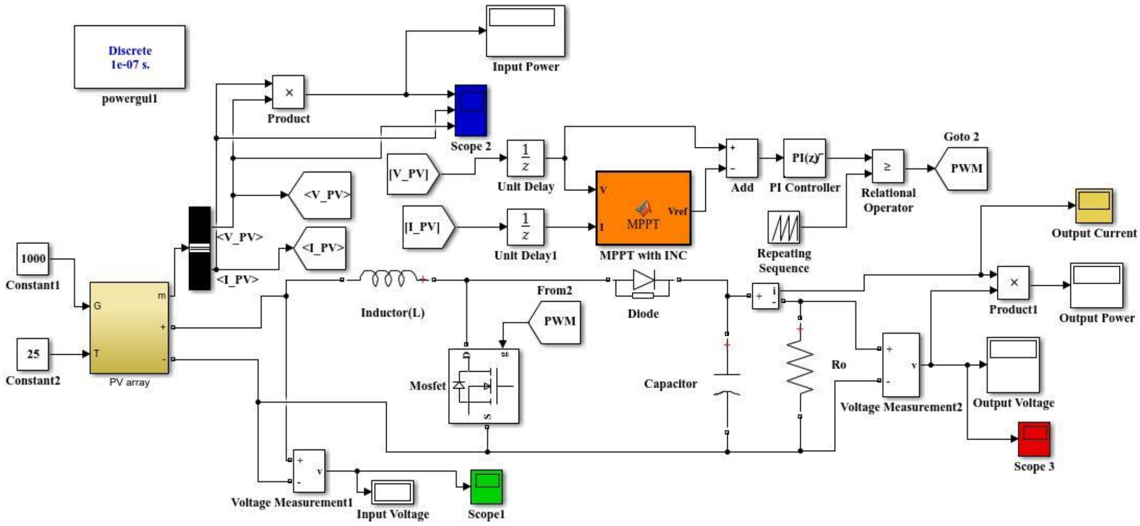

Figure 4-19 MPPT based on Incremental conductance with PV power system Simulink

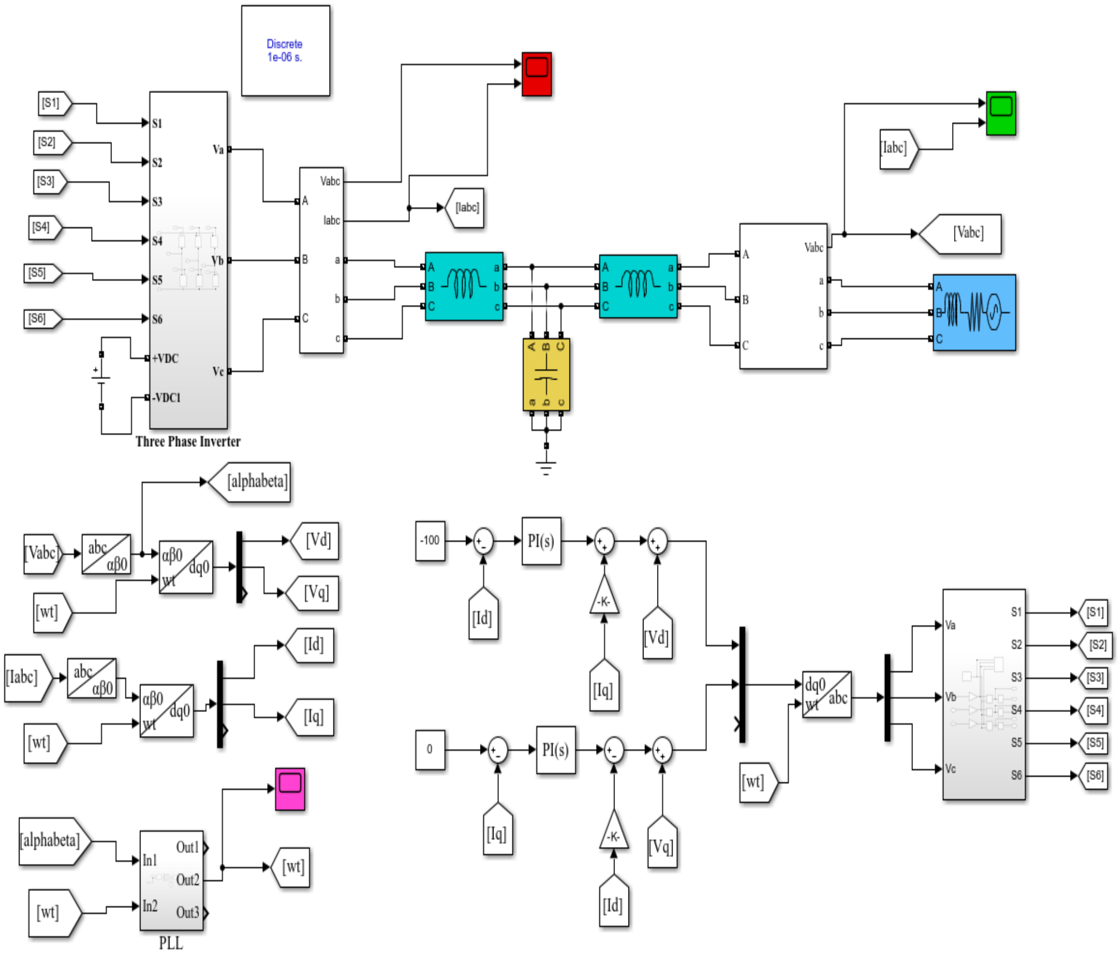

Figure 4-20 Grid tied PV power system MATLAB Simulink

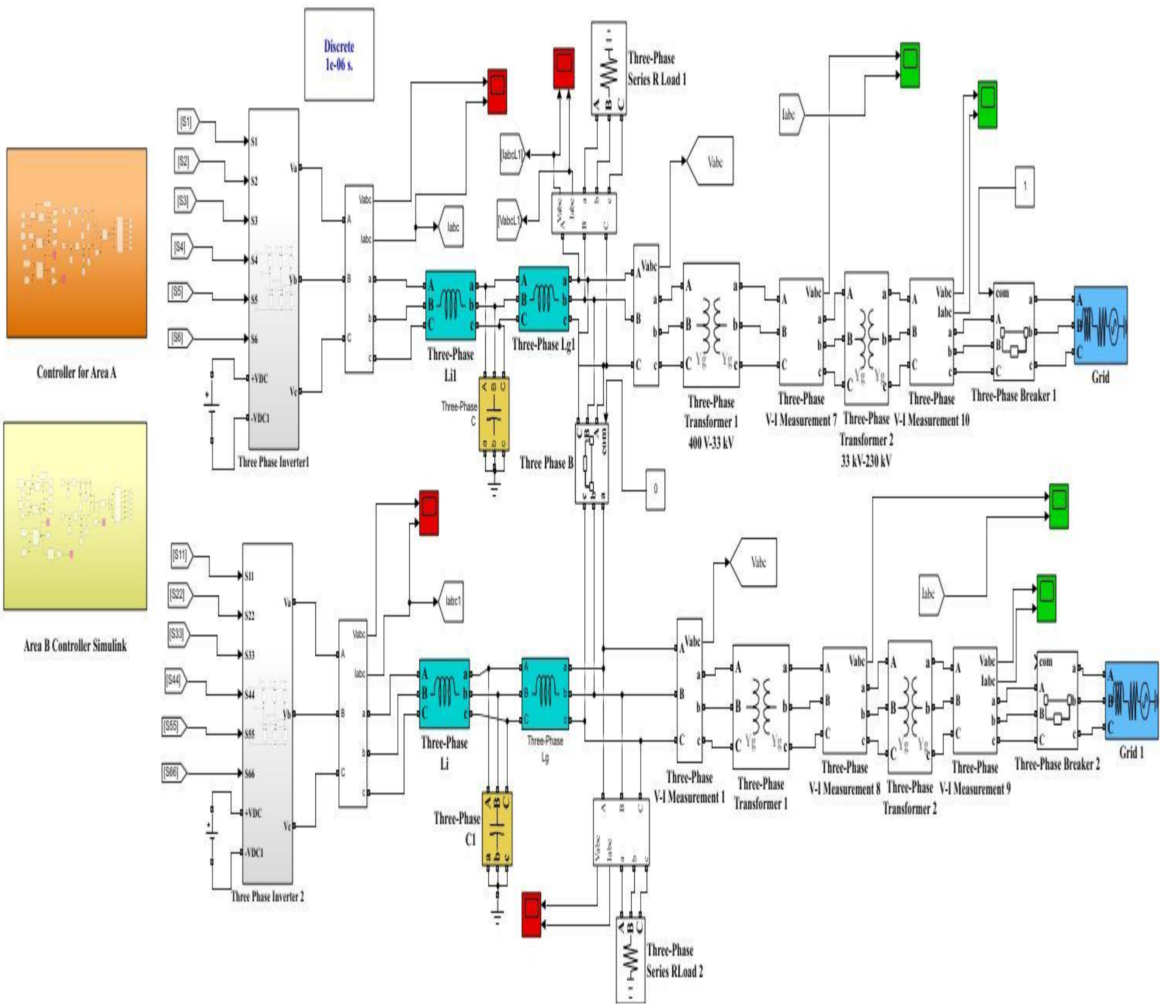

Figure 4-21 Two- areas grid connected PV power system overall Simulink.

The both areas are connected to single electrical grid as shown in Figure 4-21.

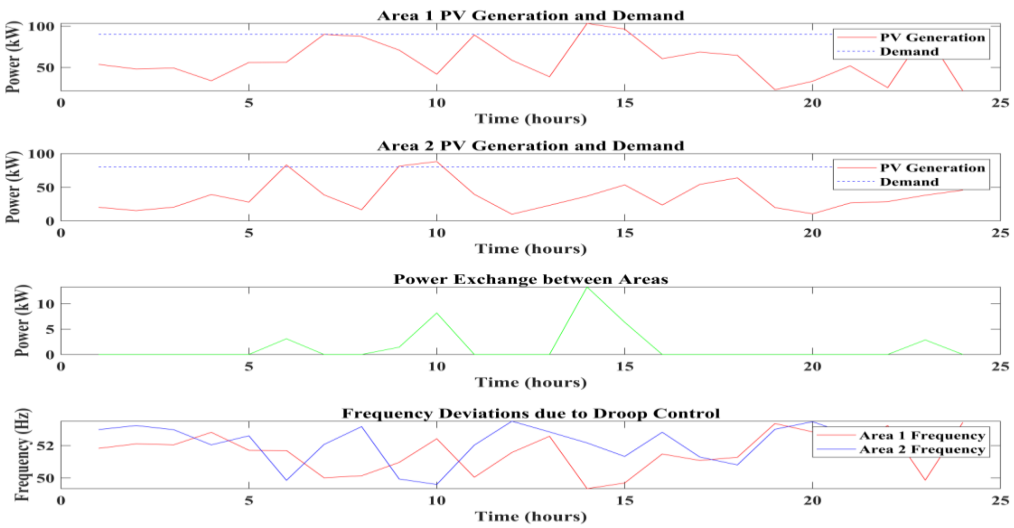

Figure 4-22 Demand and Supply

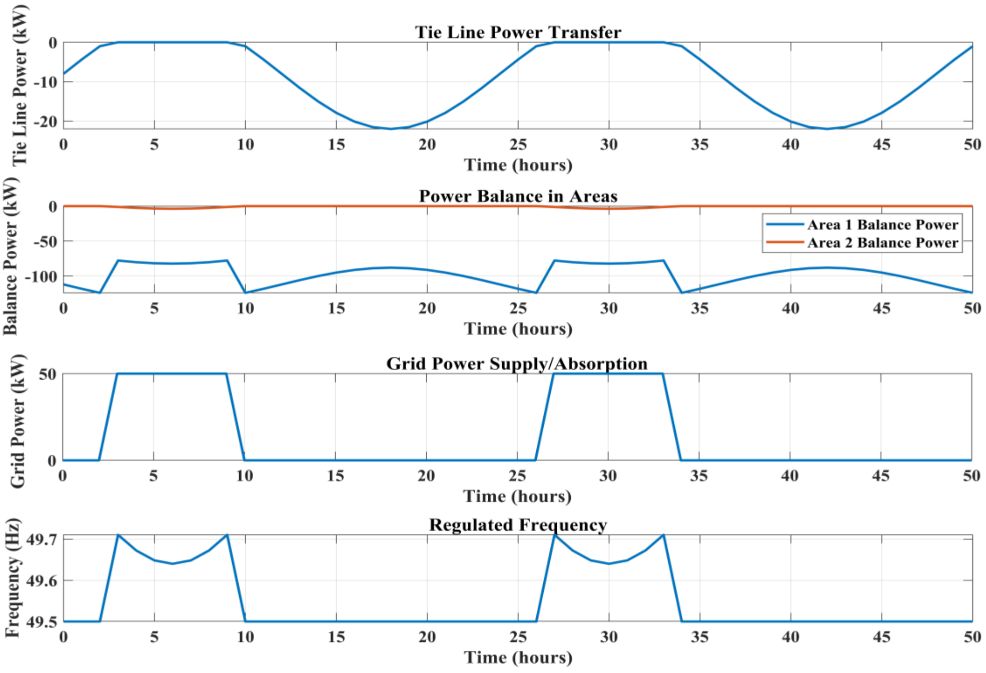

Figure 4-23 Two Areas Power Sharing and regulated frequency

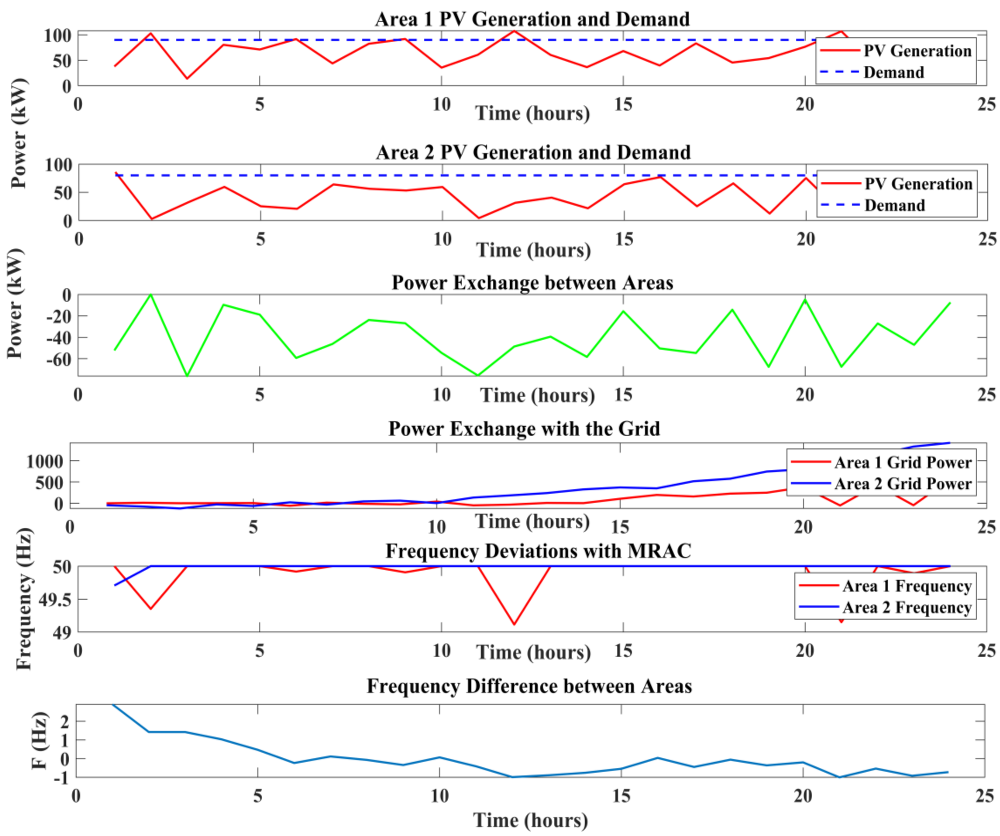

Figure 4-24 Regulated Frequency of both regions.

Area 1(Area A) PV Generation and Demand

Graph in the Figure 4-24: The first subplot shows the power generated by the PV system in Area 1 (in red) and the power demand in Area 1 (in blue dashed line).

Explanation: This graph illustrates the comparison between the power generated by the photovoltaic (PV) system in Area 1 and the demand within that area over the 24-hour period. When the red line (PV generation) is above the blue dashed line (demand), Area 1 has surplus power, and when it is below, there is a power deficit.

Area 2(Area B) PV Generation and Demand

Graph in the Figure 4-24: The second subplot is similar to the first but for Area 2. It shows the PV generation (in red) and the demand (in blue dashed line) for Area 2.

Explanation: This graph provides a similar comparison for Area 2, showing how well the PV system meets the demand in that area. The interaction between generation and demand in this graph will indicate the power surplus or deficit in Area 2.

Power Exchange between Areas

Graph: The third subplot shows the amount of power exchanged between Area 1 and Area 2 (in green).

Explanation: This graph visualizes the power exchange between the two areas to balance their power requirements. Positive values indicate that power is transferred from one area to the other to help meet its demand. This exchange is driven by the frequency difference between the areas, ensuring stability across the network. The MRAC system adjusts the power exchange dynamically to minimize the frequency deviation.

Power Exchange with the Grid

Graph: The fourth subplot shows the power exchanged with the grid by Area 1 (in red) and Area 2 (in blue).

Explanation: This graph demonstrates how each area interacts with the main grid. Positive values represent the power sent to the grid (surplus), while negative values indicate power drawn from the grid (deficit). When local generation is insufficient to meet demand, the area relies on the grid for additional power, and when there's excess generation, it supplies power back to the grid.

Frequency Deviations with MRAC

Graph: The fifth subplot shows the frequency deviations for Area 1 (in red) and Area 2 (in blue) around the nominal frequency of 50 Hz.

Explanation: This graph depicts how the frequency in each area deviates from the nominal value of 50 Hz over time. The MRAC system works to minimize these deviations by dynamically adjusting the control parameters. Ideally, the frequency should remain close to 50 Hz, indicating a stable power system. The MRAC aims to reduce fluctuations and ensure that the frequency remains within the 49-50 Hz range.

Frequency Difference between Areas

Graph: The sixth subplot shows the frequency difference between Area 1 and Area 2 (in light blue).

Explanation: This graph illustrates the difference in frequency between the two areas over time. The goal is to minimize this difference, indicating synchronized operation between the two areas. A smaller frequency difference means that the areas are better balanced, which is crucial for the stability of the interconnected system. The MRAC controller helps reduce this difference, leading to improved overall system stability.

These explanations provide context for each graph, helping you understand how the system operates and how different components interact to maintain stability and efficiency.

CHAPTER FIVE

5. CONCLUSION AND RECOMMENDATION

5.1. Conclusion

For the growth of one country, energy has a great role. From the renewable energy source PV solar system, the most important one due to sunlight is almost everywhere on Earth, making solar energy accessible globally, even in remote areas. A grid-tied photovoltaic (PV) solar system is one that is connected to the local electrical grid, allowing homeowners or businesses to use solar power alongside grid electricity. From the PV systems, DC voltage is obtained, solar panels generate electricity in the form of direct current (DC). This is because the photovoltaic effect, which occurs in the solar cells, naturally produces DC electricity. Since this DC voltage has some fluctuation or chattering, it is very necessary to filter it by using the DC link and apply the maximum power tracking controller to get the desired DC voltage. The electrical grid operates on AC voltage because it is more efficient for transmitting electricity over long distances and is the standard for power distribution worldwide. To integrate solar power with the grid, the electricity generated by the solar panels must be converted from DC to AC to match the grid's voltage and grid nominal frequency. A well-regulated frequency is essential for ensuring grid resilience and reliability. Fluctuations in frequency can lead to power outages, equipment damage, and even system-wide failures. The simulated desired frequency is 49.5 Hz to 49.7 Hz. After being controlled by the PI and droop method, the result is close to 50 Hz for Area A and 49.2 Hz for Area B. This thesis shows two different PV systems that have different power and loads are designed to share power with each other when one load is high and the other as low power with a stable system before connected to the grid, which is linked together by a tie line. When the power of the system from both PV systems is low, the system obtains power from the grid. Finally, when both areas have deficiency, then electrical grid supply power for both areas.

5.2. Recommendation

Currently, the system is designed to operate under constant temperature and irradiance. Future work could involve testing and optimizing the system under varying environmental conditions, such as fluctuating irradiance levels, temperatures, and shading, to ensure the robustness and adaptability of the control strategies. Implementing advanced weather and load forecasting techniques could further enhance the system's reliability and efficiency. By predicting changes in environmental conditions, the control strategies can proactively adjust, maintaining frequency stability and power balance more effectively.

The current setup focuses on a two-area grid-connected system. Extending this work to include multiple interconnected areas could provide valuable insights into the scalability of the control strategies. This expansion could also explore the impact of additional tie-line and the increased complexity of grid synchronization and power balancing.

While MRAC PID control is applied to the DC-DC boost converter, investigating other adaptive control strategies, such as fuzzy logic or neural network-based controllers, could offer improved performance, particularly under non-linear and uncertain conditions. Introducing energy storage systems (ESS) into the grid-connected PV system could further enhance frequency control and power balancing, especially during sudden load changes or PV generation fluctuations. Future work could explore the integration of ESS and its impact on system dynamics.

Finally, exploring optimization algorithms for power flow management and loss minimization across the grid could significantly improve the system's overall efficiency. This could involve the use of advanced techniques such as genetic algorithms, particle swarm optimization, or other heuristic methods.

REFERENCES

Abd-Elazim, S. M., & Ali, E. S. (2018). Load frequency controller design of a two-area system composing of PV grid and thermal generator via firefly algorithm. *Neural Computing and Applications*, *30*(2), 607–616. https://doi.org/10.1007/s00521-016-2668-y

Azad, A. H., & Shateri, H. (2019). A Novel Control Strategy for On-Grid Photovoltaic Systems Based on Adaptive PI Control. *2019 Iranian Conference on Renewable Energy and Distributed Generation, ICREDG 2019, June 2019.*

Choudhary, N., Parkh, K., & Jangid, R. (2019). *Load Frequency Control of 2-Area System by Whale Optimization Algorithm*. *12*.

Civelek, Z., Gorel, G., Luy, M., Barısci, N., & Cam, E. (2018). Effects on load-frequency control of a solar power system with a two-area interconnected thermal power plant and its control with a new BFA algorithm. *Elektronika Ir Elektrotechnika*, *24*(6)

D, U. R. I., Member, X., Vrxufhv, H., Ri, F., Lvwulexwhg, G., Dssurdfkhv, W., Fhqwudol, L., Ru, H. G., & Hg, G. (n.d.). *'hvljq ri dq $gdswlyh 6hqglqj 5dwh iru)uhtxhqf\ 5hjxodwlrq ri d 6pduw 0lfurjulg zlwk 2swlpdo /45 &rqwuroohu*.

Dandoussou, A., & Kenfack, P. (2023). Modelling and analysis of three - phase grid - tied photovoltaic systems. *Journal of Electrical Systems and Information Technology*. https://doi.org/10.1186/s43067-023-00096-z

Fay, D. L. (2017). Solar Photovoltaic generating system and grid Integration -modeling, cntroller design and optimization. *Angewandte Chemie International Edition, 6(11), 951–952.*

Fu, R., Chung, D., Lowder, T., Feldman, D., Ardani, K., Fu, R., Chung, D., Lowder, T., Feldman, D., & Ardani, K. (2016). U.S. Solar Photovoltaic System Cost Benchmark: Q1 2016. *National Renewable Energy Laboratory*, *September*, 37.

Ghosh, A., & Kandpal, M. (n.d.). *State-space average Modeling of DC-DC Converters with parasitic in Discontinuous Conduction Mode (DCM).*

Jiang, J., Trundle, P., Ren, J., Cheng, Y.-L., Lee, C.-Y., Huang, Y.-L., Buckner, C. A., Lafrenie, R. M., Dénommée, J. A., Caswell, J. M., Want, D. A., Gan, G. G., Leong, Y. C., Bee, P. C., Chin, E., Teh, A. K. H., Picco, S., Villegas, L., Tonelli, F., … García-Díaz, V. (2010). We are IntechOpen , the world ' s leading publisher of Open Access books Built by scientists , for scientists TOP 1 %. *Intech*, *34*(8), 57–67. detection-in-biometrics%:

Katinas, V., Marčiukaitis, M., & Tamašauskiene, M. (2016). Analysis of the wind turbine noise emissions and impact on the environment. *Renewable and Sustainable Energy Reviews*, *58*, 825–831.

Kumar, N., Singh, B., & Panigrahi, B. K. (2019). Integration of Solar PV With Low-Voltage Weak Grid System: Using Maximize-M Kalman Filter and Self-Tuned P&O Algorithm. *IEEE Transactions on Industrial Electronics*, *66*(11), 9013–9022.

Kumar, Y. V. P., & Bhimasingu, R. (2021). Design of voltage and current controller parameters using small signal model - based pole - zero cancellation method for improved transient response in microgrids. *SN Applied Sciences*.

Minda, W. (2019). *Addis Ababa Institute of Technology School of Electrical and Computer Engineering Grid Connection and Synchronization Inverter Control for Solar Power System Using Synchronously Rotating Reference Frame By A Thesis submitted to Addis Ababa Institute of Te*.

Mirzaeva, G., Goodwin, G. C., McGrath, B. P., Teixeira, C., & Rivera, M. E. (2016). A Generalized MPC Framework for the Design and Comparison of VSI Current Controllers. *IEEE Transactions on Industrial Electronics*, *63*(9), 5816–5826.

Mokhtar, M., Marei, M. I., Sameh, M. A., & Attia, M. A. (2022). An Adaptive Load Frequency Control for Power Systems with Renewable Energy Sources. *Energies*, *15*(2), 1–22.

Naz, F. (2021). *Closed loop Buck & Boost Converter Mathematical Modeling , Analysis and Simulation using MATLAB*. *8958*(4), 263–271.

Negi, P., Pal, Y., & Leena, G. (2023). Grid - Connected Photovoltaic System Stability Enhancement Using Ant Lion Optimized Model Reference Adaptive Control. *Differential Equations and Dynamical Systems*, *31*(2), 503–525.

Omar, O. A. M., Badra, N. M., & Attia, M. A. (2018). Enhancement of On-grid PV System under irradiance and temperature variations using new optimized adaptive controller. *International Journal of Electrical and Computer Engineering*, *8*(5), 2650–2660.

Ortiz, O. J. R., Castelblanco, J. S. U., & Fonseca, G. L. V. (2020). MRAC and MPC Controllers for Load Application System of the Accelerated Testing Equipment of Pavements. *International Journal on Advanced Science, Engineering and Information Technology*, *10*(5), 1946–1953.

Roberts, J. J. M. (2020). Prophets and Kings: *A God So Near*, 341–354.

Rohouma, W., Metry, M., Balog, R. S., Peerzada, A. A., & Begovic, M. M. (2020). Adaptive model predictive controller to reduce switching losses for a capacitor-less

D-STATCOM. *IEEE Open Journal of Power Electronics*, *1*(July), 300–311.

Sheril, A. A., & Ramesh Babu, M. (2017). Synchronization Control of Grid Connected Photovoltaic System. *Middle-East Journal of Scientific Research*, *25*(4), 864–870.

Workshop, S. (2014). *Design of Grid Connect PV systems*. *August*.

Zhang, R., Lu, H., Yang, J., & Zhang, T. (2018). *Single-phase Photovoltaic Grid-connected Inverter Current Control Method Based on MRAC*. *163*(Iceesd), 226–233.

APPENDIXES

Appendix A: single diode PV panel's curves plot MATLAB code

```
iT=input ('Enter the number of curves you aim to plot: 1,2...4: ');
for N=1:iT;                                  %PV Module DATA
T=input ('Give the value of Ti in degree Celsius: ')
G=input ('Give the value of solar irradiance in W/m2: ');
ai=0.09/100;                                 % Current Temperature coefficient(ki)
av=-0.36/100;                                % Voltage Temperature coefficient(kv)
Isc_r=9.4;                                   % Short-circuit current
Voc_r=51.5;                                  % Open circuit voltage
Vmp=43;                                      % Maximum voltage @ STC
Imp=8.13;                                    % Maximum current @ STC
Pmax=350;                                    % Maximum power   @ STC
Nse=60;                                      % number of Cells
a=1.045;                                     % Diode ideality factor% Internal parameters
G_n=1000;                                    % reference irradiance
T=Ti+273.6;
Tref= 25 +273.6;
dT=T-Tn;
Isc=Isc_r+aI*dT;                             % variation of Isc with T°
Voc=Voc_r+aV*dT;                             % variation de Vco with T°
Q=1.60217646*power(10,-19);                  % charge constant
K=1.3806503*power(10,-23);                   % Boltzmann constant
Vt=(Nse*a*K*T/Q);                            % Thermal voltage
EG=1.12;                                     % gap energy
I_ph=Isc*(G/G_n);                            % photo-current
Io=(Isc)/(exp( Voc/Vt )-1 );                 % saturation current
IRs=Io*( (T/Tn)^3 ) * exp ( ( (Q*EG)/(a*K) )*((1/Tn)-(1/T)) );%saturation current
Rse=0.22828;                                 % series resistance in ohm
Rpa=47.9694;                                 % parallel resistance in ohm
I=I_ph;                                      % initial codition
V=0:(V_oc/100): V_oc;                        % input voltage array
for n1=1:length(V)
```

```
for n2=1:20                    % Newton-Raphson loop for calculating output current
Vd= (V(n1)+Rse*I);             % Diode Voltage
Id=IRs*( exp(Vd/Vt) -1);    % Diode current
Ip=Vd/Rpa;                     % Parallele resistance Current
f=Iph-I-Id-Ip;                  % f(I)=0
df=-1-(IRs*Rse/Vt)*exp(Vd/Vt)-(Rse/Rpa); % f'(I)=0
I=I-f/df; % Newton-Raphson formula
end
if I<0
I=0;
End
Ipv(n1)=I;  % Accumulation of output currant
end
P=Ipv.*V;% Output power
figure(1)
hold on
plot(V,Ipv,'linewidth',N)%
grid on
figure(2)
plot(V,P,'linewidth',N)%
Plot(V,Ipv,P,'linewidth',N)
hold on
grid on
end
```

Appendix B: Power sharing code for two areas power system

```
% Parameters

pv_capacity_area1 = 110; % Capacity of PV system in area 1 (kW)

pv_capacity_area2 = 90; % Capacity of PV system in area 2 (kW)

demand_area1 = 90; % Demand of area 1 (kW)

demand_area2 = 80; % Demand of area 2 (kW)

nominal_frequency = 50;   % Nominal frequency (Hz)

droop_coefficient = 0.05;    % Droop coefficient (Hz/kW)
```

```
Kp_initial =0 .015;            % Initial proportional gain for PI controller
Ki_initial = 4000;              % Initial integral gain for PI controller
damping_factor = 0.8;         % Damping factor to reduce frequency changes over time
frequency_min = 49;            % Minimum allowable frequency (Hz)
frequency_max = 50;            % Maximum allowable frequency (Hz)
adaptation_rate = 0.01;        % Adaptation rate for MRAC
% Simulation
time_steps = 24; % Number of time steps (hours)
% Generate random PV generation profiles for demonstration
pv_generation_area1 = rand (1, time_steps) * pv_capacity_area1;
pv_generation_area2 = rand (1, time_steps) * pv_capacity_area2;
% Initialize variables
net_power_area1 = zeros (1, time_steps);
net_power_area2 = zeros (1, time_steps);
exchange_power = zeros (1, time_steps);
grid_power_area1 = zeros (1, time_steps);
grid_power_area2 = zeros (1, time_steps);
frequency_deviation_area1 = zeros (1, time_steps);
frequency_deviation_area2 = zeros (1, time_steps);
cumulative_error_area1 = 0;
cumulative_error_area2 = 0;
frequency_difference = zeros (1, time_steps);
% Initialize MRAC parameters
Kp_area1 = Kp_initial;
Ki_area1 = Ki_initial;
Kp_area2 = Kp_initial;
Ki_area2 = Ki_initial;
```

```
% Power exchange logic with MRAC-based frequency control

for t = 1: time_steps

% Calculate net power for each area

net_power_area1(t) = pv_generation_area1(t) - demand_area1;

net_power_area2(t) = pv_generation_area2(t) - demand_area2;

% Calculate frequency deviations based on net power

requency_deviation_area1(t) = -droop_coefficient *    net_power_area1(t);

frequency_deviation_area2(t) = -droop_coefficient *  net_power_area2(t)

% Calculate the frequency difference between the two areas

frequency_difference(t) = frequency_deviation_area1(t) -  frequency_deviation_area2(t);

% Damping the frequency difference over time

if t > 1

frequency_difference (t) = damping_factor * frequency_difference(t-1) + (1 -
damping_factor) * frequency_difference(t);

end

% MRAC Adaptation for Area 1

error_area1 = frequency_min - nominal_frequency - frequency_deviation_area1(t);

Kp_area1 = Kp_area1 + adaptation_rate * error_area1 * frequency_difference(t);

Ki_area1 = Ki_area1 + adaptation_rate * error_area1 * cumulative_error_area1;

% MRAC Adaptation for Area 2

error_area2 = frequency_min - nominal_frequency - frequency_deviation_area2(t);

Kp_area2 = Kp_area2 + adaptation_rate * error_area2 * frequency_difference(t);

Ki_area2 = Ki_area2 + adaptation_rate * error_area2 * cumulative_error_area2;%
Frequency synchronization by power exchange between areas

if frequency_difference(t) > 0

% Area 1 has higher frequency, transfer power to Area 2

correction_power = Kp_area1 * frequency_difference(t);

exchange_power(t) = min (correction_power, net_power_area1(t));
```

net_power_area1(t) = net_power_area1(t) - exchange_power(t);

net_power_area2(t) = net_power_area2(t) + exchange_power(t);

else if frequency_difference(t) < 0

% Area 2 has higher frequency, transfer power to Area 1

correction_power = Kp_area2 * abs(frequency_difference(t));

exchange_power(t) = min (correction_power, net_power_area2(t));

net_power_area2(t) = net_power_area2(t) - exchange_power(t);

net_power_area1(t) = net_power_area1(t) + exchange_power(t);

else

exchange_power(t) = 0; % No exchange if frequencies are equal

end % PI controller with MRAC to maintain frequency within desired range

if frequency_deviation_area1(t) < frequency_min - nominal_frequency

cumulative_error_area1 = cumulative_error_area1 + error_area1; correction_power_area1 = Kp_area1 * error_area1 + Ki_area1 * cumulative_error_area1; grid_power_area1(t) = grid_power_area1(t) + correction_power_area1;

frequency_deviation_area1(t) = frequency_min - nominal_frequency; % Clamp frequency to lower limit

elseif frequency_deviation_area1(t) > frequency_max - nominal_frequency

cumulative_error_area1 = cumulative_error_area1 + error_area1;

correction_power_area1 = Kp_area1 * error_area1 + Ki_area1 * cumulative_error_area1;

grid_power_area1(t) = grid_power_area1(t) - correction_power_area1;

frequency_deviation_area1(t) = frequency_max - nominal_frequency; % Clamp frequency to upper limit

end

if frequency_deviation_area2(t) < frequency_min - nominal_frequency

cumulative_error_area2 = cumulative_error_area2 + error_area2;

correction_power_area2 = Kp_area2 * error_area2 + Ki_area2 * cumulative_error_area2;

grid_power_area2(t) = grid_power_area2(t) + correction_power_area2;

```
frequency_deviation_area2(t) = frequency_min - nominal_frequency; % Clamp frequency to lower limit

elseif frequency_deviation_area2(t) > frequency_max - nominal_frequency

cumulative_error_area2 = cumulative_error_area2 + error_area2;

correction_power_area2 = Kp_area2 * error_area2 + Ki_area2 * cumulative_error_area2;

grid_power_area2(t) = grid_power_area2(t) - correction_power_area2;
frequency_deviation_area2(t) = frequency_max - nominal_frequency; % Clamp frequency to upper limit

end

% Interaction with the grid for remaining net power

if net_power_area1(t) > 0

grid_power_area1(t) = grid_power_area1(t) + net_power_area1(t); % Surplus to grid

net_power_area1(t) = 0;

elseif net_power_area1(t) < 0

grid_power_area1(t) = grid_power_area1(t) + net_power_area1(t);  % Deficit from grid

net_power_area1(t) = 0;

end

if net_power_area2(t) > 0

grid_power_area2(t) = grid_power_area2(t) + net_power_area2(t);  % Surplus to grid

net_power_area2(t) = 0;

elseif net_power_area2(t) < 0

grid_power_area2(t) = grid_power_area2(t) + net_power_area2(t);  % Deficit from grid

 net_power_area2(t) = 0;

end
```

```
end
% Plotting
time = 1: time_steps;
figure;
% PV Generation and Demand for Area 1
Subplot (6,1,1);
plot (time, pv_generation_area1, 'r-', time, demand_area1*ones(size(time)),
'b--');
title ('Area 1 PV Generation and Demand');
legend ('PV Generation', 'Demand');
xlabel('Time (hours)');
ylabel('Power (kW)');
% PV Generation and Demand for Area 2
subplot (6,1,2);
plot (time, pv_generation_area2, 'r-', time, demand_area2*ones(size(time)),
'b--');
title ('Area 2 PV Generation and Demand');
legend ('PV Generation', 'Demand');
xlabel ('Time (hours)');
ylabel ('Power (kW)');
% Power Exchange between Areas
subplot (6,1,3);
plot (time, exchange_power, 'g-');
title ('Power Exchange between Areas');
xlabel ('Time (hours)');
```

```
ylabel ('Power (kW)');

% Power Exchange with the Grid

subplot (6,1,4);

plot (time, grid_power_area1, 'r-', time, grid_power_area2, 'b-');

title ('Power Exchange with the Grid');

legend ('Area 1 Grid Power', 'Area 2 Grid Power');

xlabel ('Time (hours)');

ylabel ('Power (kW)');

% Frequency Deviations

subplot (6,1,5);

plot (time, nominal_frequency + frequency_deviation_area1, 'r-', time,
nominal_frequency + frequency_deviation_area2, 'b-');

title ('Frequency Deviations with MRAC');

legend ('Area 1 Frequency', 'Area 2 Frequency');

xlabel ('Time (hours)');

ylabel ('Frequency (Hz)');

% Frequency Difference between Areas

subplot (6,1,6);

plot (time, frequency_difference, 'k-');

title ('Frequency Difference between Areas');

xlabel ('Time (hours)');

ylabel ('Frequency Difference (Hz)');
```

Link: L_{in1}, L_{in2}, L_{in3} and L_{in4}, L_{in5} :https://www.electricrate.com/wp-content/uploads/2023/02/difference-between-polycrystalline-and-monocrystalline-solar-panels.jpg